INFORMATION TO USERS

This manuscript has been reproduced from the microfilm master. UMI films the text directly from the original or copy submitted. Thus, some thesis and dissertation copies are in typewriter face, while others may be from any type of computer printer.

The quality of this reproduction is dependent upon the quality of the copy submitted. Broken or indistinct print, colored or poor quality illustrations and photographs, print bleedthrough, substandard margins, and improper alignment can adversely affect reproduction.

In the unlikely event that the author did not send UMI a complete manuscript and there are missing pages, these will be noted. Also, if unauthorized copyright material had to be removed, a note will indicate the deletion.

Oversize materials (e.g., maps, drawings, charts) are reproduced by sectioning the original, beginning at the upper left-hand corner and continuing from left to right in equal sections with small overlaps.

Photographs included in the original manuscript have been reproduced xerographically in this copy. Higher quality 6" x 9" black and white photographic prints are available for any photographs or illustrations appearing in this copy for an additional charge. Contact UMI directly to order.

Bell & Howell Information and Learning
300 North Zeeb Road, Ann Arbor, MI 48106-1346 USA
800-521-0600

Université d'Ottawa · University of Ottawa

Secondary Structure of the Channel Forming Transmembrane Segments from the Nicotinic Acetylcholine Receptor

Nathalie Méthot

Thesis submitted to the Department of Biochemistry in partial fulfillment of the requirements for the degree of Doctor of Philosophy in Biochemistry

University of Ottawa
Ottawa, Ontario, Canada
September 1999

Je dédie cette thèse à ma grand-mère Marie-Blanche Poulin Bruyère (1904-1999), qui nous a quittés le jour de la soutenance.

Abstract

The goal of the research was to investigate the secondary structure and orientation of the channel forming transmembrane segments in the nicotinic acetylcholine receptor (nAChR) and their change in orientation upon desensitization. The long term objective is to further characterize the desensitized state of the nAChR as a basis of better understanding how the modulation of synaptic transmission is involved in brain function. FTIR spectroscopy was first used to probe the secondary structure of the nAChR and the changes in structure induced upon channel inactivation. Both qualitative and quantitative analysis of the secondary structure-sensitive amide I band of FTIR spectra of the nAChR support a mixed α/β type protein with a predominance of α-helices. Stabilization of the nAChR in channel inactive conformations by either prolonged exposure to the agonist carbamylcholine, to the non-competitive antagonist tetracaine or upon reconstitution into membranes lacking anionic phospholipids and cholesterol revealed no changes in the amide I band, hydrogen/deuterium exchange kinetics or exchange difference spectra attributed to a change in protein conformation. Several approaches were directed toward the elucidation of the secondary structure of the transmembrane segments in the nAChR. Hydrogen/deuterium exchange experiments revealed the presence of an exchange resistant core of hydrogen peptides, corresponding to roughly 25% of the protein, mainly α-helical, and likely located in the solvent inaccessible transmembrane domain. $^{1}H/^{2}H$ exchange experiments at alkaline pH and upon reconstitution of the nAChR in egg phosphatidylcholine membranes to increase the rate and extent of exchange were

performed and support a high proportion of α-helical peptides in the exchange resistant core of the nAChR.

The amide I band of FTIR spectra of the transmembrane domain of the nAChR isolated by pronase under membrane disruption conditions (less than 3.7 kDa in size) revealed a very high content of α-helices. Similarly, we analyzed the secondary structure of individual transmembrane segments from the nAChR isolated by Dr. Michael Blanton at Texas Tech University and observed a high α-helical content. Taken together, these results support an α-helical transmembrane domain in the nAChR. Polarized FTIR spectroscopy revealed, for the first time, an average calculated tilt angle of roughly 41° of the transmembrane segments in proteolyzed nAChR and no detectable net change in orientation was observed upon carbamylcholine induced desensitization.

Résumé

Le but de ce projet de recherche était d'étudier la structure secondaire et l'orientation des segments transmembranaires formant le canal ionique du récepteur nicotinique d'acétylcholine (nAChR) et leur changement d'orientation dans l'état désensibilisé. L'objectif à long terme était de mieux comprendre comment la modulation de la transmission synaptique est impliquée dans le fonctionnement du cerveau. Premièrement, la structure secondaire du nAChR et les changements conformationnels induits lors de l'inactivation du canal ont été étudiés par spectroscopie FTIR. L'analyse qualitative et quantitative de la bande amide I des spectres FTIR, hautement sensible à la structure secondaire des protéines, révèle la présence d'hélices α en majorité et de feuillets β dans le nAChR. La stabilisation du nAChR dans un état de canal inactivé, soit par exposition prolongée à l'agoniste carbamylcholine, à l'antagoniste non-compétitif tétracaïne ou suite à la reconstitution dans des membranes ne contenant pas de phospholipides anioniques et de cholestérol, n'a révélé aucun changement dans la bande amide I, dans la cinétique d'échange hydrogène/deutérium et dans les spectres de différence d'échange reliés à un changement de conformation. Plusieurs approches ont été utilisées afin de déterminer la structure secondaire des segments transmembranaires du nAChR. Des expériences d'échange d'hydrogène/deutérium ont révélé la présence d'un noyau d'hydrogènes peptidiques résistant à l'échange, correspondant à environ 25% de la protéine, majoritairement fait d'hélices α, et probablement localisé dans les domaines transmembranaires inaccessibles au solvent. Des expériences d'échange hydrogène/deutérium à pH alcalin après reconstitution du

nAChR dans des membranes de phosphatidylcholine d'oeuf afin d'augmenter le taux et le degré d'échange ont révélé une haute proportion d'hélices α dans le noyau résistant à l'échange. La bande amide I des spectres FTIR du domaine transmembranaire du nAChR isolé par la pronase sous des conditions de perturbation membranaire (moins que 3.7 kDa de masse moléculaire) a révélé un taux très élevé d'hélices α. Similairement, l'étude de la structure secondaire des segments transmembraires du nAChR isolés par Dr Michael Blanton à l'Université Texas Tech suggère une majorité d'hélices α. Ensemble, ces résultats appuient un domaine transmembranaire fait d'hélices α dans le nAChR. Des spectres FTIR polarisés ont révélé un angle d'inclinaison moyen d'environ 41° des segments transmembranaires du nAChR protéolysé et aucun changement net d'orientation n'a été observé suite à la désensibilisation par l'acétylcholine.

Acknowledgements

I sincerely want to thank my supervisor John (Dr. John E. Baenziger) for the privilege I was given to do research and his patience and support in my research project.

I wish to thank the professors in the Department of Biochemistry, Microbiology and Immunology for letting me use their equipment and I would like to express a special thank to both Dr. Danielle Carrier et Dr. Odette Laneuville for their friendship and support.

The members of my Advisory Committee; Dr. Danielle Carrier, Dr. Harold Jarrell and Dr. Vas Mezl are acknowledged for their advice and support.

I am grateful to Dr. Michael Blanton from Texas Tech University for providing me the transmembrane segments of the nAChR.

I also want to thank my past and present friends in the department: Hanane, Anu, Pascale, Jean, Nathalie, Vanisree, Maroun, Sonia and Roxanne, my labmates: Caroline, Jennifer, Stuart, Marcin, Roula, Mary-Lou, Phuc Hoa, Tim, Blair and especially Steve Ryan for his friendship over the years.

Thanks to the secretaries of the department: Julie Aubé, Joanne Barlow and Crystal Perry, for their friendship and technical support.

During my doctoral studies I received excellent financial support from the Natural Sciences and Engineering Research Council of Canada, le Fonds pour Chercheurs et l'aide à la recherche from the Province of Québec and the School of Graduate Studies and Research of the University of Ottawa. I would like to express my sincere thanks to these people.

Enfin, je voudrais remercier mon mari Bernard, pour sa patience et son soutien à l'égard de ces interminables études, et aussi pour son amour et son humour qui rendent la vie si agréable. Camille et Laurie, continuez d'être des petits rayons de soleil dans nos vies.

Si je suis ce que je suis, je le dois à mes parents, Paul et Pierrette. Pour leur exprimer mon amour et ma gratitude à leur égard, j'aurais besoin de toutes les pages de cette thèse. J'aimerais aussi remercier mon frère François pour m'avoir communiqué son intérêt pour la science durant notre enfance et aussi de m'avoir encouragée à poursuivre au doctorat. Finalement, je désire saluer ma soeur Manon pour ses petits mots d'encouragement, via internet, durant l'écriture de ma thèse.

Table of content

List of tables

List of figures

Chapter 1

Chapter 2

Chapter 3

Chapter 4

List of abbreviations and formulas

ATR	Attenuated total reflectance
a.u.	Absorbance units
BAC	Bromoacetylcholine bromide
$CaCl_2$	Calcium chloride
CaF_2	Calcium fluoride
Carb	Carbamylcholine
CD	Circular dichroism
Chol	Cholesterol
DMPC	Dimyristoylphosphatidylcholine
DOPA	Dioleoylphosphatidic acid
DPPC	Dipalmitoylphosphatidylcholine
dp	Depth of penetration
DTNB	5,5'-dithiobis-2-nitrobenzoic acid
DTT	Dithiothreitol
EDTA	Ethylenediaminetetraacetic acid
EGTA	Ethylene glycol-bis(β-aminoethyl ether) N,N,N'N'-tetraacetic acid
EMR	Electromagnetic resonance
EPC	Egg phosphatidylcholine
FTIR	Fourier transform infrared
$^1H/^2H$	Hydrogen/deuterium
HPLC	High performance liquid chromatography
N_2	Nitrogen
nAChR	Nicotinic acetylcholine receptor
$NaHCO_3$	Sodium bicarbonate
Na_2HPO_4	Disodium phosphate
NaN_3	Sodium azide
NMR	Nuclear magnetic resonance
$MgCl_2$	Magnesium chloride
MOPS	3-(N-morpholino)propanesulfonic acid
PAGE	Polyacrylamide gel electrophoresis
PMSF	Phenylmethylsulphonyl fluoride
rpm	Revolution per minute
SDS	Sodium dodecyl sulphate
S/N	Signal-to-noise
Tet	Tetracaine
TFA	Trifluoroacetic acid
TID	(3-(trifluromethyl)-3-(m-[^{125}I]iodophenyl)diazirine
Tm	Transition or melting temperature
TR	Torpedo Ringer
Tris	Tris(hydroxymethyl)aminomethane
ZPD	Zero path difference

Chapter 1- General Introduction

The human brain is a highly complex network of ~10^{11} interconnected neurons which convey information electrically and chemically to generate cognitive functions like perception, actions, emotions, language, memory and learning. It is subdivided into regions specialized in specific functions. For example, in the cerebral hemispheres, the cortex is involved in language whereas the hippocampus is linked to memory storage. However, the precise mechanisms by which these functions are produced are poorly understood.

At the turn of the 20th century, the mechanism underlying the propagation of nerve impulses in neurons and synaptic transmission began to emerge (Kandel, Schwartz and Jessell, 1995). Charles Sherrington introduced the term synapse for the zone of contact by which one neuron communicates with another. In the 1920s, Otto Loewi showed that a chemical compound, acetylcholine, conveys signals from the vagus nerve to the heart. This discovery resulted in a controversy in the 1930s regarding the means by which neurons transmit signals at synapses, either electrically or chemically. In the 1950s and 1960s, it became evident that both kinds of transmission exist.

At the dawn of the 21st century, it is clear that synaptic transmission at chemical synapses in both the central and peripheral nervous systems is an extremely complex biochemical event and is an important component of nervous system function. Changes in effectiveness of synaptic transmission, referred to as synaptic plasticity, can occur through modulation of neurotransmitter receptor function. However, it is unclear how these changes in synaptic efficiency are linked to cognitive functions of the brain. In

order to understand mind, we must elucidate how neurons are organized and how they communicate with each other by means of synaptic transmission. Importantly, understanding how neurotransmitter receptors function and how their activity can be modulated is crucial in order to better perceive how the brain works and will likely be a major challenge of research interest in the 21st century. The work in this thesis is focused on understanding the structure and mechanism of function in one neurotransmitter receptor, the nicotinic acetylcholine receptor (nAChR). This research was initiated in September 1992 as an honour's project and continued as graduate studies in September 1993. Before beginning to discuss the nAChR in detail, a brief discussion of the mechanism of neurotransmission and the role of neurotransmitter receptors will be presented.

1. Neurotransmission

There are two distinct classes of cells in the nervous system: the nerve cells or neurons and the glial cells. Neurons are the fundamental unit of the nervous system, they are responsible for transmitting and processing information. The three types of glial cells, oligodendrocytes, Schwann cells and astrocytes are not essential for information processing, however they perform important roles. For example, they surround neurons and serve as supporting elements providing firmness and structure to the brain, some are scavengers removing debris after injury or neuronal death.

Neurons are characterized by four distinct regions: cell body, dendrites, axon and presynaptic terminals (figure 1.1). The cell body (soma) contains the nucleus and

Figure 1.1 Schematic representation of the main features of a vertebrate neuron: the cell body, dendrites, axon and nerve terminals. Also shown myelin sheath, nodes of Ranvier and synapse with a post-synaptic cell. From Kandel et al., 1995.

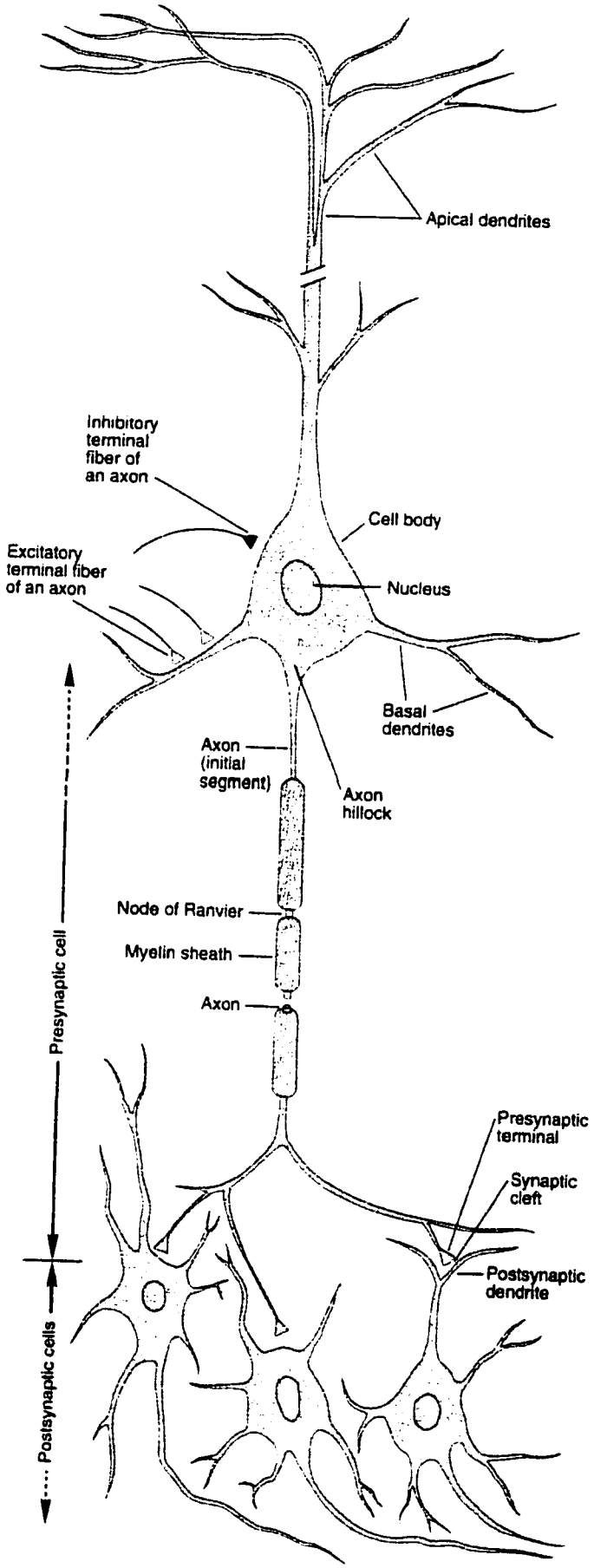
Apical dendrites
Inhibitory terminal fiber of an axon
Cell body
Excitatory terminal fiber of an axon
Nucleus
Basal dendrites
Axon (initial segment)
Axon hillock
Node of Ranvier
Myelin sheath
Axon
Presynaptic terminal
Synaptic cleft
Postsynaptic dendrite
Presynaptic cell
Postsynaptic cells

organelles and is the metabolic center of the cell. The cell body gives rise to two types of outgrowths (processes), the dendrites and the axon. The dendrites resemble branches of a tree and receive the signals from other neurons. The axon is the main conducting unit of the neuron and can convey electrical signals over long distances. Near its end, the axon splits into branches in order to reach several targets. The contact between the presynaptic terminal and the post-synaptic cell is called synapse.

To understand how signals are propagated along neurons we must introduce the basic concepts of membrane potential and ion channels. Neuronal membranes have an unequal distribution of charges on the two sides of the membrane. Both intracellular and extracellular fluids contain organic and inorganic ions, but the composition is different. The intracellular fluid contains a higher concentration of organic ions, such as amino acids and proteins (negatively charged) and K^+ ions. On the other hand, the extracellular fluid contains a higher concentration of both Na^+, Cl^- and Ca^{2+} ions. This distribution of charges across the neuronal membrane gives rise to a resting membrane potential between –60 to –70 mV, which means that the interior of neurons is more negative than the exterior. In other words, the membrane is polarized. The electrochemical driving force is defined as the sum of the electrical driving force, due to charge distribution, and the chemical driving force, due to the concentration gradient. In the resting condition, the electrochemical driving force across the membrane leads to a small influx of Na^+ and a small efflux of K^+ of equal magnitude through slightly permeable Na^+ and K^+ channels. This current is called the leakage current. Meanwhile, the sodium-potassium pump moves both Na^+ and K^+ against their concentration gradient, preventing the dissipation of the ionic gradient.

The membrane of axons contains voltage-gated Na^+ and K^+ channels which open ion channels in response to a change in membrane potential (voltage). The opening of ion channels leads to a flux of ions across the membrane and change in membrane polarization, either depolarization or hyperpolarization. Nerve impulses or action potentials travel in axons's by membrane depolarization. A depolarization of the membrane causes Na^+ channels to open rapidly resulting in an inward Na^+ current. This current increases the membrane potential and depolarizes adjacent sections of the membrane. This newly depolarized section of the membrane will also respond by opening Na^+ channels and Na^+ influx. This regenerative process moving along the neuron axon's constitutes the action potential. Membrane depolarization also leads to the delayed opening of voltage-gated K^+ channels and outward K^+ current which repolarize the membrane. Na^+ channels close spontaneously after a time where they adopt an inactivated state as long as the membrane remains depolarized. In contrast, K^+ channels stay open as long as the membrane is depolarized and close only when the membrane returns to the resting level. The action potential is followed by a period of diminished excitability, or refractoriness, which last a few milliseconds.

In the dendrites are located neurotransmitter receptors which receive signals from other neurons and are responsible for initiating action potentials. Neurotransmitter receptors are divided in two major groups according to the coupling mechanism between the receptor and effector, either directly or indirectly and are often named after the neurotransmitter's name. One group called ligand-gated ion channels (or ionotropic receptors) directly gate ion channels and will be presented in section 3. The second group of neurotransmitter receptors gate channels indirectly, they are separate molecules

from the ion channels that they modulate. One family of those neurotransmitter receptors includes the following receptors: α- and β-adrenergic, muscarinic acetylcholine, $GABA_B$, glutamate, serotonin, dopamine and receptor for neuropeptides (such as opioid peptides, β-endorphin, met-enkephalin, leu-enkephalin, somatostatin...). Ligand binding to these receptors is coupled to GTP-binding proteins (G-proteins) and production of second messengers triggering intracellular events. Often, second messengers can alter the activity of ion channels by phosphorylating the channel protein. These latter neurotransmitter receptors will not be discussed further as they are not the focus of this thesis.

Ligand binding to neurotransmitter receptors in the neuron's dendrites causes the opening of ion channels, ion flux across the membrane and a change in membrane potential called synaptic potential. Excitatory ligand-gated ion channels opening results in an important influx of Na^+ and Ca^{2+} ions, a small efflux of K^+ ions and membrane depolarization. On the other hand, inhibitory ligand-gated ion channels opening causes Cl^- influx and membrane hyperpolarization. Signaling between neurons is complicated by the fact that each neuron can receive connections from hundreds of other neurons, both excitatory and inhibitory inputs, mediated by a variety of neurotransmitters. In addition, presynaptic neuronal nAChR were identified recently and were suggested to be involved in modulation of transmitter release (Coggan, Paysan, Conroy and Berg, 1997).

The concept of synaptic integration refers to the fact that neurons must coordinate a response by integrating diverse sets of inputs and decide whether or not a response will be generated. In the case where neurotransmitter receptor activation at the synapse causes a localized membrane depolarization, voltage-gated Na^+ channels will respond to

membrane depolarization by opening rapidly, resulting in an inward Na^+ current and subsequent membrane depolarization.

Two types of glial cells are involved in the rapid propagation of action potentials in neurons. The oligodendrocytes in the brain and the Schwann cells in the peripheral nervous system insulate axons by wrapping their membrane process concentrically around the axon in a tight spiral, forming a myelin sheath. The sheath is interrupted every 1-2 mm by bare patches of 2-5 μm in length called nodes of Ranvier where the density of Na^+ channels is high. This high density of Na^+ channels generates an intense depolarizing inward Na^+ current. Myelination increases the conduction velocity in the axons since the action potential spreads quite rapidly between nodes due to the low capacitance of the myelin sheath. The action potential slows down as it crosses the high-capacitance region of each bare node. Consequently, as the action potential moves down the axon, it seems to jump from node to node, a process called saltatory conduction.

When the action potential reaches the nerve terminal, membrane depolarization induces the influx of Ca^{2+} by activating voltage-gated Ca^{2+} channels. The increase in intracellular Ca^{2+} activates a protein cascade that leads to membrane fusion of synaptic vesicles with the presynaptic membrane and exocytosis of neurotransmitter molecules in the synaptic cleft (figure 1.2). Following release, the neurotransmitters diffuse across the synaptic cleft and reach the post-synaptic membrane where they bind to neurotransmitter receptors.

Figure 1.2 Schematic diagram of a chemical synapse showing the nerve terminal, the post-synaptic cell and sequence of events involved in synaptic transmission. From Kandel et al., 1995.

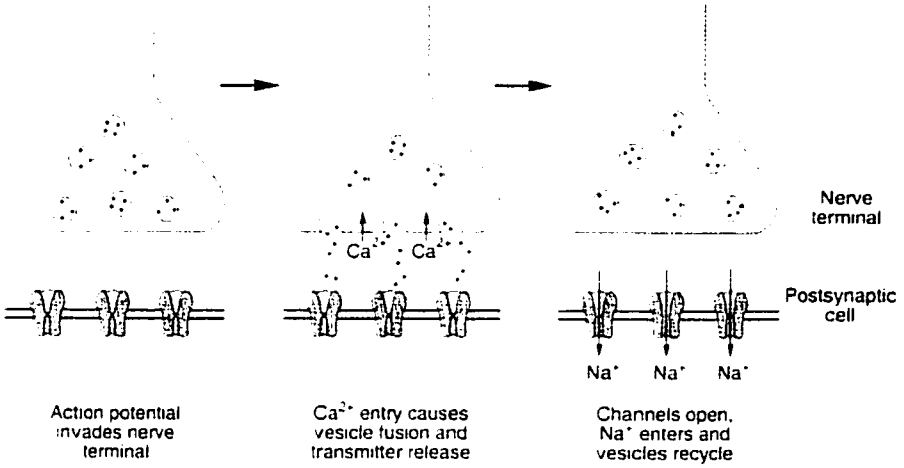
Nerve terminal
Postsynaptic cell
Ca2+
Ca2+
Na+
Na+
Na+
Action potential invades nerve terminal
Ca2+ entry causes vesicle fusion and transmitter release
Channels open, Na+ enters and vesicles recycle

2. The complexity of neurotransmission and cognition

Although our understanding of the various components of the brain has improved significantly in the last 20 years, the question remains: "How are the cognitive functions generated?" The previous sections presented some of the important aspects of neurotransmission, but in a simplistic fashion. The brain is in fact an extremely complex network of billions of neurons and connections. Synapses exist usually between nerve terminals and dendrites, however connections are also possible between nerve terminals and somas and axons. In addition, in recurrent collaterals, a neuron sends a portion of its axon back to synapse its own cell body, thus providing a self-regulatory control between neural circuits. Consequently, the organization of neurons and connections in the brain gives rise to a very complex architecture. Moreover, the existence of numerous neurotransmitters acting on distinct neurotransmitter receptors complicates the picture.

Behavior is generated by sensory inputs, intermediate processing and motor outputs and involves different groups of neurons organized in parallel. Parallel processing refers to such architecture of the brain involving several pathways to convey similar information and makes the brain a reliable system. We know that specific aspects of information processing such as sensory perceptions and motor commands are restricted to particular regions of the brain. The neurons that make up these representations have similar electric properties and the difference in their functions is due to the type of connection they make. The complexity of the connections between the various neuronal networks, not the neurons themselves, makes complex information processing possible. These connections, established during development of the brain, can

be modified later through learning. Consequently, since the types of neurotransmitters secreted by presynaptic neurons and the types of neurotransmitter receptors in the postsynaptic membrane are responsible for modulation of synaptic transmission, these components therefore appear to play a crucial role in brain function. Understanding signal transduction at chemical synapses and the role of neurotransmitter receptors in synaptic transmission is essential in order to better define both normal and abnormal brain function.

A variety of pharmacological agents can modulate the function of neurotransmitter receptors, for example, benzodiazepines (tranquilizers) potentiate the inhibitory action of certain GABA receptor species. The elucidation of the effect of pharmacological agents on neurotransmitter function might eventually support the design of new therapeutic drugs in the treatment of various disorders of the nervous system such as epilepsy, schizophrenia, Alzheimer's disease and mood disorders (Léna and Changeux, 1997). Toward the achievement of this objective, the focus of this thesis is the study of one ligand-gated ion channel: the nicotinic acetylcholine receptor isolated from the electric fish *Torpedo californica*.

3. Ligand-gated ion channels

Ligand-gated ion channels are integral membrane proteins that respond to ligand binding by directly opening an ion channel. They are separated into three genetic families, the acetylcholine, glutamate and ATP families, according to sequence homology. Members of the families are presented in table 1.1 along with their principal

Table 1.1 Members of the three genetic families of ligand-gated ion channels and their principal ionic selectivity. Modified from Conley, 1996.

Family	Ligand	Ligand-gated ion channel subtype	Principal ionic selectivities
Acetylcholine	Acetylcholine (e)	nAChR (neuronal)	Na^+, K^+, Ca^{2+}
	Acetylcholine (e)	nAChR (muscle)	Na^+, K^+, Ca^{2+}
	5-hydroxytryptamine (e)	5-HT_3	Na^+, K^+
	γ-aminobutyric acid (i)	$GABA_A$	Cl^-, HCO_3^-
	Glycine (i)	GlyR	Cl^-, HCO_3^-
Glutamate	Glutamate (e)	NMDA	Na^+, K^+, Ca^{2+}
	Glutamate (e)	non-NMDA	Na^+, K^+, (Ca^{2+})
ATP	ATP (e)	P_{2x}	Ca^{2+}, Na^+, Mg^{2+}

ionic selectivities (Conley, 1996). As indicated in the table, most ligand-gated ion channels are excitatory.

The two types of nAChR, i.e. the muscle-type nAChR, and the neuronal-type nAChR are located at the neuromuscular junction and neuronal synapses, respectively. They are part of a superfamily of ligand-gated ion channels including the serotonin (5-HT_3), $GABA_A$ and glycine receptors. These ligand-gated ion channels exhibit a high sequence homology especially in the transmembrane domain and in the ligand binding site and likely share a similar mechanism of action despite a distinct pharmacology and ionic selectivity. The muscle-type nAChR is the best characterized ligand-gated ion channel due to extensive studies on a highly homologous nAChR isolated from the electric organ of the electric fish, *Torpedo californica*. Since *Torpedo*-nAChR can be purified in large quantities, it serves as a model for the elucidation of the mechanism of action of ligand-gated ion channels in the acetylcholine superfamily.

4. The nicotinic acetylcholine receptor

Both muscle and neuronal nACh are heteropentamers made of five homologous subunits. Muscle-nAChR and *Torpedo*-nAChR are composed of four types of subunits (α,β,γ and δ) while the neuronal-nAChR are thought to be composed of only two types of subunits, the α-type subunits (7 distinct subunits exist) and β-type subunits (3 distinct subunits exist). Both muscle and *Torpedo* nAChR appear as one combination, ($\alpha_2\beta\gamma\delta$), whereas, the neuronal nAChR forms a wide variety of functional heteropentamers (for example, $\alpha 2_2\beta 2_3$ or $\alpha 1\alpha 5\beta 2_3$) (Changeux, Bertrand, Corringer, Dehaene, Edelstein, Léna,

Le Novère, Marubio, Picciotto and Zoli, 1998; Lindstrom, Anand, Gerzanich, Peng, Wang and Wells, 1996). The various combinations of neuronal-nAChR are located at strategic positions in the brain.

Despite an average 18% sequence identity between the muscle-type and the neuronal-type nAChR (Hucho, Tsetlin and Machold, 1996), their ionic selectivity and pharmacology are distinct (Changeux et al., 1998). In general, they interact with some of the same ligands (nicotine, acetylcholine...) but with different binding affinities and some ligands bind specifically to the muscle-type or to the neuronal-type (Galzi and Changeux, 1992). Similarly, the relative permeabilities for Ca^{2+} and Na^{+} vary with the nature and combination of subunits forming the receptor. For example, the homopentamers $\alpha 7$ and $\alpha 8$ are 15 times more permeable to Ca^{2+} than to Na^{+}. In contrast, the muscle-type nAChR is 5 times more permeable to Na^{+} than to Ca^{2+} (Changeux et al., 1998). The functional difference between the various subtypes of the nAChR is explained by different subunit combinations.

4.1 The conformational states of the nAChR

The nAChR is known to exist in at least three different conformations characterized by the state of the channel and the binding affinity for agonists (fig. 1.3) (Adams, 1981). In the absence of agonist, the channel alternates between two closed channel conformations: the low agonist binding affinity resting state (~80% of the time; dissociation constant (K_d) 800 nM for acetylcholine) and the high affinity desensitized state (~20% of the time; K_d 2 nM for acetylcholine) (Neubig, Boyd and Cohen, 1982).

Upon binding two molecules of agonist, the nAChR is rapidly converted into an active or open-channel state where the energy released by agonist binding leads to channel opening. Upon prolonged exposure to agonist, the nAChR is converted into a non-functional desensitized state where an increase in binding affinity is observed.

The role of desensitization in the nAChR function is not clear, however, it has been suggested that desensitization of neuronal nAChR could modulate the efficiency of synaptic transmission and possibly be involved in brain functions such as memory and learning (Changeux, 1993).

4.11 Modulators of the nAChR function

Pharmacological studies have defined four classes of effectors of the nAChR. 1) The agonists like acetylcholine and carbamylcholine which activate ion flux through the channel. 2) The partial agonists like nicotine which behave as weak agonists and antagonists. 3) The competitive antagonists like snake venom α-toxins or curare which bind at the agonist binding sites but inhibit ion flux. 4) The non-competitive antagonists which block ion flux by binding to either a high affinity site located within the ion channel or multiple low affinity sites located at the interface between membrane lipids and the nAChR (Arias, 1996).

The conformational equilibrium of the nAChR can be modified in the presence of agonists and through various allosteric effectors. Prolonged exposure to agonists and to non-competitive antagonists converts the nAChR into the desensitized state.

Figure 1.3 Schematic diagram of three distinct conformations of the nAChR. In absence of agonist, the channel is closed and the nAChR is in the resting state; upon agonist binding the nAChR, is activated and opens transiently and upon prolonged exposure to agonists, the nAChR is converted to a desensitized state where the channel is closed and the affinity for the agonist is increased. From Changeux, 1993.

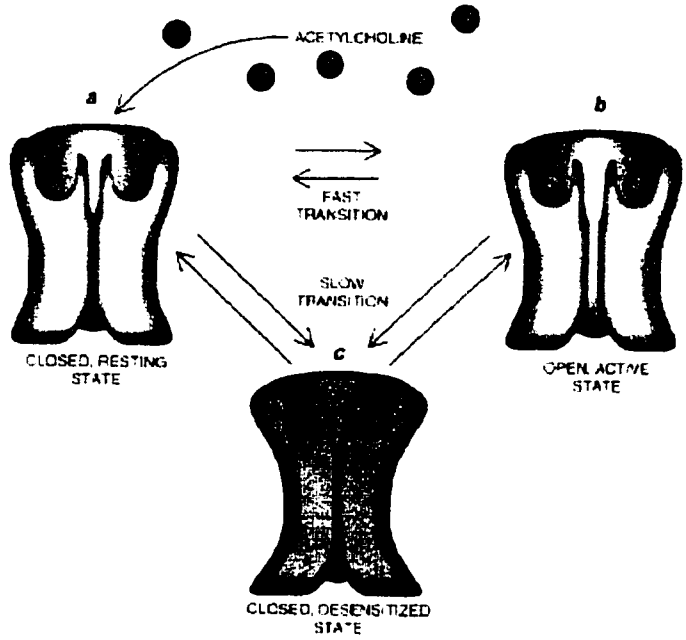
ACETYLCHOLINE
a
b
FAST
TRANSITION
SLOW
TRANSITION
c
CLOSED, RESTING
STATE
OPEN, ACTIVE
STATE
CLOSED, DESENSITIZED
STATE

However, *in vivo*, the acetylcholine released at the synapse level is rapidly hydrolyzed by the enzyme acetylcholinesterase, so that the nAChR will not be exposed to neurotransmitter for long enough to induce desensitization (Stroud, McCarthy and Shuster, 1990). Most neurotransmitter receptors have been shown to be regulated by protein phosphorylation or to contain consensus sequences for phosphorylation by protein kinases. For instance, several phosphorylation sites have been identified in the intracellular domain of the nAChR (Yee and Huganir, 1987; Wagner, Edson, Heginbotham, Post, Huganir and Czernik, 1991). Protein phosphorylation in the nAChR was shown to induce receptor clustering at synaptic sites and to regulate its assembly (Swope, Moss, Blackstone and Huganir, 1992). It was also shown to increase the rate of desensitization (Huganir, Delcourt, Greengard and Hess, 1986) which could play an important role in modulation of synaptic transmission.

Ca^{2+} ions, which exhibit a high permeation through the neuronal nAChR channel, also act as a positive effector of neuronal nAChR. It was shown that the binding of Ca^{2+} to specific external regulatory sites increased the opening frequency of the nAChR channel (Changeux et al., 1998) and the rate of desensitization (Ochoa, Chattopadhyay and McNamee, 1989).

In addition, upon reconstitution of the nAChR into egg phosphatidylcholine (EPC) membranes lacking cholesterol and anionic phospholipids, the nAChR may be stabilized in a desensitized like state (McCarthy and Moore, 1992; Fong and McNamee, 1986). In contrast, recent studies proposed that the nAChR in EPC is stabilized in a resting like conformation (Rankin, Addona, Kloczewiak, Bugg and Miller, 1997; Raines and Krishnan, 1998).

4.2 Structural features of the nAChR

In order to elucidate the mechanism of ligand binding, coupling between ligand binding and channel opening, channel gating and desensitization in the nAChR, its three-dimensional structure must be resolved. The structure of the nAChR has not been determined yet at a high resolution either by x-ray crystallography due to the difficulty in obtaining suitable protein crystals or by NMR spectroscopy due to its large dimension. The following sections present the actual knowledge regarding the various levels of the nAChR's structure.

4.21 Primary structure and transmembrane topology models

In the early 80s, the primary sequence of the nAChR (muscle-type) was determined from a few species including Torpedo (Noda, Takahashi, Tanabe, Toyosato, Furutani, Hirose, Asai, Inayama, Miyata and Numa, 1982; Noda, Takahashi, Tanabe, Toyosato, Kikyotani, Furutani, Hirose, Takashima, Inayama, Miyata and Numa, 1983; Claudio, Ballivet, Patrick and Heinemann, 1983), human, calf, bovine, rat and chicken and the percentage sequence identity between these species is above 80% (Hucho et al., 1996). It was determined that the *Torpedo* nAChR is composed of four homologous subunits with the following stoichiometry: $\alpha_2\beta\gamma\delta$. The four polypeptide chains have the following lengths: α: 437, β: 469, γ: 489 and δ: 501 amino acids. In human, the γ subunit is embryonic and replaced postnatally by an ε subunit. Roughly 20% of the nAChR's mass is composed of carbohydrates mainly of the high-mannose type and some sialylated

complex type. The N-glycosylation sites are located on all subunits with a higher proportion on the γ and δ subunits. Consequently, the apparent molecular weights of the subunits on SDS-PAGE are respectively 40, 48, 60 and 65 kDa for the α, β, γ and δ subunits (Hucho et al., 1996) and the molecular weight of the complex is roughly 300 kDa. These polypeptides are the product of different genes and in some cases localized on different chromosomes. They share on average 35% sequence homology and 18% sequence identity (Hucho et al., 1996).

Transmembrane topology models of the nAChR were developed following the publication of the primary sequence. The model shown in figure 1.4 includes a large extramembranous domain, four putative transmembrane α-helices and a small intracellular domain. This model, referred to as the four helix model, is based on extensive experimental evidence and assumes that the four subunits are folded in a similar way according to their sequence homology (Karlin, 1991). Initial hydrophobicity analysis of the nAChR's primary structure identified four stretches of ~19-25 hydrophobic amino acids which were attributed to transmembrane α-helical segments and were named M1 to M4 (Claudio et al., 1983). Secondary structure prediction of transmembrane segments in membrane proteins by hydrophobicity analyses is based on a correlation between hydrophobic stretches of roughly 20 amino acids residues in length and α-helical transmembrane segments identified in membrane proteins such as the photosynthetic reaction center and bacteriorhodopsin (White, 1994). Note that porins, which are made of transmembrane β-barrels do not contain such long hydrophobic segments (Cowan, Schrimer, Rummel, Steiert, Ghosh, Pauptit, Jansonius and Rosenbusch, 1992). Based on the fact that the signal sequence for the nAChR is cleaved

Figure 1.4 Currently accepted transmembrane topology model of the nAChR. Each small cylinders denoted M1 to M4 represents one putative transmembrane segments while the big cylinders denoted by a Greek letter correspond to one subunit. The inset shows the pattern of assembly of the five subunits (see text). From Changeux, 1993.

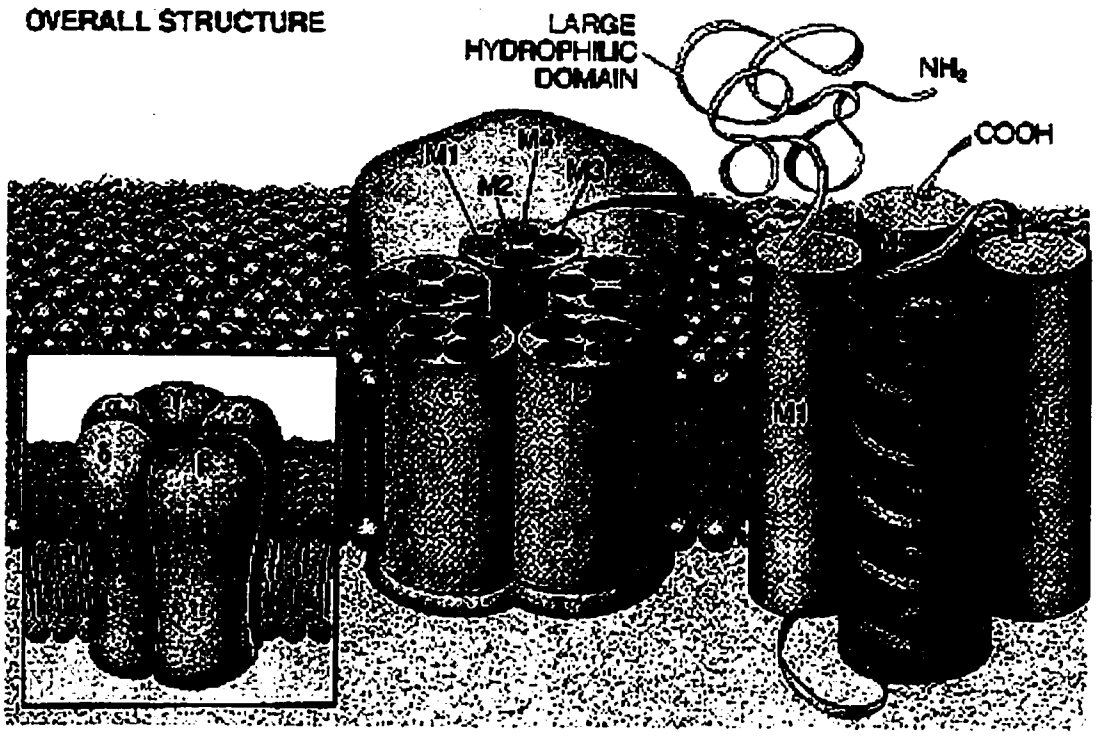
OVERALL STRUCTURE
LARGE
HYDROPHILIC
DOMAIN
NH_2
COOH
M1
M2
M3
M4
M1

(Sabatini, Kreibich, Morimoto and Adesnik, 1982 and Anderson, Walter and Blobel, 1982) and glycosylation sites identified at α-Asn141, δ-Asn70, δ-Asn143 and δ-Asn208 are located extracellularly according to the model (Hucho et al., 1996), the N-terminus is likely extracellular. The C-terminus is also probably extracellular due to the accessibility of δCys500 to sulphydryl reagents (Czajkowski, DiPaola, Bodkin, Salazar-Jimenez, Holtzman and Karlin, 1989; DiPaola, Czajkowski and Karlin, 1989). These two observations support an even number of transmembrane segments. All the phosphorylation sites established up to now are located in the intracellular loop between the predicted M3 and M4 transmembrane segments of each subunit (Yee and Huganir, 1987; Wagner et al., 1991). Chavez and Hall, 1992, have constructed fusion proteins of the α and δ subunits of the nAChR inserted in microsomes and containing a fragment of prolactin inserted after each of the postulated transmembrane segments to test the validity of the model. The location of the prolactin fragments was determined by proteolysis while assuming that intramicrosome (equivalent to the extracellular domain) peptides bonds are protected from cleavage. Only prolactin fusion proteins with the prolactin domain fused after M2 and M4 were recovered, suggesting their intramicrosome location which is topologically equivalent to the extracellular space. These results provide further support for the transmembrane location of the M1-M4 segments in the orientation proposed in the model.

Chemical labelling experiments indicate that M1, M3 and M4 are exposed to the hydrophobic environment of the lipid bilayer (Giraudat, Montecucco, Bisson and Changeux, 1985; Blanton and Cohen, 1992 and 1994). However, the transmembrane segment M2 is not lipid exposed and lines the ion channel pore (see below).

4.22 Quaternary structure

The quaternary structure of the nAChR was revealed by electron microscopy first at a resolution of 25 Å (Brisson and Unwin, 1985), at 18 Å resolution (Unwin, Toyoshima and Kubalek, 1988), at 9 Å resolution (Unwin, 1993 and 1995) and very recently at 4.6 Å resolution (Miyazawa, Fujiyoshi, Stowell and Unwin, 1999). According to the electron microscopy images, from the synaptic side, the nAChR appears to be ~65 Å in diameter with a central 25 Å wide depression and five peaks of electron density surrounding the central pore assigned to the five subunits. The four subunits of the nAChR are organized as a barrel surrounding the central ion pore, however the precise clockwise arrangement is still controversial. By photolabeling studies with α-neurotoxins, Machold, Weise, Utkin, Tsetlin and Hucho (1995) have suggested an αγαδβ arrangement viewed from the synaptic cleft. In contrast, recently, Miyazawa et al. (1999) proposed an αβαδγ arrangement. The nAChR from *Torpedo* occurs predominantly as a dimer in post-synaptic neuronal membranes where two nAChR molecules are linked through a disulphide bridge between the δ subunits. The role of the dimerization in the nAChR is unclear since the muscle-type nAChR occurs as monomers and that there appears to be no change in binding affinity or channel properties between the monomeric and the dimeric form.

Figure 1.5 Model of subunit assembly in the nAChR (see text). Each subunit is identified by a Greek letter. One the right, a cross section of the nAChR showing the two ligand binding sites on the α-subunits and the central ion channel. From Changeux, 1993.

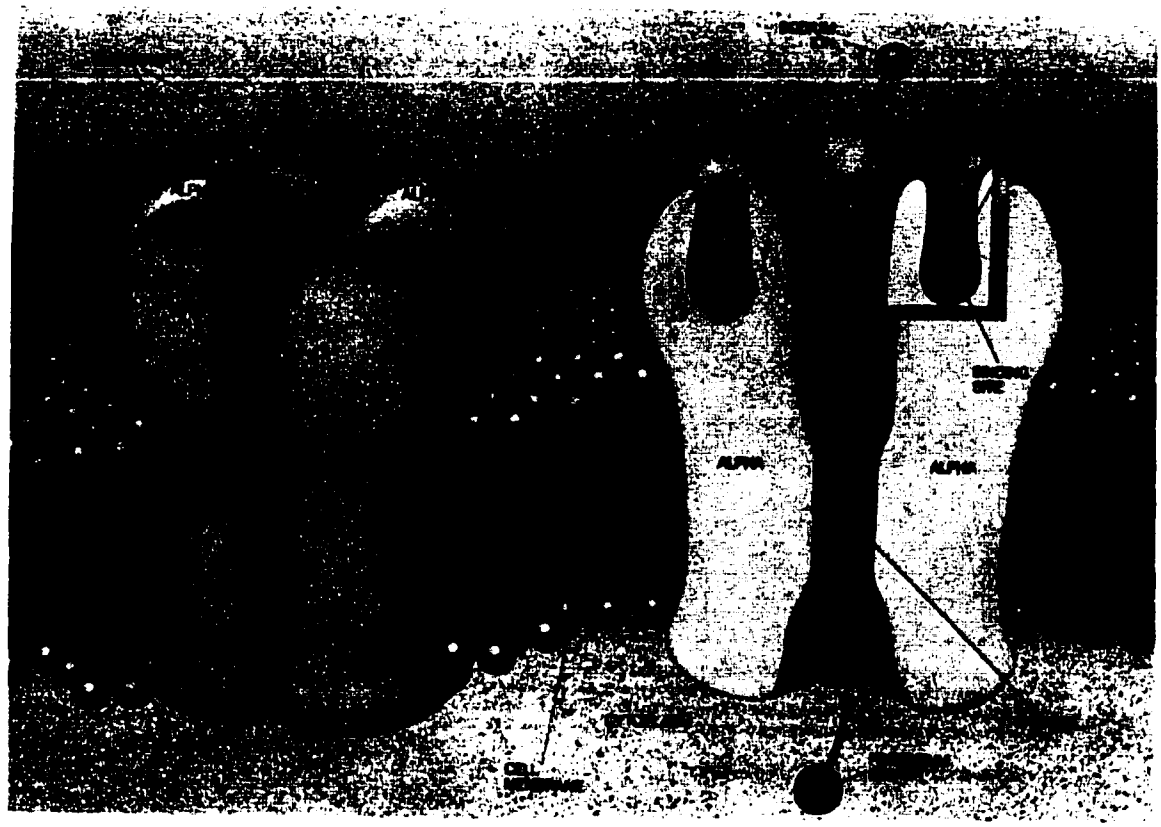

4.23 Secondary structure

Knowledge of the secondary structure of large integral membrane proteins can provide important information for the development of structural models. This is particularly true for the nAChR since high resolution structural information is not available. In 1992, when this research project started, the secondary structure of the nAChR had been studied using numerous spectroscopic techniques such as circular dichroism (CD) (Mielke and Wallace, 1988; Wu, Sun and Yang, 1990), Raman spectroscopy (Yager, Chang, Williams, Dalziel, 1984) and Fourier Transform infrared (FTIR) spectroscopy (Fong and McNamee, 1987). The proportion of the secondary structure components estimated in these studies varied significantly, for instance the percentage of α-helices ranged from 20 to 40% (table 1.2). This variation could not be explained by a difference in the purity of the nAChR samples since in all cases the nAChR was purified through an affinity column which removes contaminating proteins. However, the reliability of the study by Yager et al. (1984) is questionable due to the fact that the nAChR was reconstituted into non-functional dielaidyl phosphatidylcholine (DEPC) membranes. The FTIR study of Fong and McNamee (1987) focused on weak skeletal stretching vibrations for which the correlation with secondary structure is not well established. These vibrations are located in a region of the infrared spectrum which overlaps with lipid vibrations. A low proportion of α-helices in the nAChR (~20%) is not sufficient to account for four transmembrane helices per subunit and extramembraneous helices. Consequently, it was suggested that the transmembrane domain of the nAChR could contain β-sheets (Mielke and Wallace, 1993).

Table 1.2 Secondary structure estimates of the nAChR published before 1991 from CD, Raman and FTIR spectroscopy.

Reference	Technique	α-helix (%)	β-sheets (%)	β-turns (%)	unordered structures (%)	Type of sample
Mielke and Wallace, 1988	CD	23	43	6	28	Affinity-purified
Wu et al., 1990	CD	40	20	10	30	Affinity-purified
Yager et al., 1984	Raman	38	33	15	10	Affinity-purified
Fong and McNamee, 1987	FTIR	20	24			Affinity-purified

Early in this research project, we collected preliminary data on the nAChR secondary structure which were suggestive of a much higher proportion of α-helices. These results and their implication in transmembrane topology models of the nAChR drove us to further investigate the secondary structure of the nAChR. In the following years, additional secondary structure analyses of the nAChR were published and the results are presented in table 1.3. Again, the proportion of α-helices varies significantly, from 14 to 48%. These discrepancies are partially explained by differences in purity. Two of these studies used nAChR-rich membranes which contain a significant amount of non-nAChR material (Naumann, Schultz, Görne-Tschelnokow, Hucho, 1993; Aslanian et al., 1993). In addition, the study of Butler and McNamee (1993) was based on low quality FTIR spectra.

Moreover, several rods of electron density at 9 Å resolution on the nAChR's surface were interpreted as α-helices but since the protein interior was relatively featureless, it was suggested that the secondary structure of the nAChR would be along the estimations of Mielke and Wallace, 1988, with a majority of β-sheets (Unwin, 1993). Very recently, based on a structure prediction algorithm, Le Novere, Corringer and Changeux (1999) predicted roughly 24% of α-helices in the nAChR.

Table 1.2 Secondary structure estimates of the nAChR published after 1991 from CD, Raman and FTIR spectroscopy.

Reference	Technique	α-helix (%)	β-sheets (%)	β-turns (%)	unordered structures (%)	Type of sample
Butler and McNamee, 1993	FTIR	14 ($^1H_20$) 19 ($^2H_20$)	37 ($^1H_20$) 42 ($^2H_20$)	29 ($^1H_20$) 24 ($^2H_20$)	20 ($^1H_20$) 15 ($^2H_20$)	Affinity-purified
Naumann et al., 1993	FTIR	32-33	36-43	14-24	18-19	nAChR-rich membranes
Castrasana et al., 1992	FTIR	43	48	0	0	Affinity-purified
Aslanian et al., 1993	Raman	47	25	18	11	nAChR-rich membranes
West et al., 1997	CD (spectra of Mielke and Wallace, 1988	48	26	13	12	Affinity-purified

4.24 The secondary structure of the channel forming transmembrane segments

The nAChR's channel is an non-selective cation channel which increases the membrane's permeability of Na^+ and K^+ ions by ~10 000 fold for ~1 ms upon agonist binding. The nAChR has developed an extremely efficient mechanism in order to maintain the physiological membrane barrier of the neuron in absence of agonist and allow high current of cations in the presence of agonist. Recently, insights in the mechanism of channel gating of the potassium channel emerged based on the crystal structure at 3.4 Å resolution (Doyle, Morais Cabral, Pfuetzner, Kuo, Gulbis, Cohen, Chait and MacKinnon, 1998). In contrast, the mechanism by which the nAChR facilitates the passage of charged atoms across the hydrophobic bilayer of the membrane in such an efficient way is unknown.

Electron microscopy suggested a five-fold axis of symmetry for the transmembrane domain of the nAChR. The overall structure of the ion channel appears funnel shaped since from the side, the transmembrane domain appears wider at the cytoplasmic side and thinner at the synaptic side (Unwin, 1993). More precisely, the entrance of the channel is roughly 2.0-2.5 nm in diameter (Unwin, 1993), the non-competitive channel blocker site appears 1.15 nm wide according to the size of triphenylphosphonium (TPMP+) determined by x-ray crystallography (McPhail, Semenink and Chestnut, 1971). The narrowest part was evaluated to be at least 0.64 nm according to the size of the largest permeating cation (Huang, Catterall and Ehrenstein, 1978).

The four transmembrane segments per subunit in the transmembrane domain of the nAChR have all been suggested to be part of the ion channel and involved in channel gating (muscle-nAChR M1: Akabas and Karlin, 1995; Wilson and Karlin, 1998: muscle-nAChR M2; Labarca, Nowak, Zhang, Tang, Deshpande and Lester, 1995; Wilson and Karlin, 1998 and Filatov and White, 1995; neuronal-nAChR M3: Campos-Caro, Rovira, Vicente-Agulló, Ballesta, Sala, Criado and Sala, 1997; *Torpedo*-nAChR M4: Lee, Li, Lasalde, Rojas, McNamee, Ortiz-Miranda and Pappone, 1994 and Lasalde, Tamamizu, Butler, Vibat, Hung and McNamee, 1996). However, functional analysis suggested that the M4 transmembrane segment could be replaced by foreign transmembrane sequences without loss of channel activity (Tobimatsu, Fujita, Fukuda, Tanaka, Mori, Konno, Mishina and Numa, 1987).

Several groups have identified the M2 segments as lining the lumen of the channel (Hucho et al, 1986; Giraudat, 1987; Leonard, Labarca, Charnet, Davidson and Lester, 1988; Revah et al., 1990; Unwin, 1993; Akabas et al., 1994). Electron microscopy at 9Å reported a kink in the M2 segments near the middle of the bilayer where it comes closest to the axis of the pore and tilts radially by ~12° toward the extracellular side and by ~45° toward the intracellular side (Unwin, 1995). Solid-state NMR studies of M2 peptides suggest a slightly curved structure for the M2 segments, tilted 12° from the lipid bilayer without evidence of a kink (Opella, Marassi, Gesell, Valente, Kim, Oblatt-Montal and Montal, 1999).

The secondary structure of the hydrophobic stretches identified by hydrophobicity plots and assigned to transmembrane α-helices has been the subject of considerable controversy questioning the validity of the four helix model (Hucho, Görne-Tschelnokow

and Stecker, 1994; Ortells and Lunt, 1996). Knowledge of the secondary structure of the transmembrane segments in the nAChR is important in the development of models of channel gating and desensitization since these segments form the ion channel. Several investigations attempted to determine the secondary structure of the transmembrane segments in the nAChR, and at the present the majority support the α-helical nature of the five M2 channel lining segments. More precisely, Hucho, Oberthür and Lottspeich (1986), Giraudat et al. (1987) and Revah et al. (1990) by photolabeling with non-competitive channel blockers identified residues in contact with the lumen of the channel, all located in the M2 segments. In addition, the pattern of labeling was in an α-helical manner. In the electron micrographs at 9Å resolution, Unwin (1993) reported 5 clear rods of electron density assigned to one M2 transmembrane helix per subunit as lining the channel. Site-directed mutagenesis and chemical labeling identified several residues in the M2s as lining the pore and organized in α-helices according to the pattern of labeling (Akabas et al., 1994). NMR spectroscopy also supports the α-helical nature of the M2 transmembrane segments (Bechinger, Kim, Chirlian, Gesell, Neumann, Montal, Tomich, Zasloff, Opella and 1991; Opella, Marassi, Gesell, Valente, Kim, Oblatt-Montal and Montal, 1999).

In contrast, the secondary structure of the M1, M3 and M4 is controversial. Both M3 and M4 exhibit an α-helical exposure to the lipid bilayer as monitored using photoactivatable hydrophobic probes, while the labeling of M1 correlates with a slightly distorted α-helix, due to the presence of a proline residue (Blanton and Cohen, 1994 and 1996). Site-directed mutagenesis experiments also support an irregular structure for the M1 segment which is partially exposed to the channel lumen (Akabas and Karlin, 1995).

Recent NMR evidence support the α-helical secondary structure of a synthetic peptide corresponding to the M3 transmembrane segment in the nAChR (Lugovskoy, Maslennikov, Utkin, Tsetlin, Cohen and Arseniev, 1998).

Even though the great majority of crystallized membrane proteins display α-helical transmembrane segments, the presence of transmembrane β-strands was proposed in the nAChR. Mielke and Wallace (1988) using CD, identified a relatively low amount (20%) of α-helices, insufficient to account for both transmembrane and extramembraneous helices. Note that the CD spectra of Meilke and Wallace were recently re-interpreted as reflecting a much higher α-helical content (West, Bjorkman, Dougherty and Lester, 1997). In the electron micrographs, Unwin (1993) observed a diffuse pattern of electron density in the periphery of the ion channel that could correspond to five or seven transmembrane β-strands. The presence of both α-helices and β-sheets in the transmembrane domain of the nAChR was also suggested based on FTIR spectra of proteolysed nAChR (to remove the extramembraneous domains) and molecular modeling studies (Görne-Tschelnokow, Stecker, Kaduk, Naumann and Hucho, 1994; Ortells and Lunt, 1996). Very recently, secondary structure predictions of the nAChR proposed an overall low amount of α-helices (24%) and the transmembrane domain was predicted to be a mixed α/β topology with a predominance of α-helices (Le Novere et al., 1999).

Modeling studies have constructed models of the nAChR's channel based on numerous experimental evidence. In the model by Tikhonov and Zhorov, 1998, the M2 helices are kinked and come in contact at the cytoplasmic side but diverge at the synaptic side. In addition, the model proposes a contribution to the pore of the N-termini of M1

segments based on experimental results from Akabas and Karlin, 1995. Ortells and Lunt, 1996 proposed a model of the nAChR by assuming a structural homology of the transmembrane domain from the nAChR with the heat-labile enterotoxin. The model proposes a central pore composed of slightly bent α-helical M2s with a majority of β-strands in the remaining transmembrane segments.

Non-competitive blockers such as chlorpromazine and triphenylmethyl-phosphonium which sterically block ion flux in the nAChR have been used to identify the amino acid residues in the channel involved in the binding. Chlorpromazine photolabels threonine, serine and leucine residues belonging to homologous domains of each M2 subunit within which they occupy a homologous position. These data support the notion that homologous regions from each subunit contribute to the formation of an ion channel located in the axis of quasi-symmetry of the receptor molecule (Galzi and Changeux, 1992). Consequently, models of the nAChR's ion channel were developed based on stratified rings of amino acid residues (fig.1.6).

Site-directed mutagenesis studies were conducted on the channel lining residues of the nAChR to determine their role in ionic selectivity, channel gating and desensitization. The nAChR is a non-selective cation channel and it was established that two rings of charged and polar residues located at the cytoplasmic end of M2 are responsible for the selectivity for monovalent cations. Moreover, two rings of residues have been involved in Ca^{2+} versus Na^{+} selectivity. Interestingly, three mutations with homologous residues from the glycine α1 subunit (anionic channel) were sufficient to convert the cationic selectivity of the neuronal α7 nAChR to anionic (Galzi et al., 1992).

Figure 1.6 Stratified organization of the ion channel in the nAChR showing the rings of residues thought to be involved in channel selectivity and gating. Also shown, the putative binding site of non-competitive antagonists. From Bertrand et al., 1993.

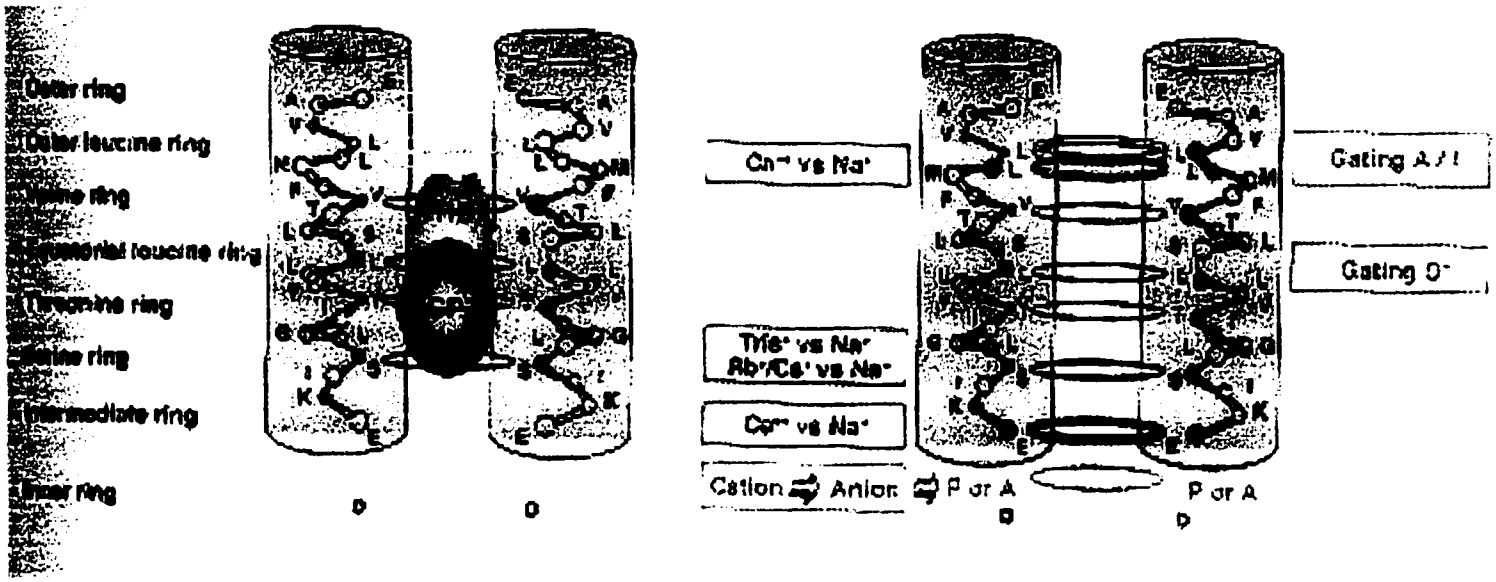
Outer ring
Outer leucine ring
Inner ring
Hydrophobic leucine ring
Threonine ring
Serine ring
Intermediate ring
Inner ring
D
D
Cn⁺⁺ vs Na⁺
Trie⁺ vs Na⁺
Rb⁺/Cs⁺ vs Na⁺
Ca⁺⁺ vs Na⁺
Cation ⇄ Anion ⇄ P or A
P or A
D
D
Gating A / I
Gating D⁻

These mutations included the insertion of an uncharged residue (proline and alanine) at the amino-terminal end of M2. This result suggests that the length of the segment linking M1 with M2 is a critical determinant of channel selectivity. Mutation of residues in the three rings of residues photolabeled by chlorpromazine (threonine, serine and leucine) increased the apparent affinity for acetylcholine and abolished desensitization. These results lead to the hypothesis that these three rings of residues are involved in channel gating (Bertrand, Galzi, Devillers-Thiéry, Bertrand and Changeux et al., 1993). Moreover, Miyazawa et al. (1999) observed a narrow strip of electron density bridging the pore close to the middle of the membrane. This electron density was assigned to the gate of the channel. However, Wilson and Karlin (1998), based on cysteine substitution experiments, proposed a more cytoplasmic location of the gate in the nAChR' channels.

5. Mechanism of nAChR desensitization

The detailed structural features responsible for the increase in binding affinity at the agonist binding site and the closed state of the ion channel in the desensitized state of the nAChR are poorly understood. An important alteration in the quaternary structure was reported in the desensitized state of the nAChR. In the presence of Carb, Unwin et al. (1988) and Unwin (1995) using cryoelectron microscopy at 18 and 9 Å resolution, respectively, observed a quaternary rearrangement of the nAChR involving predominantly the δ-subunit. The rearrangement consisted of a less than 10° apparent rotation of the axis of the subunits. An FTIR secondary structure study of the changes in conformation of the nAChR in the desensitized state have reported large rearrangements

in the protein. Castresana, Fernandez-Ballester, Fernandez, Laynez, Arrondo, Ferragut and Gonzalez-Ros (1992) reported FTIR spectra recorded in the presence of Carb which were interpreted as a decrease of β-pleated sheet from ~48% to ~24% concomitant with an increase in unordered structures. Similarly, important modifications in the nAChR's secondary structure were reported for the channel inactive conformation stabilized in absence of cholesterol and anionic phospholipids, which some studies suggest is analogous to the agonist induced desensitized state (McCarthy and Moore, 1992; Fong and McNamee, 1986). Fernandez-Ballester, Castresana, Fernandez, Arrondo, Ferragut and Gonzalez-Ros (1994) interpreted changes in the FTIR spectra of nAChR samples reconstituted in absence of cholesterol as a decrease of the proportion of both α-helices and β-sheets, from roughly 45% and 50%, respectively, in the presence of cholesterol down to 30% and 40%, respectively, in absence of cholesterol.

In contrast, Fernandez-Ballester, Castresana, Arrondo, Ferragut and Gonzalez-Ros (1992), Mielke and Wallace (1993) and McCarthy and Stroud (1989a) reported only negligible alterations in the secondary structure of the nAChR following agonist binding. The structural changes induced in the desensitized state appear to be very small and restricted at the amino acid level (Baenziger, Miller and Rothschild, 1993).

The amino acids involved in agonist binding in the nAChR were identified using the ligand and photoaffinity probe p(N,N)-dimethylaminobenzene diazonium fluoroborate (DDF) and were located in three loops of the α-subunits (Galzi, Revah, Bouet, Ménez, Goeldner, Hirth and Changeux, 1991). In the resting state, DDF interacts predominantly with amino acids in loop II. The same probe was used to investigate the conformational changes in the binding area upon desensitization. Stabilization in the

high affinity state by a non-competitive inhibitor resulted in an increase in the labeling of the α- and δ-subunit, a decrease in the labeling of the γ-subunit while no change in the β-subunit were observed. A differential labeling in two of the three loops of the α-subunits was detected, the labeling in loop III was unchanged whereas the labeling of loop I and II increased up to 6 fold upon desensitization. It was suggested that the higher affinity of ligands for the desensitized receptor would result from increased interactions with additional peptides, possibly including the three amino acid loops.

Changes in conformation of the transmembrane segments were reported upon carbamylcholine binding by photoincorporation of an uncharged nicotinic noncompetitive antagonist (3-(trifluoromethyl)-3-(m-[^{125}I]iodophenyl)diazirine ([^{125}I]TID)). The labeling pattern revealed a decrease in the level and stoichiometry of [^{125}I]TID in the subunit incorporation in the desensitized state (McCarthy and Stroud, 1989a). In absence of agonist, TID labels homologous aliphatic residues in the M2 segment of the β and δ subunits (βL-257, δL-265, βV-261 and δV-269). Upon agonist binding, the labeling decreases by ~90% and the distribution of labeled residues is broadened to include an homologous set of serine residues at the amino terminus of M2 (White and Cohen, 1992). Moreover, site-directed mutagenesis and labeling experiments revealed that the M1 transmembrane segment is exposed in the channel and that its exposure changes in the presence of agonist (Akabas and Karlin, 1995).

In contrast, Baenziger and Chew (1997) found by FTIR difference spectroscopy that desensitization involves mainly a structural change in solvent-accessible regions of the nAChR as opposed to the transmembrane domain. Finally, fluorescence spectroscopy experiments using eserine (putative agonist) support the notion that desensitization

involves conformational changes in the ligand binding site but not in the ion channel. Eserine binding through a distinct binding site than the neurotransmitter binding site induces channel opening even under preincubation with acetylcholine suggesting that the ion channel in the desensitized state is still activatable (Kuhlmann, Okonjo and Maelicke, 1991).

6. Rationale and objectives

The initial objective of this thesis was to better characterize the nature of the conformational changes in the desensitized state of the nAChR. The first goal, given the above noted controversial data, was to examine the magnitude of the conformational changes upon ligand and lipid induced desensitization. In the course of this study, it became evident first that simple questions regarding the nAChR secondary structure were still controversial. This knowledge is important for the development of structural models of the nAChR. Consequently, the secondary structure investigation of the nAChR was undertaken.

Second, it was also realized that I had tools to investigate the secondary structure of the transmembrane segments in the nAChR. As mentioned earlier, the secondary structure of the M2 transmembrane segments is likely α-helical. However, the secondary structure of the three remaining transmembrane segments per subunit in the nAChR is controversial but central in the development of models of channel gating. This important question became the major focus of the thesis.

Finally, I wanted to test the structural organization and more precisely, the tilt angle of the transmembrane α-helices in the nAChR. In addition, I wanted to investigate the involvement of the transmembrane segments in the desensitized state by probing any change in their tilt angle upon desensitization.

The results suggest a mixed α-β-type secondary structure in the nAChR with a majority of α-helices. The transmembrane segments appear all α-helical with an overall perpendicular orientation with respect to the membrane plane. Moreover, according to the results, the desensitized state of the nAChR is characterized by a lack of large conformational changes and no large change in the tilt angle of the transmembrane α-helices.

7. Organization of the thesis

The thesis starts with a general introduction to the complexity of neurotransmission and cognition, to ligand-gated ion channels and to the nicotinic acetylcholine receptor.

Chapter 2 presents the theory of Fourier transform infrared spectroscopy and the rationale for using this technique in the study of the nAChR.

Chapter 3 presents the secondary structure determination of the nAChR in both the active and inactive conformations. The results presented in Chapter 3 have been published in: Méthot, McCarthy and Baenziger (1993) and Méthot, Demers and Baenziger (1995).

In Chapter 4, the different strategies employed in an attempt to provide new information regarding the secondary structure of the transmembrane domain of the nAChR are presented. The data reported in chapter 4 have been published in the following articles: Baenziger and Méthot, 1995; Corbin, Méthot, Wang, Baenziger and Blanton, 1998; Méthot and Baenziger, 1998 and Méthot and Baenziger, 1999.

Chapter 5 presents the orientation of the transmembrane α-helices in the nAChR and the effect of carbamylcholine on their orientation. The results have been presented at conferences.

Finally Chapter 6 consists of a general discussion.

Chapter 2- Fourier Transform Infrared Spectroscopy

Proteins are central in the various functions of the cells such as metabolism, transport, communication, catalysis, etc. The diversity of protein function is linked to the diversity of protein structure. Each protein is uniquely designed into a particular conformation to perform its role. Moreover, understanding protein function depends on the ability to probe the unique structure adopted by the protein and how this structure allows a specific function. High-resolution techniques such as NMR spectroscopy and x-ray diffraction have been developed to investigate the three-dimensional structure of proteins at the atomic level. However, these techniques are difficult to apply to large integral membrane proteins such as the nAChR.

The use of infrared spectroscopy in the determination of protein structure originated from the work of Elliot and Ambrose (1950) who observed an empirical relationship between protein secondary structure and the infrared spectra. Due to the low signal-to-noise ratio of the infrared spectra, it was difficult to extract detailed structural information and the interest in the technique was low.

A major improvement in the infrared instrumentation was introduced with the design of spectrometers based on Michelson interferometers (Michelson, 1891) and the application of the fast Fourier transform algorithm (Cooley and Tukey, 1965) to data collection which allowed a substantial improvement in the signal-to-noise ratio. FTIR spectroscopy offers several advantages over other techniques such as its relatively low-cost, rapidity and easiness to record spectra, use of small amounts of protein (~50 μg) and importantly the unique possibility of studying integral membrane proteins in their

membrane environment. This chapter presents the theory of Fourier transform infrared (FTIR) spectroscopy and its application to protein structure investigations.

1. Vibrational spectroscopy

Spectroscopy is the study of the interaction of electromagnetic radiation (EMR) with matter. EMR can be described as either a particle, called a photon, or a wave with perpendicular electric and magnetic fields, which oscillate sinusoidally. The energy of the wave is,

$$E = \frac{hc}{\lambda} = h\nu \qquad (1.1)$$

where h is Planck's constant (6.626×10^{-34} Js), c the velocity of light in vacuum (2.997925×10^{10} cm/s), λ its wavelength (cm) and ν its frequency (Hz or s^{-1}).

Infrared spectroscopy is based on the measurement of vibrational transitions in molecules. When EMR is absorbed by a molecule, the energy of the incident radiation causes a mechanical transition between two vibrational energy levels. The frequency of the EMR absorbed corresponds to the vibrational frequencies of the bonds and results in an increase in the amplitude of the bonds vibration. When the molecule goes back to the ground state, the energy is dissipated as heat.

In order to absorb infrared radiation, there must be a change in dipole moment at least along one Cartesian coordinate of a bond. For example, two atoms with a difference in electronegativity will produce a dipole moment change upon bond vibration. In such a case, the vibration is categorized as infrared active.

To describe the energy of the radiation, wavelength (λ, in cm), frequency (ν, in Hz or s^{-1}) and wavenumber ($\bar{\nu}$, in cm^{-1}) are used. Wavenumbers are proportional to frequency according to,

$$\bar{\nu} = \frac{\nu}{c} = \frac{1}{\lambda} \tag{1.2}$$

where c is the velocity of the light. Wavenumbers are more conveniently used when referring to infrared spectra compared to the large frequency numbers. A plot of absorption in function of the wavenumber is called an absorption spectrum. The absorption (A) at a wavenumber is calculated according to Beer-Lambert's law,

$$A = \varepsilon c l \tag{1.3}$$

where ε is the molar absorption coefficient ($M^{-1}cm^{-1}$), c the molar concentration (M) and l length of optical path (cm).

1.1 Molecular vibrations

A normal mode of vibration is one in which each atom in a molecule executes a simple harmonic oscillation about its equilibrium position. All atoms move in phase with the same frequency and the center of gravity of the molecule does not move. Each atom in a molecule has three degrees of freedom of motion, in the x, y and z directions which are the Cartesian coordinates used to define its position. Therefore a molecule with N atoms will have a total of 3N degrees of freedom of motion for all atoms in the molecule.

However, when all the atoms move or rotate simultaneously in the same direction, x, y or z, no change in bond length or angle is taking place. Consequently, a non-linear molecule with N atoms has 3N-6 normal modes of vibration. A linear molecule has 3N-5 degrees of freedom since rotation about the molecular axis is not considered a degree of freedom, no displacements of nuclei are involved.

The bond vibrations in molecules are classified as "stretching" vibrations where there is a change in bond lengths and "bending" vibrations where there are changes in bond angles. In-plane bending vibrations include scissoring and rocking modes and out-of-plane bending include wagging and twisting modes (fig.2.1). The vibrational frequency depends on the atoms involved in the bond and is calculated according to classical mechanics using the following equation

$$\nu = \frac{1}{2\pi c}\sqrt{\frac{k}{Ma\,Mb/Ma + Mb}} \qquad (1.4)$$

where k is the force constant of the bond (N m^{-1}) and M_a and M_b the masses of the atoms and c the velocity of the light (m/s).

Figure 2.1 Types of normal vibration in a linear (A) and non-linear (B) triatomic molecule. Atomic displacements are represented by arrows (in the plane the page) and by + and – symbols (out of the plane of the page). From Arrondo et al., 1993.

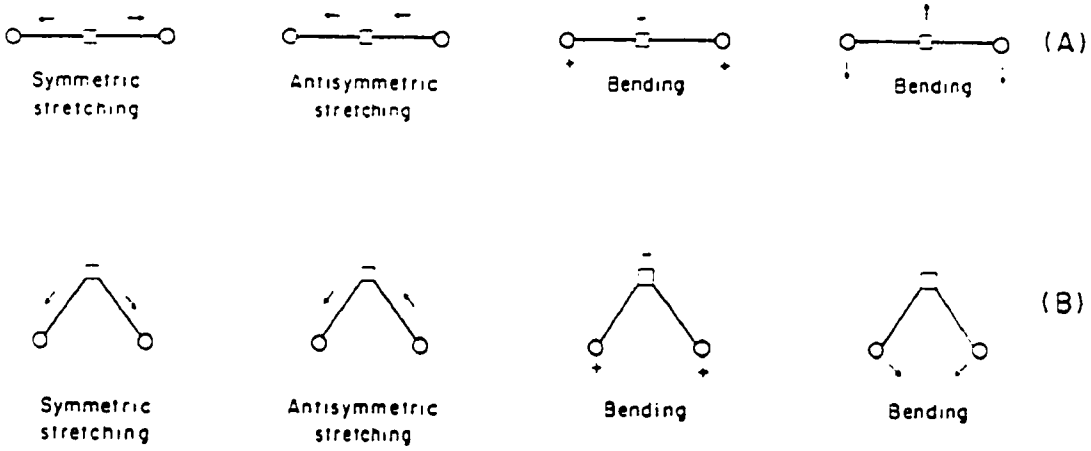
Symmetric stretching
Antisymmetric stretching
Bending
Bending
(A)
Symmetric stretching
Antisymmetric stretching
Bending
Bending
(B)

2. FTIR spectroscopy of proteins

An infrared spectrum is the result of the absorption of all bond vibrations in a molecule and is therefore very complex, especially for macromolecules such as proteins which contain thousands of atoms. However, functional groups (-OH, $-CH_2$, -C=O,..) in molecules, are known to absorb at a range of frequencies which allows their identification. In addition, the intrinsic vibrational frequency of chemical bonds can be affected by inter and intra molecular interactions such as hydrogen bonding. Such effects make FTIR spectroscopy a good tool to investigate protein structure.

To obtain insight into protein structure, one approach is to probe the backbone conformation of the protein, that is the conformation of peptide groups. The peptide groups in proteins give rise to infrared absorption bands in the infrared spectrum called amide bands, which are sensitive to protein conformation. The amide I band is a broad feature observed in the frequency region between 1600-1700 cm^{-1}. The amide I band represents primarily the carbonyl stretching vibration (about 80%) coupled to the in-plane NH bending and C-N stretching modes. The amide II band located at 1547 cm^{-1} represents N-H bending (60%) and C-N stretching modes (40%) (Miyazawa and Blout, 1961; Krimm and Bandekar, 1986). The amide I band is the most useful amide band for protein structural determination since it is highly sensitive to protein secondary structure. The pattern of hydrogen bonding of the carbonyl groups in the various secondary structures of proteins (α-helices, β-sheets, β-turns, unordered structures...) influences the frequencies of vibration and allows their identification according to the frequency of absorption of the amide I band.

Several approaches have been used to predict the frequency of vibration of secondary structure components in proteins. The pioneer empirical observations of Elliot and Embrose (1950) of a correlation between the infrared spectra and the secondary structure motifs identified by x-ray diffractions studies led to the identification of specific ranges of frequencies for both α-helices (1652-1657 cm^{-1}) and β-sheets (1628-1635cm^{-1}). Similar observations have been performed on proteins in both $^{1}H_2O$ and $^{2}H_2O$ (Susi, Timasheff and Stevens, 1967).

Normal mode calculations were conducted in order to determine the frequency of vibration of secondary structures based on interchain and intrachain interactions (Miyazawa and Blout, 1961) and force field treatments of amide vibrational modes (Krimm and Bandekar, 1986).

The empirical observations between protein structure and the infrared spectra, recently studied in both soluble and membrane proteins (Surewicz and Mantsch, 1988; Byler and Susi, 1986 and Goormaghtigh, Cabiaux and Ruysschaert, 1990) have been explained by a correlation between chain geometry, hydrogen bond strength, C=O electron group density and amide I frequencies for the various secondary structures (Jackson and Mantsch, 1991 and 1995). The backbone geometry of a protein influences the length and direction of the hydrogen bonds and in turn, the strength of hydrogen bonding between the peptide groups. This results in characteristic amide I frequencies for the peptidic carbonyls according to the strength of hydrogen bonding. The stronger the hydrogen bond, the lower the electron density in the C=O group, which leads to a lower vibrational frequency. Using this approach, Jackson and Manstch (1991 and 1995) predicted the frequency of absorption of protein secondary structures, in general. For

example, extended polypeptide chains in denatured proteins exhibit extremely strong intermolecular hydrogen bonds and would be expected to produce a low frequency of vibration for the peptide C=O groups. In fact, this is what is observed, denatured proteins absorb around 1610-1628 cm^{-1}. β-sheets extended in an anti-parallel fashion with internal hydrogen bonds form weaker hydrogen bonds compared to denatured extended chains and therefore, the C=O vibration absorbs at a higher frequency (observed 1630-1640 cm^{-1}). α-helices absorb at a further higher frequency (observed 1648-1658 cm^{-1}) due to the slightly longer length of the hydrogen bonds. Exceptions to this general relationship exist, for example, antiparallel β-sheets also give rise to a high-frequency absorption that arises from transition dipole coupling (Moore and Krimm, 1975).

A consensus emerges from these various approaches and ranges of frequencies of secondary structures components are presented in table 2.1 (Jackson and Mantsch, 1995). However, it should be kept in mind that despite a strong correlation between vibrational frequencies and protein structure, some proteins exhibit frequencies outside these ranges. For example, bacteriorhodopsin, which is known to form mainly transmembrane α-helices, exhibits an amide I band maximum at 1662 cm^{-1} (Lee, Hayward, Restall, and Chapman, 1985). Also, loop structures in trypsin were shown to absorb at 1655 cm^{-1} in ^2H_2O (Prestrelski, Byler and Liebman, 1991).

Table 2.1 Typical frequencies of absorption of secondary structure components in the amide I band of FTIR spectra. From Jackson and Mantsch, 1995.

Secondary structure	Amide I frequency (cm^{-1})
antiparallel β-sheet/aggregated strands	1675-1695
3_{10}-helix	1660-1670
α-helix	1648-1660
Unordered	1640-1648
β-sheet	1625-1640
Aggregated strands	1610-1628

3. Fourier transform infrared spectrometers

The amide I band of proteins is often broad due to the fact that the various secondary structures absorb at frequencies close to one another. This resulting overlap produces a composite band from which a rough and limited estimation of the secondary structure can be obtained. Numerous strategies have been applied to the analysis of infrared bands in order to increase the resolution and extract more information from the spectra such as Fourier self-deconvolution and derivative. Before presenting the various resolution-enhancement techniques, details of the FTIR instrumentation are presented.

The parts of FTIR spectrometers: the light source, sample compartment, interferometer and detector are illustrated in fig.2.2. The major advances in infrared spectroscopy are due to the introduction of Michelson interferometers in infrared spectrometers and fast-Fourier transformations in data processing. This allowed a significant improvement in the signal-to-noise ratio of the infrared spectra. Michelson interferometers are optical devices invented by and named after Albert Abraham Michelson (fig. 2.3). The purpose of an interferometer is to produce interference in the incident polychromatic radiation in order that all frequencies interact with the sample at the same time. The monochromator takes the incident beam of EMR, splits it into two and makes one beam of light travel a different distance than the other. The difference in distance traveled by these two beams of light is called the optical path difference. The Michelson interferometer consists of four arms. The first arm consists of a source of infrared light, the second arm consists of a fixed mirror, the third arm contains a moving mirror, and the fourth arm is open. At the intersection of the four arms is a beam splitter,

Figure 2.2 Simplified representation of an FTIR spectrometer and resulting FTIR spectrum. At the bottom right is shown the FTIR spectrometer which includes an infrared light source, a Michelson interferometer, the sample and a detector. In the top left insert is shown an interferogram and single-beam spectrum obtained after Fourier transformation. From Braiman and Rothschild, 1988.

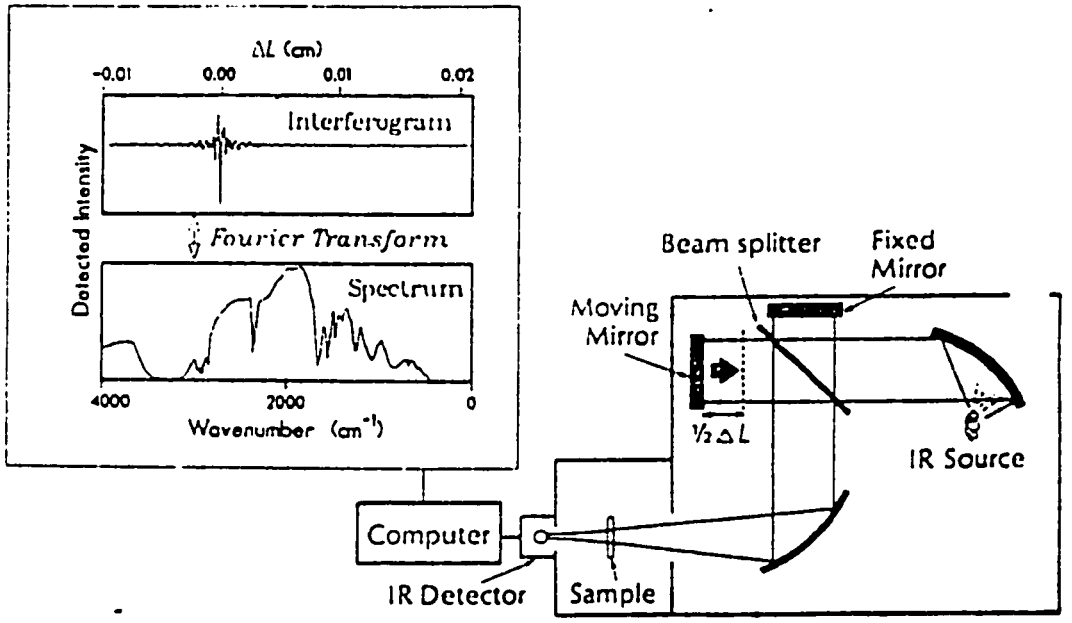
ΔL (cm)
-0.01
0.00
0.01
0.02
Interferogram
Detected Intensity
Fourier Transform
Spectrum
4000
2000
0
Wavenumber (cm⁻¹)
Beam splitter
Fixed Mirror
Moving Mirror
½ΔL
IR Source
Computer
IR Detector
Sample

Figure 2.3 Schematic representation of a Michelson interferometer. Inset: representation of the resultant intensity at different optical retardation with a monochromatic light as a source. From Arrondo et al., 1993.

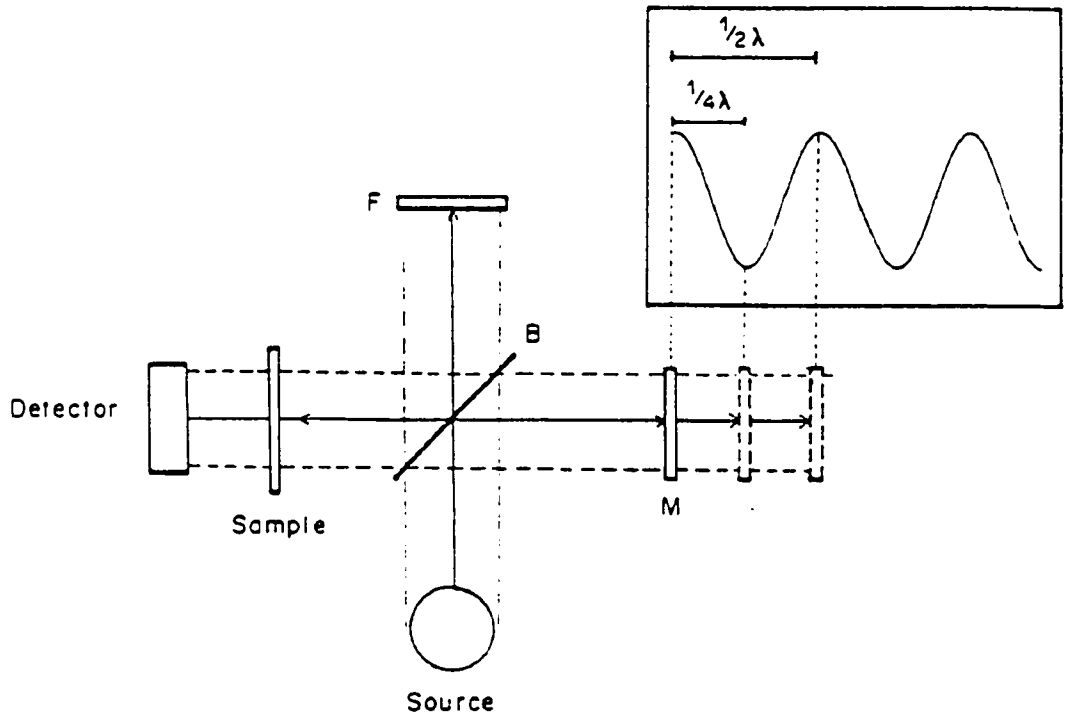
1/2 λ
1/4 λ
F
B
Detector
Sample
M
Source

which is designed to transmit half the radiation and reflect half. The light transmitted strikes the fixed mirror, and the light reflected strikes the moving mirror. After reflecting off their respective mirrors, the light beams recombine at the beamsplitter, then leave the spectrometer to interact with the sample and end in the detector.

If the moving and fixed mirrors are at the same distance from the beamsplitter, no difference in phase is created between the two beams of light, a condition known as zero path difference (ZPD). An optical path difference or retardation is introduced when the moving mirror is displaced at a greater distance from the beamsplitter than the fixed mirror. The light beams are no longer in phase. The distance that the mirror is moved from ZPD is called the mirror displacement. If the mirror is moved at a constant velocity, the two light beams will interfere and depending on the distance of the moving mirror, positive or destructive interference will be created. Consequently, the intensity of the infrared radiation will increase and decrease smoothly and the variation of light intensity with optical path difference is measured by the detector as a cosine wave. An interferogram is a plot of light intensity versus optical path difference and one movement of the moving mirror back and forth is called a scan.

The FTIR spectrometer measures an interferogram of a sample at all wavelengths at the same time which is Fourier transformed to obtain a single beam spectrum (fig. 2.2, inset). The Fourier transform is calculated using the fast Fourier algorithm developed by Cooley and Tukey (1965). In simple terms, the Fourier transformation is a mathematical procedure which transforms a function from the time or Fourier domain to the frequency domain (fig.2.4).

The length of the mirror displacement in the interferogram influences spectral resolution. If the mirror displacement is small, a few data points will be collected and bands will not accurately be defined. On the other hand, when the mirror displacement is longer, more data points are collected, increasing the resolution. Resolutions of 2, 4 and 8 cm^{-1} represent respectively 1, 2 and 4 data point(s) per cm^{-1}. At a greater resolution, the noise level is higher since the intensity of the signal decays in the interferogram and reaches a point where it is lower than the intensity of the noise. Therefore, upon collection of data points at a further distance from ZPD, a lot of noise is collected. To circumvent this problem, when acquiring infrared spectra at a higher resolution, more scans are averaged to reduce the intensity of the noise level which is random over the spectrum since the signal-to-noise ratio is proportional to the square root of the number of scans. The resulting single-beam spectrum of the sample is ratioed over a single beam background spectrum to yield an absorbance spectrum:

$$A = -\log \%T = -\log \frac{I}{I_o} \tag{1.5}$$

where %T is transmittance, I is the intensity of the sample spectrum and I_0 the intensity of the background spectrum (without sample). The signal-to-noise ratio improvement in infrared spectra brought by interferometers is two fold. First, the throughput or Jacquinot advantage of FTIR is based on the fact that no slit is used to restrict the frequency range and intensity of the light that strikes the detector. The infrared light passes through the sample and strikes the detector at once in an FTIR spectrometer. Therefore, the intensity

of the source is not reduced as in monochromators in old dispersive instruments. Second, the multiplex or Fellget advantage is based on the fact that in a FTIR spectrometer, all the frequencies of the light pass through the sample at once compared to a small frequency range at a time. The practical advantage of multiplexing is the rapidity of FTIR spectrometers. Therefore, more scans can be averaged in a short time reducing the signal-to-noise ratio.

4. Resolution enhancement

Fourier deconvolution was introduced to infrared spectroscopy in 1981 as a method to reduce the width of component bands (Kauppinen, Moffatt, Mantsch and Cameron, 1981; Griffiths and Pariente, 1986). In essence, this procedure allows one to mathematically improve the resolution of the component bands in the amide I band. This is important in the secondary structure investigation of proteins by FTIR spectroscopy since as stated above, the spectra are often broad and featureless.

Infrared spectra are recorded by the detector in the spectrometer as an interferogram which is Fourier transformed to produce the actual spectrum. The interferogram is an exponentially decaying cosine function which rate of decay influences the width of the band. For a fast decaying function, the resulting spectrum is broad (fig. 2.4, upper panel). The principle behind self-deconvolution is that the cosine decaying function is multiplied by an exponential function to decrease the rate of decay and consequently narrow the band. Concomitantly, this procedure has the disadvantage that it increases the noise level in the spectra. To reduce noise contribution, the multiplied

Figure 2.4 A broad band and its fast decaying interferogram (top) and a narrow band and its slow decaying interferogram (bottom). From Arrondo et al., 1993.

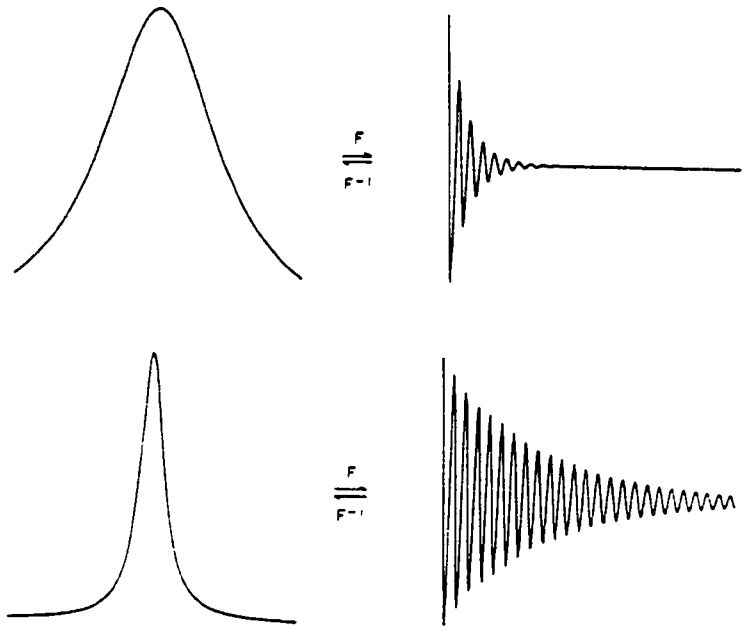

interferogram is subsequently truncated through an apodisation function which varies from 1 (maximal truncation) to 0 (no truncation). Two parameters are used to describe spectral deconvolution, the resolution enhancement factor, $K = \gamma/\gamma'$ were γ is the half-width at half height (HWHH) of the original spectrum and γ' is the HWHH of the deconvolved spectrum and the smoothing factor which varies between 0 (complete truncation) and 1 (no truncation) (Surewicz and Mantsch, 1988). Fourier self-deconvolution was achieved in this thesis by the software package Ramop (Kauppinen, Moffatt, Mantsch and Cameron, 1981) using typically a bandwidth (γ') of 17.0 and a resolution enhancement factor (K) of 2.0-2.4.

Spectral deconvolution is easy to perform on FTIR spectra with the availability of computers. However, care should be applied upon recording the FTIR spectra to ensure the appropriate choice of resolution at which the spectra are recorded, sufficient scan averaging to maximize the signal-to-noise ratio and avoid water vapours in the spectrum. In the latter case, the selective subtraction is possible, but a low initial level is preferable. All these factors can potentially limit the ability to obtain a resulting high quality deconvolved spectrum. In addition, one must be careful in the selection of the deconvolution parameters. For example, if the value of K is too high, this will result in overdeconvolution and appearance of side lobes on each side of the band. On the other hand, if the value of K is too small, the spectrum will appear unchanged.

Spectral derivation is another technique by which the frequencies of overlapping component bands in the infrared spectra are determined. Even order derivatives either in the frequency domain or in the Fourier domain, can be calculated. In the frequency domain it is done in two steps, first, the derivative is taken by convolution of functions

with the spectrum and second, smoothing is applied to reduce the amplification of the noise. The major problem in calculating the derivative in the frequency domain is the rapid degradation of the signal-to-noise ratio as the order of the derivative increases. In contrast, Fourier derivation has the advantage over the frequency domain that it maximizes the signal-to-noise ratio, band narrowing and good lineshape. The Fourier transform of the nth derivative of a spectrum is the complex product of the transform of the spectrum and a weighting function.

The most common method of quantitation of protein secondary structure involves curve fitting of the amide I band (Jackson and Mantsch, 1995). As an initial step, deconvolution and derivation are performed to determine the number of component bands and their frequencies. In addition, observation of the original spectrum provides an estimation of their intensities and widths. Using these initial parameters, the curve-fitting algorithm will summate the peaks and change their parameters in order to "fit" the actual spectrum. The computer calculates the area of each peak which can be ratioed over the area of the whole band in order to get the percentage of absorption of each peak. This approach is based on a number of assumptions that are not necessarily justified (Surewicz, Mantsch and Chapman, 1993). First, it is assumed that the molar absorptivities of amide C=O groups in different secondary structures are the same. Second, the number and positions of the component bands revealed by deconvolution and derivation may not be an accurate reflection of the real number and position of the component bands. Third, the type of band shape (Lorentzian, Gaussian, or mixed) of the various secondary structure components is unknown and must be assumed (Jackson and Manstch, 1995).

The curve fit algorithm provides a statistical analysis including a χ^2 value which is proportional to the difference between the original and fitted spectra. A small value of χ^2 means that the fit is very close to the original spectrum. However, this does not mean that this fit is the one that represents the actual component bands the best. Therefore, a lot of precautions have to be taken when using curve-fitting. We developed a way to verify if the fit is a close representation of the original spectrum. Spectral deconvolution of the curve-fit is achieved and compared with the spectral deconvolution of the original spectrum, giving a good idea of the quality of the estimation of all the component bands.

5. Attenuated total reflection

Most of the FTIR spectra presented in this thesis have been recorded by a method called attenuated total reflection (ATR) (Harrick, 1967 and Fringeli and Günthard, 1981). Total internal reflection in a prism of high refractive index (such as a crystal of germanium) is dependant on the angle of incidence θ of the incident radiation with the prism and the refraction indices of the rare medium (n_2, air or sample) to the dense medium (n_1, prism) (fig 2.5). If $\sin \theta > n_2/n_1$, the radiation is reflected back into the dense medium, a process called total internal reflection. It was established that an evanescent electromagnetic wave exists in the rare medium beyond the reflecting interface of total reflection. It exhibits the same frequency as the incoming light but the amplitude falls off exponentially with the distance z from the surface

$$E = E_o e^{-z/d_p} \qquad (1.6)$$

Figure 2.5 Schematic representation of a path of a ray of light for total internal reflection. The ray penetrates a fraction of a wavelength (d_p) beyond the reflecting surface into the rarer medium of refractive index n_2 and there is a certain displacement (D) upon reflection. From Harrick, 1967.

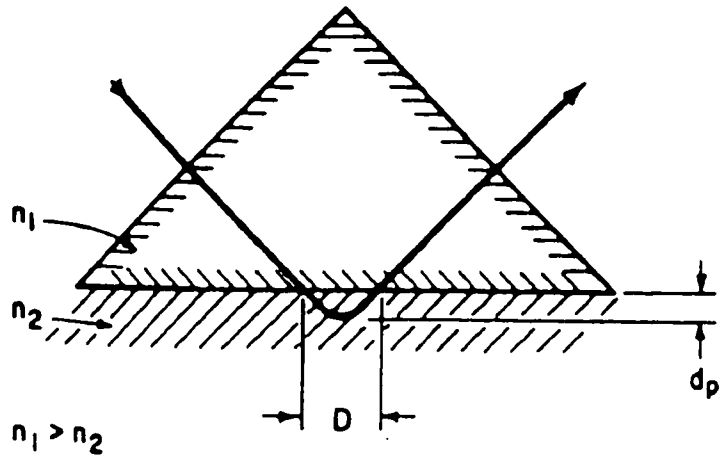
n_1
n_2
d_p
D
$n_1 > n_2$

where d_p is the depth of penetration and is given by

$$d_p = \frac{\lambda_1}{2\pi\left(\sin^2\theta - n_{21}\right)^{1/2}} \qquad (1.7)$$

where θ is the angle of incidence and where $n_{21} = n_2/n_1$ which are the refractive indices of the air (1.007) and the crystal (germanium 4.0), respectively. In a germanium crystal with an angle of incidence of 45°, the depth of penetration varies between 2 and 0.2 μm in the frequency range 400 to 4000 cm^{-1}. Molecules close to the surface of the crystal absorb the infrared radiation and give rise to a spectrum.

ATR has several advantages over the transmission technique in the study of membrane protein structure. First, samples of membrane proteins, upon drying on the surface of the ATR crystal under a gentle stream of N_2 (g), remain attached to the surface. Upon mounting in an ATR liquid cell, the sample film can be hydrated and subsequently, the buffer in contact with the sample can be easily changed without disturbing the sample film. This is particularly important in order to record spectra of the same protein film under different conditions and avoid variations due to the sample. For example, hydrogen/deuterium exchange measurements are possible after seconds of exposure (described in chapter 3), upon exchange of the ^1H_2O buffer in contact with the sample with ^2H_2O buffer. Similarly, ligand-induced conformational changes in a membrane protein can be obtained by cycles of difference spectroscopy where the difference between a spectrum recorded in absence of ligand and a second spectrum recorded in presence of ligand is calculated. Transmission liquid cells are available but their main

disadvantage consists of the strong absorption of water due to the thick path length in the cell (50 μm).

The second main advantage of ATR is the possibility to perform orientation measurements of ordered molecules both in the membrane and the protein. This technique is further described in chapter 5.

Chapter 3- Secondary Structure of the nAChR in both the Active and Inactive Conformations

1. Introduction

The importance of defining precisely the secondary structure of the nAChR is linked to the development of transmembrane topology models which provide insights into the secondary structure and organization of the transmembrane segments. This knowledge is particularly important in the nAChR as a basis to understand the mechanism of action of the ion channel.

Several spectroscopy techniques accumulated divergent experimental results regarding the nAChR's secondary structure. Initially, Fong and McNamee (1987) and Mielke and Wallace (1988) proposed a low proportion (~20%) of α-helices in the nAChR. This proportion is sufficient to account for four transmembrane helices but not for any other α-helices in the extramembraneous domains. Since this latter possibility is unlikely, the existence of transmembrane β-sheets was proposed. Later on, Butler and McNamee (1993), Unwin (1993) and recently Le Novere et al. (1999) also proposed a low content of α-helices in the nAChR. On the other hand, other studies reported a greater proportion (from 32% to 48%) of α-helices (Yager et al., 1984; Wu et al., 1990; Castresana et al., 1992, Naumann et al., 1993 and West et al., 1997).

At the same time, conflicting views were published on the extent of the conformational changes in the desensitized state of the nAChR. Electron microscopy

studies reported rotations, of less than 10°, of the subunits of the nAChR in the desensitized state (Unwin et al., 1988 and Unwin, 1995)

An FTIR secondary structure study of the changes in conformation of the nAChR in the desensitized state have reported large rearrangements in the protein. Castresana et al. (1992) interpreted the FTIR spectral changes observed in the presence of Carb in terms of a decrease of β-pleated sheet from ~48% to ~24% concomitant with an increase in unordered structures. In contrast, Fernandez-Ballester et al. (1993), Mielke and Wallace (1993) and McCarthy and Stroud (1989b) reported only negligible alterations in the secondary structure of the nAChR following agonist binding. The structural changes induced in the desensitized state appear to be very small and restricted to the amino acid level (Baenziger et al., 1993).

Important modifications of the nAChR's structure have also been reported for the channel-inactive conformations induced in the absence of cholesterol and anionic lipids. Those include a possible change in the α-helical character of the M2 segments leading to the inactivation of the ion channel (Fong and McNamee, 1987 and Butler and McNamee, 1993). Fernandez-Ballester et al. (1994) interpreted changes in the FTIR spectra of nAChR samples reconstituted in the absence of cholesterol as a decrease of both α-helix and β-sheets proportions from roughly 45% and 50%, respectively, in the presence of cholesterol down to 30% and 40%, respectively, without cholesterol.

In order to clarify the nature of the secondary structure of the nAChR and the magnitude of the conformational changes induced in the channel-inactive conformations, FTIR spectra of the nAChR were recorded both in $^{1}H_2O$ and $^{2}H_2O$ buffer in the presence and absence of desensitizing agents (1 mM Carb and 5 mM tetracaine (Tet)) and upon

reconstitution into lipid mixtures of various compositions. In addition, the kinetics of hydrogen/deuterium ($^1H/^2H$) exchange was examined to precisely investigate the changes in the nAChR's structure upon desensitization.

A detailed analysis of the various spectral features clearly demonstrates that the nAChR is an α/β type protein with a predominance of α-helices and that the secondary structure is essentially unaffected by channel inactivation, regardless of whether the inactive conformation is ligand- or lipid-activated.

2. Experimental procedures

2.1 nAChR purification from *Torpedo californica*

2.1.1 Crude homogenization

The nAChR was purified from the electric organ of *Torpedo californica* according to McCarthy and Moore (1992). A crude membrane fraction was prepared at 4 °C from frozen electric tissue (the tissue was purchased frozen), typically 500 g of the tissue was cut in dice-size pieces and homogenized in homogenization buffer: 10 mM sodium dihydrogen orthophosphate (Na_2HPO_4), 5 mM ethylenediaminetetraacetic acid (EDTA), 5 mM ethylene glycol-bis(β-aminoethyl ether N,N,N',N'-tetraacetic acid) (EGTA) and 0.02% sodium azide (NaN_3), pH 7.4, containing 2 protease inhibitors: 1 mM phenylmethylsulfonyl fluoride (PMSF) (to inhibit serine proteases) and 10 mM iodoacetamide (to inhibit cysteine proteases) using a blender with three bursts of 30 s and

15 s of pause in between the bursts. The homogenate was centrifuged for 10 min at 5000 rpm in a Sorvall GSA rotor and the supernatant was filtered through four layers of cheese cloth. The pellets were rehomogenized using a Polytron in homogenization buffer and centrifuged as above. The pooled supernatants were centrifuged at 14 000 rpm for 3 hours in the same rotor. The pellets were hand homogenized, transferred into a test tube, frozen in liquid nitrogen and stored at –80 °C.

2.1.2 Synthesis of bromoacetylcholine bromide

Bromoacetylcholine bromide (BAC) was used as the immobilized ligand to purify the nAChR and was synthesized from choline bromide and bromoacetylbromide. Over a period of 40 minutes, 24.2 g of bromoacetylbromide was added to 18.4 g of choline bromide and the mixture was cooled in an ice bath for 75-90 minutes. 75 ml of absolute ethanol was added over a period of 30 minutes while keeping the flask on ice and then, the solution was filtered through a medium scintered glass funnel and washed with cold ethanol. The white powder was recrystallized two times in a 400 ml of isopropanol, placed under vacuum overnight until no smell of solvent could be detected and stored at –20 °C. Typical yield was 18 g.

2.1.3 Preparation of the affinity column

To prepare the affinity column for the purification of the nAChR, 20 ml of Affi-gel 102 was derivatized overnight at 4°C in a 1.44 M N-acetyl-DL-homocysteine

thiolactone and 1.0 M sodium bicarbonate ($NaHCO_3$) solution, pH 9.7. The next morning, the gel was washed with 1 L of cold 0.1 M NaCl solution using a scintered glass funnel. The moist gel was transferred in a beaker with 20 ml of 0.2 M dithiothreitol (DTT) and 200 mM Tris(hydroxymethyl)aminomethane (Tris) solution, pH 8.0 and stirred gently at room temperature for 30 minutes. The gel was transferred into a glass column and the DTT solution drained. 20 ml of 0.2 M DTT solution (as above) was added to the column and the column agitated on a belly dancer for 30 minutes. The gel was washed with 140 ml of buffer B (100 mM NaCl, 20 mM Na_2HPO_4, 0.02% NaN_3, pH 7.0) and the eluate was tested for the presence of free sulfhydryls using the 5,5'-dithiobis-2-nitrobenzoic acid (DTNB) colorimetric assay. 100 µl of the eluate was combined with 2 ml of the assay solution (0.6 ml of 10 mM DTNB in ethanol is combined with 18 ml of 100 mM Tris buffer, pH 8.0) and a clear solution indicates that the DTT was all eluted. Similarly, a small amount of the gel should turn yellow in contact with the assay solution. The column was resuspended with 15 ml of 50 mM sodium phosphate, pH 7.0, and 0.4 g of BAC and shaked for 60 minutes. The column was drained and the gel tested for the presence of free sulfhydryls (should be clear). The column was rinsed with 80 ml of buffer B and 0.138 g of iodoacetamide was added to the column which was mixed for 20 minutes. Finally, the column was washed with a solution of 0.02% sodium azide and stored at 4 °C.

2.1.4 Affinity purification of the nAChR

2/5 of the crude homogenate was thawed and diluted with dialysis buffer (1 M NaCl, 100 mM Tris, 1mM EDTA and 0.2% NaN_3, pH 7.8) to a final protein concentration of 4 mg/ml and cholate was added to make a 1% cholate solution. The nAChR was solubilized for 60 minutes at 4 °C and centrifuged at 35000 revolutions per minute (rpm) for 1 hour. The affinity column was washed with 60 ml of dialysis buffer and then, the supernatants of solubilized nAChR were applied to the column at a flow rate of 1-2 ml per minute. The nAChR was reconstituted in artificial membranes of controlled composition. The stock lipid solution (solution A) contains 165.7 mg of egg phosphatidylcholine (EPC), 53.24 mg of dioleoylphosphatidic acid (DOPA) and 27.24 mg of cholesterol (Chol) for a 3:1:1 molar ratio, respectively, in 110 ml of dialysis buffer and 2% cholate. When asolectin lipids (lipids extracted from soybean, mainly dioleoylphosphatidylcholine (DOPC)) are used, the total amount used is 246.2 g. Lipid solution B contains 45 ml of lipid solution A with 1% cholate in 65 ml of dialysis buffer. Lipid solution C contains 10 ml of lipid solution B with 90 ml of 0.5% cholate in dialysis buffer. Lipid solution D contains 6 ml of lipid solution B with 54 ml of 0.5% cholate elution buffer (10 mM 3-(N-morpholino)propanesulfonic acid (MOPS), 250 mM NaCl, 0.1 mM EDTA, 0.02% NaN_3, pH 7.8) and 10 mM Carb.

The column was washed with 80 ml of lipid solution B until no more protein was detected at 280 nm, 60 ml of solution A and 50 ml of lipid solution C. The nAChR was eluted with 100 ml of solution D by collecting 3 ml fractions. The presence of the nAChR was detected by reading the absorbance of each fraction at 280 nm and all fractions with

an absorbance greater than 0.05 a.u. were pooled. The solution was transferred in dialysis bags (molecular weight cut-off of 12,000-14,000 Da) which were placed in dialysis buffer (2 L beaker) and dialyzed. The buffer was changed every 12 hours and 5 times. The column was then washed with 150 ml of 0.02% NaN_3. After dialysis, the nAChR solution was spun down for 2 hours at 41 000 rpm. The pellet was resuspended in 0.5 ml of 2 mM phosphate buffer pH 8.0 and stored at -80°C. Protein concentration was measured by a Lowry protein assay modified by Hartree (1972) and purity was assessed via sodium dodecylsulphate polyacrylamide gel electrophoresis (SDS-PAGE) (Leammli, 1970) and α-bungarotoxin binding assays (Schmidt and Raftery, 1973). Typically, using a 20 ml column, roughly 15 mg of nAChR were obtained, SDS-PAGE diplayed 4 bands at 38, 47, 55 and 66 kDa and the nAChR membranes contained 7.67 ± 0.33 nmol of α-bungarotoxin binding sites/mg of protein.

The nAChR reconstituted in lipid membranes made of EPC:DOPA:Chol in a molar ratio of 3:1:1 supports agonist induced cation flux (Fong and McNamee, 1986). Moreover, the nAChR retains the ability to bind ligands and undergo the resting-to-desensitized transition (McCarthy and Moore, 1992 and Méthot et al., 1994).

2.1.5 Preparation of deuterated samples

250 μg of nAChR was spun down in a microcentrifuge at 14 000 rpm for 15 minutes. The supernatant was removed and 500 μl of 2 mM phosphate buffer, pH 6.6 (all pH values in ^2H_2O have been corrected according to the following: pD = pH + 0.4, Glasoe and Long, 1960) prepared in ^2H_2O was added. The sample was vortexed,

centrifuged and resuspended again. The sample was stored at 4°C for three days. Then, the sample was centrifuged and resuspended in 100 µl of 2 mM phosphate buffer and either dried on the ATR crystal or stored at -80°C.

2.2 FTIR spectroscopy

FTIR spectra were acquired either on a Bio-Rad FTS-40 or on a Bio-Rad FTS-40A spectrometer equipped with either a mercury cadmium telluride or a deuterated triglycine sulfate detector for transmission and attenuated total reflectance (ATR) measurements, respectively. Each spectrometer was purged with dry air (dew point, 100°C) from a Balston air-dryer. The ATR crystals were cleaned before use by soaking in chromic acid for 30 minutes and then rinsed thoroughly with distilled water. All spectra were recorded at 2 cm^{-1} resolution. Spectral deconvolution was performed according to the method of Kauppinen et al. (1981) with γ' (full width at half height) of 17.0 cm^{-1} and resolution enhancement factor of K = 2.2. Fourth-derivative spectra were obtained using a power of 3 and a band cutoff of 0.35. Prior to deconvolution, all spectra were stringently examined for the presence of water vapor using the mild spectral deconvolution procedure described in Reid, Moffatt and Baenziger, 1996 and if present they were eliminated by spectral subtraction.

Curve-fitting of both the amide I and amide I' band was performed by the software package Grams. Initial input parameters for the curve-fit routine such as the number and frequencies of the component bands and band widths and heights were obtained from the resolution-enhanced spectra. After the initial input parameters were set,

the curve fit spectrum was deconvolved and compared to the corresponding deconvolved experimental spectrum. The band widths and heights of the component bands were adjusted to obtain a rough match with the experimental data and thus establish reasonable starting conditions for the curve fit routine. The curve fit was then run iteratively, simultaneously adjusting the component band widths and heights to obtain a best fit solution. Each final curve fit was deconvolved and compared to the corresponding deconvolved experimental spectrum as a final test to ensure a close match with the experimental data. Each curve fit analysis was performed using a large region of the spectrum (roughly 1760-1500 cm^{-1}) in order to take into account the possible overlap of non-amide I vibrations in the amide I region. All peaks were fitted using a mixed Gaussian/Lorentzian line shape.

Secondary structure analysis-Transmission 10 µl of solutions of myoglobin and trypsin of 20 mg/ml were deposited and dried on the surface of a cal cium fluoride (CaF_2) window with a gentle stream of nitrogen (N_2) (g). An FTIR spectrum averaging 256 scans was recorded either of the dry protein film or after rehydration with 10 µl of 2 mM phosphate buffer, pH 7.0. Similarly, 125 µg of the nAChR were deposited and dried on the transmission window. The protein film was rehydrated with Torpedo Ringer (TR) buffer (250 mM NaCl, 5 mM KCl, 2 mM magnesium chloride ($MgCl_2$), 5 mM Na_2HPO_4, 3 mM calcium chloride ($CaCl_2$) and 0.02% NaN_3, pH 7.0) and 4096 scans were averaged.

Secondary structure analysis-ATR Typically, 250 µg of nAChR pre-exposed to ^2H_2O for three days at 4 °C, pH 7.0, was deposited on a germanium internal reflection element crystal, carefully dried with a gentle stream of nitrogen and placed in an ATR liquid sample cell connected with plastic tubing. The ATR cell was placed in the sample

compartment of the FTIR spectrometer and the nAChR was immediately rehydrated with TR buffer made in ^2H_2O. After purging the water vapours, an FTIR spectrum averaging 16000 scans was recorded.

$^1H/^2H$ exchange FTIR spectra were recorded during the time course of peptide $^1H/^2H$ exchange using the ATR technique. An aliquot of reconstituted nAChR was carefully spread and dried on the surface of the germanium element as described above, however, the sample was rehydrated with ^1H_2O TR buffer after mounting the reflection element in the ATR cell. After purging the water vapours, a spectrum averaging 256 scans was recorded. Then, the ^1H_2O buffer was removed and ^2H_2O buffer added into the ATR cell. As soon as the ATR cell was filled with ^2H_2O (roughly 1 minute), FTIR spectra were automatically recorded over a period of 12 hours with increasing number of scans (varying from 50 to 1500 scans/spectrum).

3. Theory of hydrogen/deuterium exchange

Before presenting the results in this chapter, the theory of hydrogen/deuterium ($^1H/^2H$) exchange which was used extensively in this research project (for reviews on $^1H/^2H$ exchange see Englander, Downer and Teitelbaum (1972), Englander and Kallenbach (1984) and Goormaghtigh, Cabiaux and Ruysschaert (1994a) is presented.

In 1953, Lenormant and Blout observed more or less accidentally that some peptide groups exchange their hydrogens slowly while others proceed more rapidly. Later on, several groups used the amide II band in the infrared spectra for quantitative measurements of amide $^1H/^2H$ exchange (reviewed in Englander et al., 1972b). Upon

contact with ^2H_2O, isotopic exchange of protons in the protein for deuterium atoms in the solvent is taking place and the kinetics of exchange has been used to investigate protein motions in hemoglobin (Hydrogen-tritium exchange) (Englander, Calhoun, Englander, Kallenbach, Liem, Malin, Mandal and Rogero, 1980) and conformational changes in proteins such as hemoglobin (Englender and Mauel, 1972b), cytochrome c (Heimburg and Marsh, 1993) and rhodospin (Rath, DeGrip and Rothschild, 1998).

The rate of $^1H/^2H$ exchange depends on several factors such as solvent accessibility, hydrogen bonding, temperature and pH. The effect of these factors is presented below. In order for exchange to take place, the ^2H_2O has to come in contact with the protein groups. This factor is largely related to the accessibility of the protein structures. For instance, protein groups located at the surface of the protein are easily accessible to aqueous solvent. In contrast, the structures located in the hydrophobic interior of the protein are less susceptible to exchange due to their inaccessibility to aqueous solvent. The accessibility of the hydrogen peptides located in the protein interior is largely reduced due to the hydrophobic nature of the segments. This is particularly true for the transmembrane segments of an integral membrane protein located in the hydrophobic environment of the lipid bilayer.

Ordered secondary structures like α-helices and β-sheets can undergo $^1H/^2H$ exchange only during a transient local unfolding which implies breakage of the hydrogen bonds. Therefore, the groups that are directly hydrogen bonded to the solvent will exchange much more rapidly that the ones involved in internal hydrogen bonds which involves breakage of a stabilizing hydrogen bonds. The temperature effect is related to

hydrogen bonding since increases in temperature increase fluctuations and unfolding, leading to increase in the exchange.

The hydrogen exchange rates strongly depend on pH. The hydrogen-tritium exchange rate of the polymer poly-D-L-alanine is described by the following equation:

$$t_{1/2} = \frac{200}{\left[(10^{pH-3} + 10^{3-pH})(10^{0.05T})\right]} \qquad 2.1$$

where $t_{1/2}$ is the exchange half-time (min.) and the T the temperature in °C (Englander, Downer and Englander, 1972). Equation 2.1 shows that increases in pH and temperature decrease the half-time of the reaction.

FTIR spectroscopy allows the measurement of the rate and extent of peptidic $^1H/^2H$ exchange. Upon incubation in ^2H_2O buffer there are a number of changes in the infrared bands including a slight downshift of the secondary structure components in the amide I band and a dramatic decrease in intensity of the amide II band concomitant with an increase in intensity of the amide II' band located at 1450 cm^{-1}. These spectral changes are presented below.

4. Results

4.1 Secondary structure analysis

The secondary structure analysis of the nAChR was carried through the analysis of the amide I band located between 1600 and 1700 cm^{-1} which represents mainly the carbonyl stretching vibration of the peptide groups. The amide I band is sensitive to secondary structure since the strength of hydrogen bonding of the peptide carbonyl

influence the frequency of vibration. Empirical observations and normal mode calculations have identified the typical frequency of vibration of secondary structure components (see table 2.1). Transmission FTIR spectra of a protein of known structure, for example myoglobin (87% α-helices and 0% β-sheets) is characterized by sharp amide bands with a maximal amide I absorption at 1655 cm^{-1} (figure 3.1, top spectrum) (Dousseau and Pézolet, 1990). These spectral features are highly characteristic of α-helical proteins. In contrast, trypsin (9% α-helices and 56% β-sheets) displays broader amide bands with a maximal amide I absorption at 1642 cm^{-1} and a shoulder at 1676 cm^{-1} (figure 3.1, middle spectrum). This pattern is typical of β-sheet proteins. Note that a similar pattern of absorption is observed for α-helices and β-sheets in membrane proteins (Goormaghtigh et al., 1990).

A transmission FTIR spectrum of affinity-purified nAChR in asolectin membranes recorded in $^{1}H_2O$ Torpedo Ringer buffer, pH 7.0, is presented in figure 3.2 (solid line). To help in the subtraction of the $^{1}H_2O$ buffer contribution which overlaps dramatically with the amide bands, the absolute amide I/amide II ratio was estimated from an FTIR spectrum of the nAChR in the dry state (not shown). Buffer subtraction was accomplished by obtaining a flat line around the $^{1}H_2O$ absorption band at 2100 cm^{-1} and by matching the amide I/amide II ratio in the dry state. The subtracted spectrum reveals an amide I band with an intense maximum at 1655 cm^{-1} and two broad shoulders, one near 1635 cm^{-1} and the other one between 1670 and 1700 cm^{-1}. Moreover, both amide I and amide II bands are sharp and narrow, similar to the amide bands in the spectrum of myoglobin (Dousseau and Pézolet, 1990). This implies that the nAChR is essentially α-helical.

Figure 3.1 Amide I and II region of transmission-FTIR spectra of myoglobin, trypsin and nAChR in $^{1}H_2O$ buffer. 256 scans were averaged and the contribution of buffer was subtracted from the spectra.

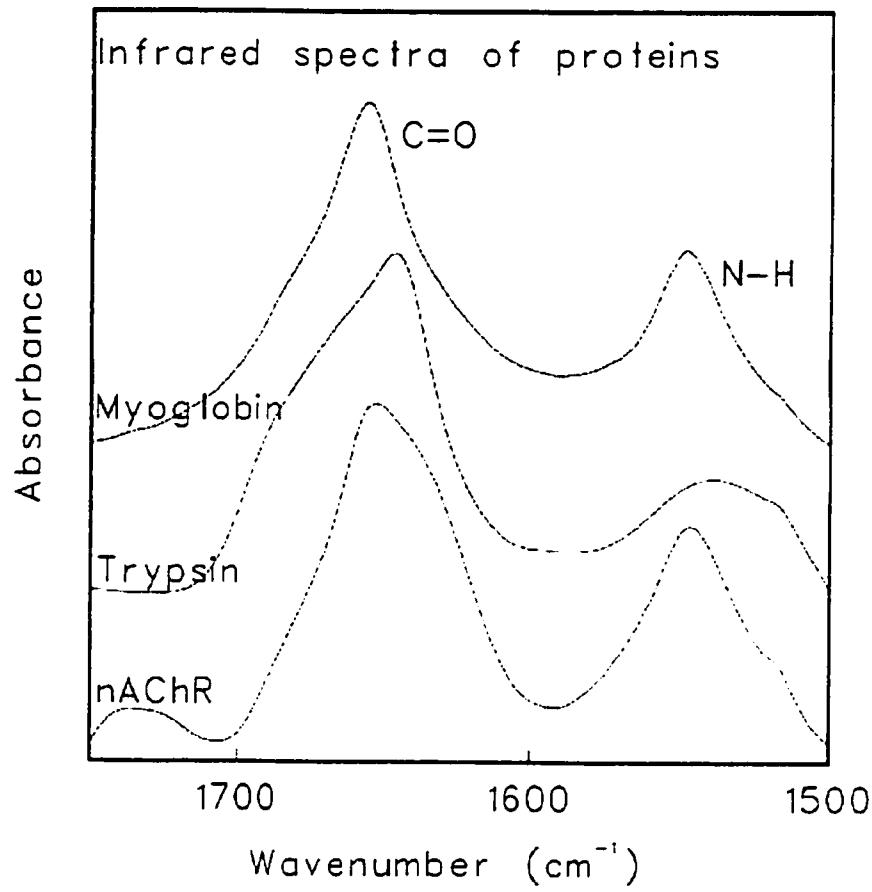
Infrared spectra of proteins
C=O
N–H
Myoglobin
Trypsin
nAChR
Absorbance
1700
1600
1500
Wavenumber (cm⁻¹)

Upon exposure of the nAChR to ^2H_2O, the solvent accessible peptide hydrogens exchange for deuterium leading to a downshift in the frequency of absorption of both amide bands (figure 3.2, dashed line). The amide I band (called amide I' in ^2H_2O) becomes more symmetrical with a decrease in intensity around 1655 cm^{-1} and concomitant increase in intensity around 1640 cm^{-1}. An important decrease in intensity of the amide II band is observed since the N-H bending vibration downshifts from 1547 to 1450 cm^{-1} in ^2H_2O.

The amide I band is a broad band which represents the summation of the individual secondary structures from which the specific frequencies of absorption can be deduced using resolution-enhancement techniques such as spectral deconvolution and fourth derivative (figure 3.3). The resolution-enhanced spectrum of the nAChR in ^1H_2O (figure 3.3a, middle) reveals the presence of an intense component band at 1655 cm^{-1} typical of polypeptide chains in the α-helical conformation. This frequency of absorption is also characteristic of unordered structures. Two shoulders are visible near 1635 cm^{-1} and between 1670 and 1700 cm^{-1}. The high frequency shoulder is composed of three poorly resolved bands around 1691, 1682 and 1670 cm^{-1}. Bands in these regions have been assigned to both β-sheets and β-turns. The low-frequency shoulder of the amide I band is resolved into 6 component bands centered at 1644, 1633, 1624, 1615 and 1605 cm^{-1}. The latter two bands are generally assigned to amino acid side chains. The bands at 1633 and 1624 cm^{-1} are characteristic of β-sheets. In ^2H_2O, most of the changes in shape of the amide I band, occur in the first seconds of exposure and are attributed to the important downshift of unordered structures from 1655 cm^{-1} to 1644 cm^{-1}.

Figure 3.2 Transmission-FTIR spectra of the nAChR in EPC:PA:Chol membranes at the molar ratio 3:1:1, showing the amide I and II regions in $^{1}H_2O$ (solid line) and after prolonged exposure to $^{2}H_2O$ (dash line). 4096 scans were averaged and the contribution of buffer was subtracted from the spectra.

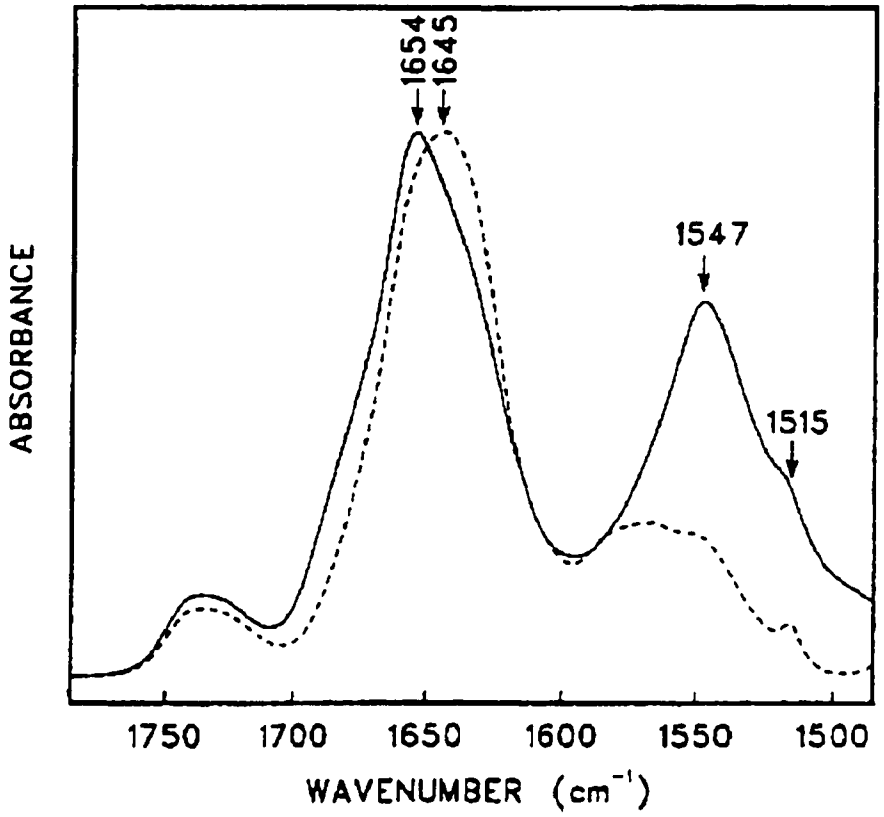
1654
1645
1547
1515
ABSORBANCE
1750
1700
1650
1600
1550
1500
WAVENUMBER (cm⁻¹)

Figure 3.3 Resolution-enhanced amide I region of transmission-FTIR spectra of the nAChR in EPC:PA:Chol membranes in the molar ratio 3:1:1, in $^{1}H_2O$ (top panel) and after prolonged exposure to $^{2}H_2O$ (bottom panel). For each panel: top, absorbance spectrum; middle spectrum after Fourier self-deconvolution; spectrum after fourth-derivative. The deconvolution parameters used were: γ' factor 17.0 and resolution-enhancement factor 2.6.

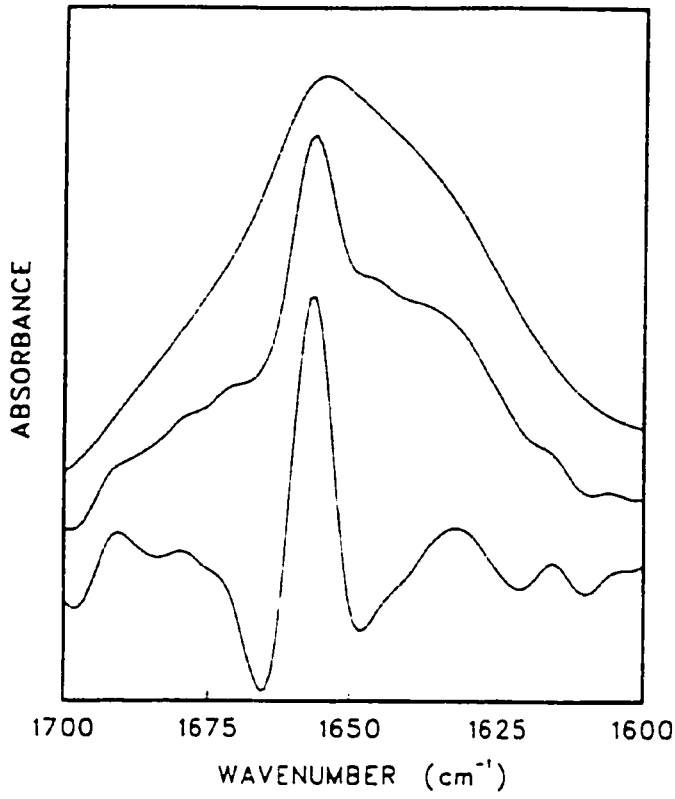
ABSORBANCE
1700
1675
1650
1625
1600
WAVENUMBER (cm⁻¹)

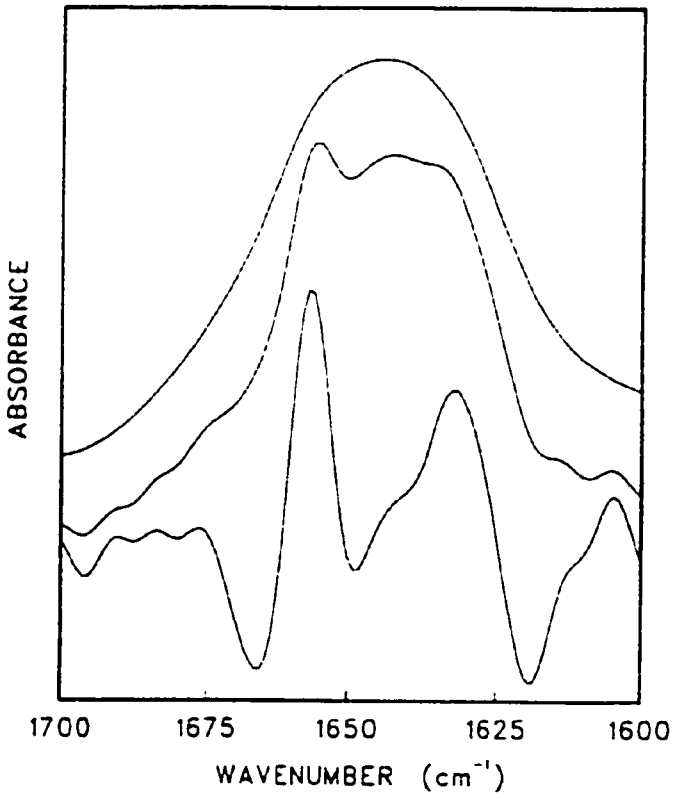
ABSORBANCE
1700
1675
1650
1625
1600
WAVENUMBER (cm⁻¹)

Affinity purified nAChR reconstituted in EPC/DOPA/Chol membranes have been recorded using the ATR technique and the spectra are essentially identical to the transmission spectra presented here. A small decrease in intensity of the band at 1655 cm^{-1} in the ATR spectrum compared to the transmission spectrum is suggestive of a predominant orientation of the transmembrane α-helices perpendicular to the membrane plane due to the intrinsic polarization of the ATR crystal. Therefore, the spectra recorded using ATR slightly underestimate the contribution of α-helices in the nAChR.

To estimate the percentage of each secondary structure in the amide I contour, a curve fitting analysis of the FTIR spectra recorded both in ^1H_2O and after prolonged exposure to ^2H_2O was performed (fig. 3.4). The area of the 1656 cm^{-1} component band in ^1H_2O was estimated to 58% of the total area of the amide I band and is assigned to the combined absorption of α-helices and unordered structures. In ^2H_2O, the unordered component displaced at 1644 cm^{-1} corresponds to 21% of the total area leaving an α-helical band of roughly 39%. The percentage of β-sheets was calculated to be roughly 35% (summation of the 1624, 1633 and 1672 cm^{-1} bands) and the β-turn content is roughly 6% (summation of the 1691 and 1680 cm^{-1} bands).

4.2 Desensitization of the nAChR

To clarify the magnitude of the changes in conformation in the nAChR in ligand- and lipid-induced channel inactive conformations, the secondary structure and kinetics of hydrogen/deuterium ($^1H/^2H$) exchange which are very sensitive to nAChR structure and conformational changes were examined. FTIR spectra recorded as a function of time

Figure 3.4 Curve fit analysis of the amide I band (top panel) and of the amide I' band (bottom panel) of transmission-FTIR spectra of the nAChR in EPC:DOPA:Chol membranes in the molar ratio 3:1:1 . In each panel: the solid line represents the experimental spectra, the dotted line superimposed onto the experimental spectra represents the curve fit spectra and the dotted lines represent the individual component bands.

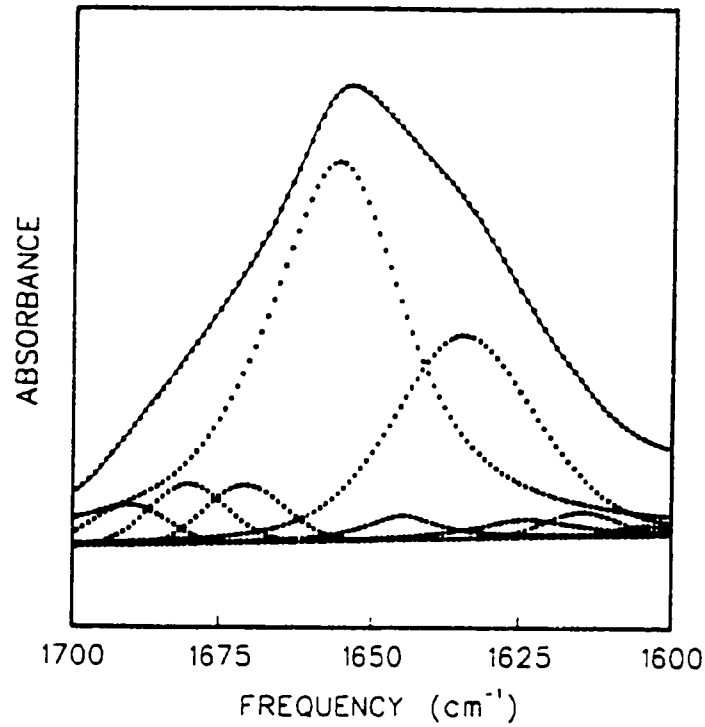
ABSORBANCE
1700
1675
1650
1625
1600
FREQUENCY (cm⁻¹)

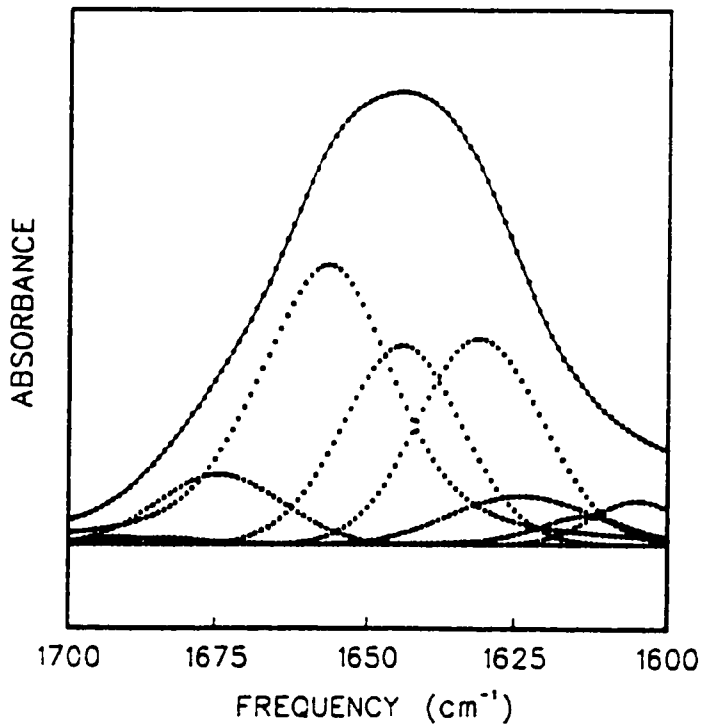
ABSORBANCE
1700
1675
1650
1625
1600
FREQUENCY (cm⁻¹)

after exposure of the nAChR to ^2H_2O exhibit spectral changes reflecting the isotopic exchange of the solvent accessible peptide N-^{1}H for N-^{2}H. These spectral changes in the affinity-purified nAChR, reconstituted in membranes composed of EPC:DOPA:Chol in the molar ratio 3:1:1 were monitored for a period of 12 hours (figure 3.5, A). In such membranes, the nAChR is able to bind ligands and undergo agonist induced channel gating and desensitization (Fong and McNamee 1986; McCarthy and Moore, 1992; Méthot et al., 1994). The decrease in intensity of the amide II band is plotted as the change in the amide II/amide I ratio as a function of time after exposure to ^2H_2O (figure 3.6, A) and provides a direct measure of the overall rates and extent of peptide $^1H/^2H$ exchange. Thus, it was calculated that roughly 30% of the nAChR hydrogen peptides exchange within ~5 seconds of exposure due to the rapid decrease in intensity at 1547 cm^{-1} in the first seconds of exposure to ^2H_2O, 50% after 30 min and 60% after 12 h. Prolonged exposure for several days at room temperature leads to the exchange of 75% of the nAChR (see chapter 4).

The most important change in shape of the amide I band in ^2H_2O which occurs in the first seconds of exposure is a downshift in frequency of a band from 1655 to 1644 cm^{-1} associated with the exchange of unordered structures. In addition, the 6% of β-turns in the nAChR are also likely to exchange rapidly. These observations correlate with the roughly 30% of the nAChR exchanging in the first seconds of exposure. Hydrogen-tritium exchange measurements on poly-DL-alanine which is a homopolypeptide in an unordered conformation, revealed an exchange half-time ($t_{1/2}$) of 0.0675 s at pH 7.0 and 22.5 °C (Englander et al., 1972). Note that the spectral changes in the amide I band

Figure 3.5 ATR-FTIR spectra recorded as a function of time after exposure of the nAChR in EPC:PA:Chol membranes in the molar ratio 3:1:1 to Torpedo Ringer buffer prepared in $^{2}H_2O$, pH 7.0. (A) The spectrum in dashed line was recorded in $^{1}H_2O$ (100 scans) and the spectra in solid line were recorded from top to bottom at 1547 cm^{-1} after 3, 6, 9,12, 22, 50, 80, 170, 360, 600 and 780 min after exposure to $^{2}H_2O$ (from 50 to 1500 scans). (B) Amide I' band after Fourier self-deconvolution of spectra recorded during the 1st (small dashed line), 3rd (long dashed line) and 12th hour (solid line) after exposure to $^{2}H_2O$ (1500 scans). The deconvolution parameters were γ' 17 and resolution enhancement factor of 2.0. The contribution of buffer was subtracted from all spectra.

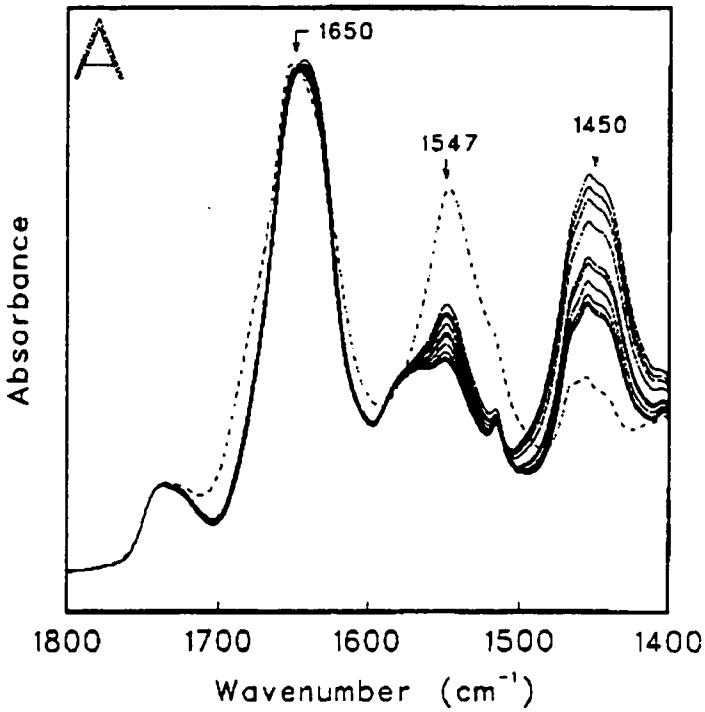
A
1650
1547
1450
Absorbance
1800
1700
1600
1500
1400
Wavenumber (cm⁻¹)

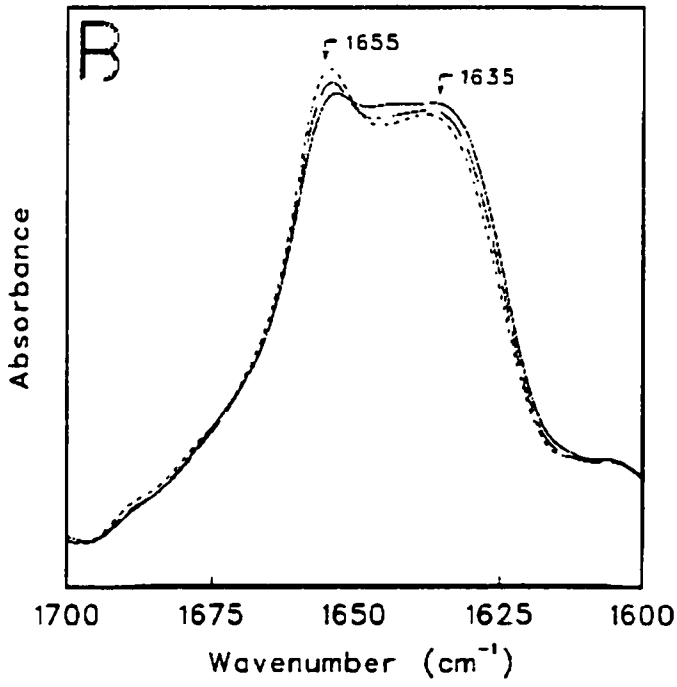
B
1655
1635
Absorbance
1700
1675
1650
1625
1600
Wavenumber (cm⁻¹)

Figure 3.6 Time course of $^{1}H/^{2}H$ exchange plotted as a function of the amide II/amide I ratio. (A) Data were taken from spectra of the nAChR reconstituted into EPC:DOPA:Chol membranes in the molar ratio 3:1:1 in the absence of ligands (o), the presence of 1 mM Carb (■), and the presence of 5 mM Tet (▲). (B) Data were taken from spectra of the nAChR reconstituted into EPC/DOPA/Chol membranes in the molar ratio 3:1:1 (▲), EPC/DOPA membranes in the molar ratio 3:1 (■) and EPC membranes (o).

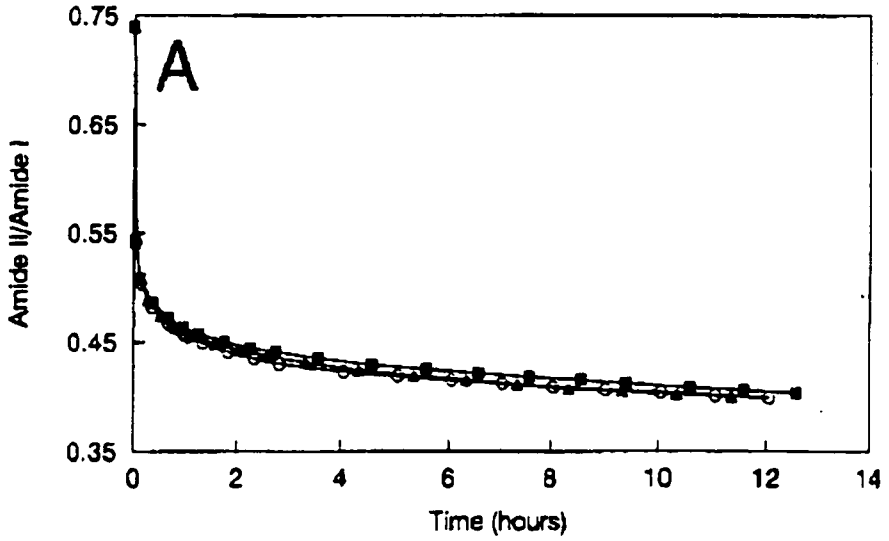
A
0.75
0.65
0.55
0.45
0.35
Amide II/Amide I
0
2
4
6
8
10
12
14
Time (hours)

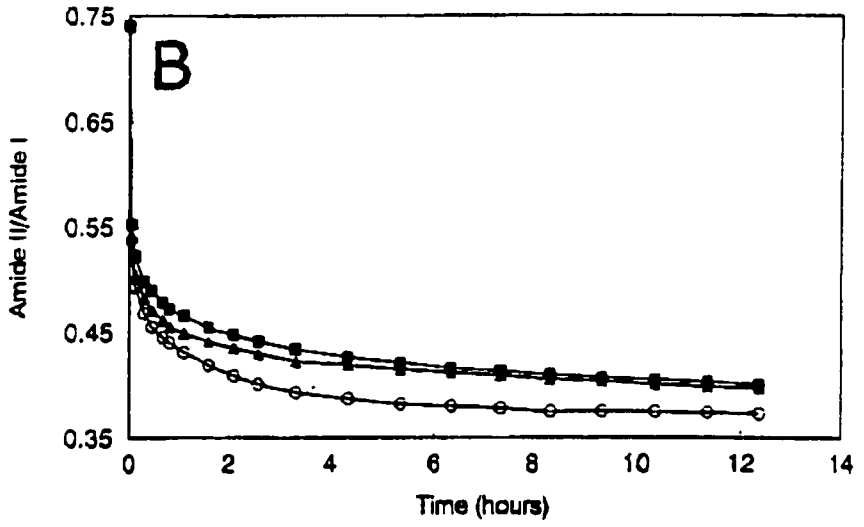
B
0.75
0.65
0.55
0.45
0.35
Amide II/Amide I
0
2
4
6
8
10
12
14
Time (hours)

associated to the downshift of unordered structures are completed before the first spectrum in ^2H_2O is recorded.

Resolution-enhanced amide I band of FTIR spectra recorded during the 1st, 3rd and 12th hour after solvent exposure exhibit a gradual decrease in intensity at 1655 cm^{-1} and a concomitant increase in a shoulder located from 1625 to 1645 cm^{-1} (fig. 3.5b). These spectral changes are associated with the slower exchange of ordered secondary structures involved in internal hydrogen bonds, such as α-helices and β-sheets. These slowly exchanging hydrogen peptides correspond roughly to 30% of the hydrogen peptides in the nAChR. The 25% of hydrogen peptides unexchanged after prolonged exposure are likely α-helical as suggested by the strong remaining intensity at 1655 cm^{-1} in the amide I' band (figure 3.3B, middle spectrum) and located in the solvent restricted hydrophobic membrane environment (see chapter 4).

$^1H/^2H$ exchange experiments were performed in the presence of 1 mM Carb or 5 mM tetracaine and as shown in figure 3.6a, the rate and extent of $^1H/^2H$ exchange were not significantly different compared to the curve in absence of agonist. Similarly, both absorbance and deconvolved amide I spectra of the nAChR recorded either in the absence or presence of ligands do not exhibit any large change in shape indicating that the magnitude of the secondary structure changes is very small (figure 3.7a and b). Note that the FTIR spectra presented in figure 3.7a and b were all recorded on the same nAChR sample, minimizing potential sample preparation artifacts. The spectra were recorded at a very high signal-to-noise ratio and carefully examined for the presence of water vapours. Noise and water vapours can lead to artifacts in the resolution-enhanced spectra

Figure 3.7 Effects of ligands and lipids on the absorbance and Fourier self-deconvolved amide I' band of the nAChR. Before data acquisition, the nAChR was incubated for 3 days in ^2H_2O at 4°C. Absorbance (A) and deconvolved (B) spectra of the nAChR recorded in either the absence of ligand (solid line in A, bottom spectrum in panel B), or the presence of either 1 mM Carb (small dashed line in panel A; center spectrum in panel B) or 5 mM Tet (long dashed spectrum in panel A; top spectrum in panel B). All spectra in panels A and B are from the nAChR in EPC/DOPA/Chol membranes. The arrows indicate the absorption of the ligand Tet. Absorbance (C) and deconvolved (D) spectra of the nAChR into either EPC/DOPA/Chol membranes (solid line in A; bottom spectrum in B) or EPC/DOPA membranes (small dashed line in A; center spectrum in B) or EPC membranes (long dashed line in A; top spectrum in B). The spectra are the average of 16000 scans, the contribution of buffer was subtracted and the deconvolution parameters were γ' 17.0 and 2.4.

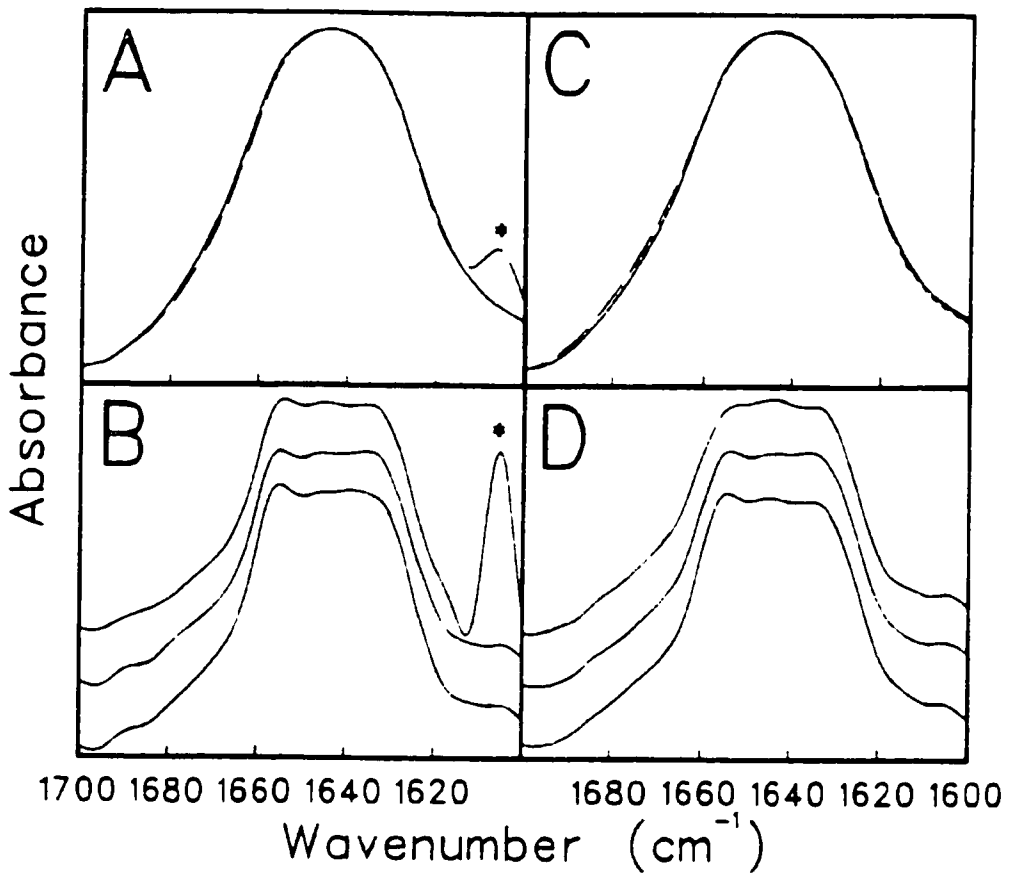
A
C
B
D
Absorbance
1700 1680 1660 1640 1620
1680 1660 1640 1620 1600
Wavenumber (cm^{-1})

that could be mis-assigned to amide I component bands (Goormaghtigh et al., 1994a; Reid et al., 1995). The results are in agreement with several studies which support the lack of a large conformational changes in the nAChR upon going to the desensitized state (Mielke and Wallace, 1988; McCarthy and Stroud, 1989; Wu et al., 1990; Fernandez-Ballester et al., 1992; Aslanian, Grof, Galzi and Changeux, 1993; Baenziger et al., 1993; Butler and McNamee, 1993) but contradict the interpretation of Castresana et al. (1992) and Fernandez-Ballester et al. (1994).

To test the effect of various membrane lipids on the secondary structure of the nAChR, an analysis similar to that presented above was performed with the nAChR reconstituted in either EPC:DOPA:CH (molar ratio of 3:1:1), EPC:DOPA (molar ratio of 3:1) or EPC membranes. Upon reconstitution into membranes lacking cholesterol and anionic lipids, the nAChR adopts a channel-inactive conformation that may be analogous to ligand-induced desensitization (McCarthy and Moore, 1992). The rate and extent of $^{1}H/^{2}H$ exchange in the nAChR reconstituted into EPC:DOPA membranes (figure 3.6b) is not different than that upon EPC:DOPA:CH reconstitution. Likewise, deconvolved amide I bands of the nAChR in EPC:DOPA membranes (figure 3.7d, center spectrum) do not exhibit any noticeable changes supporting no large structural rearrangement. However, a reproducible increase in both the rate and extent of the $^{1}H/^{2}H$ exchange was observed for the nAChR reconstituted into membranes lacking cholesterol and anionic lipids (figure 3.6b, open circle curve). Close examination of the extent of $^{1}H/^{2}H$ exchange in the nAChR revealed a smaller amount of unexchanged peptides in those samples, by roughly 5% to 10%. Also, the deconvolved amide I' band exhibited a decrease in intensity at 1655 cm^{-1} and an increase in intensity at 1645 cm^{-1} (figure 3.7d,

top spectrum). This spectral change could reflect a conformational change in the nAChR in membranes lacking cholesterol and anionic lipids leading to the enhanced $^1H/^2H$ exchange. Alternatively, the spectral change in the amide I' band could reflect 5% to 10% enhanced level of $^1H/^2H$ exchange.

To address the effect of the membrane lipids on the nAChR secondary structure and dynamics and to explore the magnitude of the conformational changes upon desensitization, the spectral changes in the amide I' band were monitored as a function of time after exposure to ^2H_2O. Upon $^1H/^2H$ exchange, the vibration of the individual secondary structures downshifts in frequency, giving rise to spectral changes in the amide I' band. In addition, the time course of the spectral changes reflects the individual rate of exchange of the individual secondary structures and is sensitive to the nAChR structure and conformational changes. Most of the changes in shape of the amide I' band in ^2H_2O (decrease in intensity at 1655 cm^{-1} accompanied with an increase in intensity around 1640 cm^{-1}) occur within seconds of exposure and are associated with the exchange of unordered structures. The smaller changes in shape in the amide I' band between 3 min. and 12 h after exposure are due to the downshifts in the frequencies of α-helices and β-sheets and are very sensitive to any change in structure, dynamics or conformation (fig. 3.5b). The band shifts can be seen more clearly in exchange difference spectra calculated by subtracting the spectra recorded at various time points from the spectra recorded after 3 min of exposure to ^2H_2O (figure 3.8). Negative bands represent a decrease in intensity, while positive bands represent an increase in intensity. The band shift of α-helices is reflected by a negative band near 1660 cm^{-1} coupled with a positive

shoulder near 1645 cm^{-1}, while the band shift of β-sheet is reflected by the negative and positive bands near 1680 and 1630 cm^{-1}.

The exchange difference spectra calculated from spectra recorded in the presence and absence of Carb are similar. In both cases, the majority of peptides in β-sheets conformation exchange within the first 2 h of exposure whereas the α-helical structures exchange on a much lower time scale. The exchange difference spectra indicate that desensitization does not modify the kinetics of $^{1}H/^{2}H$ exchange of both α-helices and β-sheets in the first 12 hours and as suggested by the secondary structure analysis (figure 3.7 A,B) and the rates and extent of $^{1}H/^{2}H$ exchange presented above (figure 3.6, A), Carb does not induce a significant change in the structure or dynamics of the nAChR. The rates of the secondary structure components in the exchange difference spectra of the nAChR reconstituted in membranes made either of EPC:DOPA:CH or EPC:DOPA are similar, suggesting again that cholesterol is not required to stabilize the native secondary structure of the nAChR. In contrast, the rates of $^{1}H/^{2}H$ exchange recorded from the nAChR in EPC membranes reveal an increase in the negative and positive intensities of the 1660 and 1645 cm^{-1} bands, respectively, suggesting an enhanced exchange of otherwise exchange-resistant α-helical peptides. Similarly, resolution-enhanced spectra ecorded after 3 days of exposure showed an increase in the extent of exchange of α-helical peptides (figure 3.6b). These results suggest that the spectral changes in the amide I' band upon reconstitution in EPC membranes are caused by an increase in the level of $^{1}H/^{2}H$ exchange and not by a change in the secondary structure of the nAChR as reported previously (Fong and McNamee, 1987; Bhushan and McNamee, 1993; Butler and McNamee, 1993 and Fernandez-Ballester et al., 1994).

Figure 3.8 Exchange difference spectra showing the spectral changes that occur in the amide I' band upon exposure of the nAChR to ^2H_2O. In each case, the spectrum recorded after 3 min of exposure to ^2H_2O was subtracted from spectra recorded after 6, 9, 16, 40, 80, 600 and 780 min of exposure to ^2H_2O. All spectra were baseline corrected between 1811 and 1600 cm^{-1}. (A) nAChR in EPC/DOPA/Chol membranes in the molar ratio 3:1:1 in absence of ligand; (B) nAChR in EPC/DOPA/Chol membranes in the molar ratio 3:1:1 in the presence of 1 mM Carb; (C) nAChR in EPC/DOPA membranes in the molar ratio 3:1 in the absence of ligand; and (D) nAChR in DOPC membranes in the absence of ligand. Bottom panel: superposition of the exchange difference spectrum calculated at 12h for the nAChR in DOPC (solid line) over the same difference spectrum recorded from the nAChR in DOPC/DOPA/Chol (dashed line).

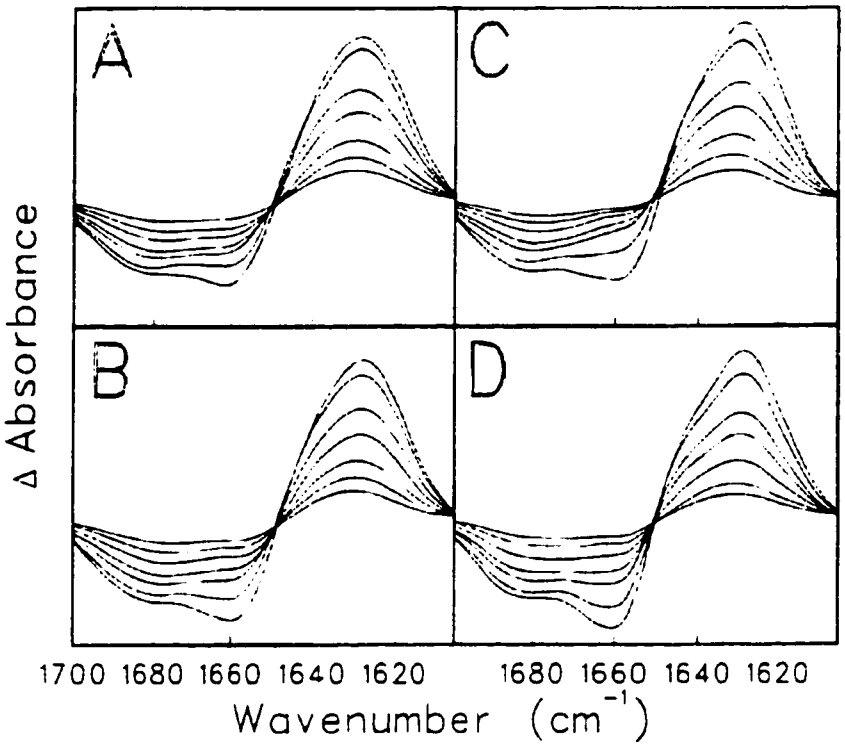
A
C
B
D
Δ Absorbance
1700 1680 1660 1640 1620
1680 1660 1640 1620
Wavenumber (cm⁻¹)

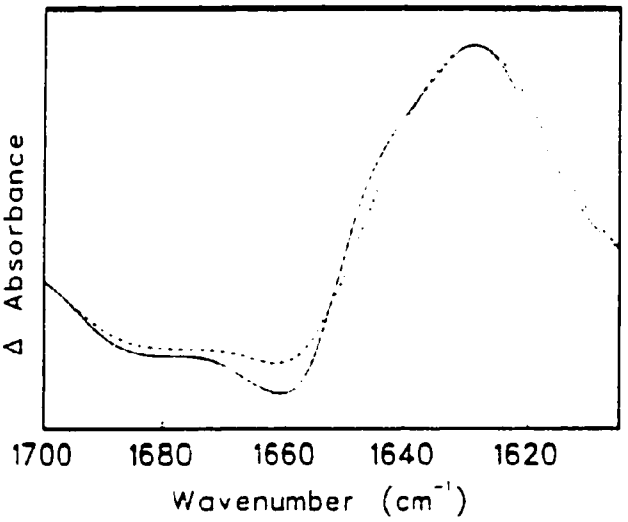
Δ Absorbance
1700
1680
1660
1640
1620
Wavenumber (cm⁻¹)

In order to further test if the decrease in intensity at 1655 cm^{-1} in the amide I' band of the nAChR in EPC is due to the enhanced $^1H/^2H$ exchange, the spectral changes observed in the resolution-enhanced amide I' bands after 3 days of exposure were compared with the spectral changes in spectra of the nAChR in EPC:PA:CH recorded after 2 and 12 h of exposure to ^2H_2O. As shown by the amide II bands in figure 3.9a, an additional 10% of the hydrogen peptides in the nAChR exchanges in the nAChR in EPC compared to the nAChR in EPC:DOPA:CH. Similarly, the extent of $^1H/^2H$ exchange in the nAChR in EPC is roughly 10% enhanced from 2 to 12 h. The spectral differences between the resolution-enhanced amide I band for the nAChR in EPC:DOPA:CH relative to the nAChR in EPC spectra (figure 3.9c) are very similar to the differences observed between spectra of the nAChR in EPC recorded during the 2^{nd} relative to the 12^{th} h of exposure to ^2H_2O (figure 3.9d). Since these latter changes are due exclusively to an enhanced level of $^1H/^2H$ exchange, it can be concluded that the increase in the rates and extent of peptide $^1H/^2H$ exchange observed in EPC is responsible for the spectral changes observed in the resolution-enhanced amide I band of the nAChR in EPC. This supports no major change in secondary structure in the nAChR in EPC membranes but likely an increase in the dynamics of the receptor and possibly an increased accessibility of the transmembrane α-helices to ^2H_2O as a result of an increase in the "fluidity" and thus the permeability of the EPC bilayers.

Figure 3.9 Comparison of the differences between absorbance and Fourier deconvolved spectra of the nAChR reconstituted into EPC/DOPA/Chol membranes in the molar ratio 3:1:1 and in EPC membranes with the differences in spectra of the nAChR in EPC membranes recorded after 2 and 12 h after exposure to ^2H_2O. (A) Absorbance and (C) Fourier-self deconvolved spectra of the nAChR in EPC/DOPA/Chol membranes (dashed line) and in EPC membranes (solid line) both after 3 days exposure to ^2H_2O at 4°C. (B) Absorbance and deconvolved spectra of the nAChR in EPC membranes after 2 (dotted line) and 12 h (solid line) of exposure to ^2H_2O. The spectra are baseline corrected between 1800 and 1350 cm^{-1}. The two spectra in A and C are normalized according to the relative intensities of the amide I band. The spectra in B and D are not normalized.

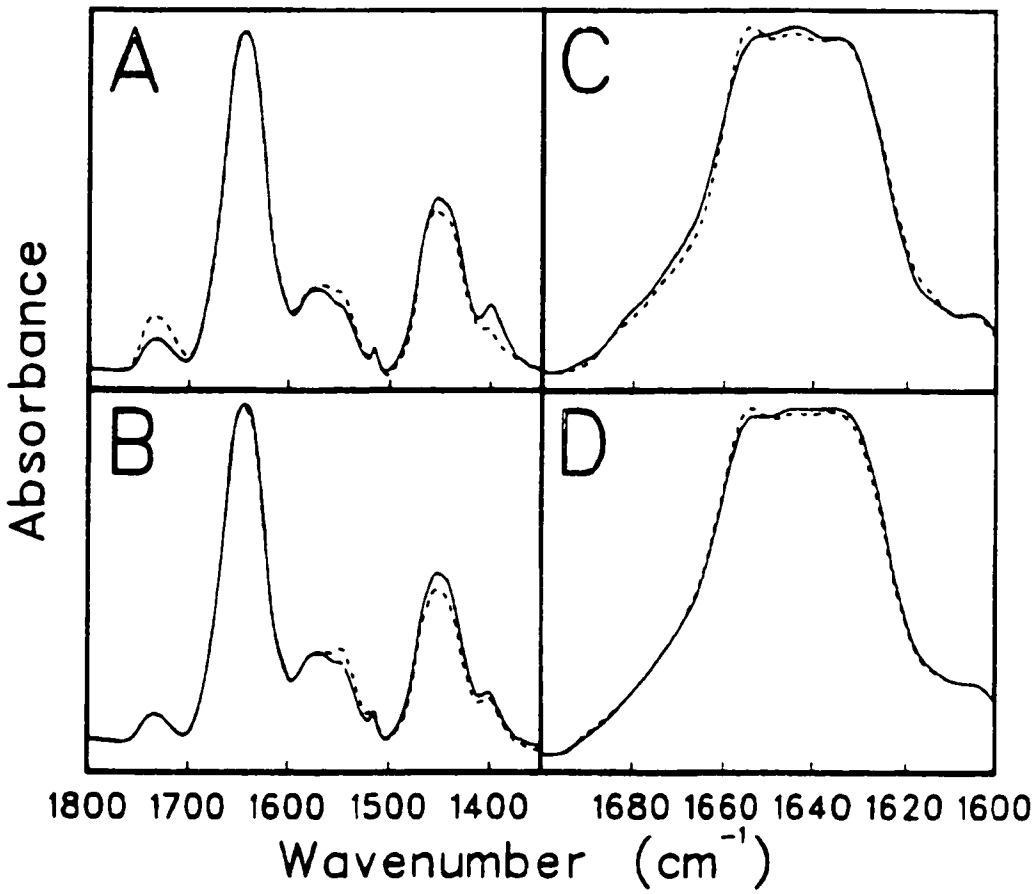
A
C
B
D
Absorbance
1800 1700 1600 1500 1400
1680 1660 1640 1620 1600
Wavenumber (cm^{-1})

5. Discussion

In absence of high resolution structural information on the nAChR, the secondary structure of affinity-purified nAChR was examined by analyzing qualitatively and quantitatively the secondary structure sensitive amide I band of FTIR spectra both in ^1H_2O and ^2H_2O buffer. The secondary structure of the nAChR was studied by several spectroscopic approaches before this work was started (table 1.2) however no consensus was reached regarding the proportion of the individual secondary structures. In particular, two of these studies (Fong and McNamee, 1987 and Mielke and Wallace, 1988), in conjunction with electron microscopy evidence, suggested a relatively low proportion of α-helices and a high proportion of β-sheets giving restrictions on the transmembrane topology models of the nAChR.

Our results suggest a higher α-helical content in the nAChR and a lower proportion of β-sheets. First, it is clear from the qualitative observation of the amide bands of FTIR spectra of the nAChR in both ^1H_2O and ^2H_2O that the nAChR has a substantial amount of α-helices. Both amide bands are narrow with maxima near 1654 and 1547 cm^{-1} and furthermore, resolution-enhancement of the amide I band reveals the important contribution of the 1655 cm^{-1} band. These observations are highly characteristic of α-helical proteins (Dousseau and Pézolet, 1990). Using a curve-fitting algorithm, the contribution of the secondary structures in the nAChR from the FTIR spectra was calculated. The estimations are the following: α-helices 39%, β-sheets 35%, unordered peptides 19% and β-turns 6%. Therefore, the results suggest that the nAChR is an α/β type of protein, with a majority of α-helices.

In order to accurately quantify the secondary structure of the nAChR, affinity purified, essentially pure nAChR samples, reconstituted into membranes supporting its functioning, were used. The spectra were recorded at a very high signal-to-noise ratio, and the presence of water vapours was examined carefully. Despite these precautions, the secondary structure estimates by curve fitting are possibly associated with up to 10% error due to the number of assumptions on which it is based, limiting its accuracy (Surewicz et al., 1993 and Jackson and Manstch, 1995). I am very much confident in a good proportion of α-helices in the nAChR, nonetheless, it must be kept in mind that the quantitative secondary structure estimates have a limited accuracy.

The estimated α-helical content of 39% is consistent with secondary structure analysis by Raman, CD and FTIR spectroscopy by Yager et al. (1984), Wu et al. (1990) and Castresana et al. (1992), although Yager et al. (1984) used non-functional nACh.. Recently, West et al., 1997 have re-interpreted the spectra of Mielke and Wallace (1988) as containing 48% of α-helices.

The results agree with the studies of Wu et al. (1990) and Castresana et al. (1992) regarding the prediction of α-helical content in the nAChR, however they contradict their estimation of the proportion of β-sheets, which is 20% and 48% respectively. Note that the proportion of β-sheets estimated from the CD spectra of Wu and co-workers varies significantly depending on the way the analysis is performed (see table 1). In addition, Wu et al. (1990) and Castresana et al. (1992) predict 30% and 0%, respectively, of unordered structures. I am confident in the presence of both β-sheets and unordered structures since in resolution-enhanced amide I bands, an important and well resolved spectral contribution around 1635 cm^{-1} is attributed to β-strands. A visual comparison of

the width and intensity of the 1635 cm^{-1} band in the amide I' band (figure 3.3) with the 1655 cm^{-1} band support a substantial amount of both α-helices and β-sheets in the nAChR with a higher proportion of α-helices. The important and rapid change in shape of the amide I' band following exposure to ^2H_2O accompanied with an increase in intensity at 1644 cm^{-1} supports a population of unordered structures in the nAChR, which was estimated to be roughly 20%. The discrepancy in the detection of unordered structures in the nAChR between this study and Castresana's et al. (1992) is likely due to two factors. First, their secondary structure analysis was performed solely in ^2H_2O and as stated above, the presence of unordered structures is well identified upon rapid spectral shift from 1655 cm^{-1} in ^1H_2O to 1644 cm^{-1} in ^2H_2O. Second, the spectra presented here were recorded at a very high signal-to-noise ratio permitting the use of substantially less smoothing (resolution enhancement factor of 2.4) compared to Castresana et al. (1992) (resolution enhancement factor of 1.8-2.0). Consequently, a better resolution of the peaks is achieved.

FTIR spectra of native nAChR membranes provide further support for a large proportion of α-helices (32-33%) in the nAChR but with a higher amount of β-sheets (36-43%) (Naumann et al., 1993). However since these samples contain only 25-50% nAChR protein by weight (Schieber and Hucho, 1978), the secondary structure predictions represent a significant amount (50-75%) of contaminating proteins which may explain the differences in the estimations.

The secondary structure predictions differ significantly from the analyses of those of McNamee's group (Fong and McNamee, 1987; Butler and McNamee, 1993), Mielke and Wallace (1988) and Aslanian et al. (1993). In the first FTIR report by Fong and

McNamee (1987) the secondary structure predictions were based on the analysis of the amide III band. The correlation of the weak skeletal stretching vibrations of the amide III band with secondary structure is not clear and in addition, the spectral subtraction of the overlapping lipid contribution in that region may distort the analysis. The second FTIR report of McNamee's group (Butler and McNamee, 1992) presents FTIR spectra recorded at a low signal-to-noise ratio (100 scans at 4 cm^{-1} of resolution). In addition, the spectra contained visible water vapour bands which were assigned to protein structures in the curve-fit analysis. Finally, the validity of circular dichroism for studying membrane proteins is questioned due to the scattering of light produced by the lipid bilayer. In addition, according to Wu et al. (1990) and West et al. (1997), the helical content estimated by Mielke and Wallace (1988) is rather low for $[\theta]_{222}$ of −17 200.

The magnitude of the conformational changes in the nAChR in the ligand- and lipid-induced inactive conformations is unclear. Several studies by CD and FTIR spectroscopy did not detect any large structural rearrangement in the nAChR upon Carb-induced desensitization (Meilke and Wallace, 1988; McCarthy and Stroud, 1989; Wu et al., 1990; Fernandez-Ballester et al., 1992; Butler and McNamee, 1993; Aslanian et al., 1993). In addition, FTIR difference spectroscopy supports conformational changes in the nAChR upon desensitization at the amino acid level (Baenziger et al., 1993). In contrast, important changes in the nAChR secondary structure have been reported in the presence of Carb (Castresana et al., 1992; Fernandez-Ballester et al., 1994) and upon reconstitution in membranes lacking cholesterol and anionic phospholipids (Fong and McNamee, 1987; Butler and McNamee, 1993; Fernandez-Ballester et al., 1994).

In order to clarify the structural changes in the channel inactive states of the nAChR and provide a better understanding of the mechanism of desensitization, FTIR spectra of affinity-purified nAChR were recorded as a function of time after exposure to ^2H_2O, for a period of 12 hours and after 3 days of exposure. The rate and extent of $^1H/^2H$ exchange are sensitive to structural changes and have previously detected changes in protein conformation (Goormaghtigh, Vigneron, Scarborough and Ruysschaert, 1994b; Rath et al., 1998). Different groups of peptide hydrogens in the nAChR were identified according to their $^1H/^2H$ exchange rates. First, the fast exchanging ones are likely solvent accessible and hydrogen bonded to solvent; second, the slow exchanging ones are less solvent accessible and involved in ordered secondary structures and third, the very slowly exchanging ones appear solvent inaccessible and likely located in the hydrophobic environment of the bilayer. The presence of Carb or Tet did not produce any variation in the rate and extent of $^1H/^2H$ exchange. Any important conformational change in the nAChR upon desensitization would be detected by monitoring the rate of $^1H/^2H$ exchange of the individual secondary structure components. The exchange difference spectra which allow a close examination of the spectral downshift in the amide I band were unchanged in the presence of Carb or Tet. Additional support for the minor effect of Carb and Tet on the nAChR structure in FTIR spectra recorded after prolonged exposure to ^2H_2O for 3 days and 4°C. These spectra were recorded at high signal-to-noise ratio which allow the use of resolution-enhancement procedures such as spectral deconvolution in order to better resolve the spectral components. Again, both absorbance and resolution-enhanced amide bands were essentially identical in the presence or absence of Carb and Tet. Taken together, the results suggest a lack of change in

secondary structure, dynamics or solvent exposure in the nAChR upon binding of desensitizing agents. However, the possibility of a conformational change which does not involve a modification of the solvent accessibility of the nAChR cannot be ruled out. For example, it was suggested that the increase in ligand binding affinity in the desensitized state could involve a localized conformational change in the ligand binding site (Galzi et al., 1991). This localized conformational change would not necessarily modify the secondary structure or $^{1}H/^{2}H$ exchange kinetics of the nAChR and therefore would not be detected in the experiments.

Using FTIR spectroscopy, both Castresana et al. (1992) and Fernandez-Ballester et al. (1994) interpreted spectral change in the amide I band of the nAChR in the presence of Carb as a conformation change upon desensitization. As reported above, important spectral changes in the amide I band of the nAChR are observed in the first 12 hours of exposure to $^{2}H_2O$ and are indicative of $^{1}H/^{2}H$ exchange and are highly similar to the spectral changes reported by Castresana's and Fernandez-Ballester's groups. Prior to recording their FTIR spectra in $^{2}H_2O$, both groups prepared their nAChR samples in $^{2}H_2O$ by "submitting the samples to at least two centrifugation-resuspension cycles in $^{2}H_2O$ buffer". This process is likely not sufficient to complete the $^{1}H/^{2}H$ exchange of solvent accessible groups and therefore, the spectral changes they report are likely due to changes in $^{1}H/^{2}H$ exchange.

The same experiments as reported above have been performed on affinity-purified nAChR reconstituted in membranes of EPC:DOPA:Chol, EPC:DOPA and EPC in order to investigate the effect of lipids on the nAChR structure. More precisely, I wanted to investigate the role of cholesterol in supporting the physiological structure of the nAChR

given that several reports suggested an absolute structural requirement for cholesterol (Fong and McNamee, 1987; Butler and McNamee, 1993 and Fernandez-Ballester et al., 1994). The decrease in intensity of the amide II band in the first 12 hours of exposure to ^2H_2O, the rate of exchange of the secondary structure components and the shape of the amide I' band after prolonged exposure were all unaffected by the absence of cholesterol in the EPC:DOPA membranes. In contrast, the lack of both cholesterol and anionic phospholipids caused a detectable change in the rate and extent of $^1H/^2H$ exchange and a slight change in the amide I' band after prolonged exposure. These results can be interpreted in two ways. First, the absence of both cholesterol and DOPA causes a conformational change in the nAChR as revealed in the amide I' band and resulting in a modification of the exchange kinetics. Alternatively, since cholesterol is known to increase the ordering of the lipid bilayers (Smith, 1984), its absence could cause an increase in the membrane "fluidity" responsible for the increase in the $^1H/^2H$ exchange and spectral changes. To better interpret the results, exchange difference spectra which highlight the changes in the amide I band in the first hours of exposure to ^2H_2O were calculated. These spectra directly probe the spectral changes in the amide I' band upon $^1H/^2H$ exchange and are also sensitive to change in conformation. The exchange difference spectra of the nAChR in EPC membranes revealed a decrease in intensity around 1660 cm^{-1} accompanied with an increase around 1645 cm^{-1}. A similar spectral shift is observed in the amide I' band after prolonged exposure to ^2H_2O. This downshift in frequency is highly characteristic of enhanced $^1H/^2H$ exchange of α-helices and may not reflect a change in secondary structure of the nAChR.

Changes in the secondary structure of the nAChR have been reported in absence of cholesterol and/or DOPA (Fong and McNamee, 1987; Butler and McNamee, 1993; Fernandez-Ballester et al., 1994). I believe that the interpretation of the results in those studies was influenced by varying levels of $^{1}H/^{2}H$ exchange (Fernandez-Ballester et al., 1994), a low signal-to-noise ratio and high levels of water vapours (Butler and McNamee, 1993), a low correlation of the amide III band with secondary structure and importantly, overlap with lipid contributions in the amide III region (Fong and McNamee, 1987).

6. Conclusion

The secondary structure of the nAChR was investigated through the analysis of the secondary structure sensitive amide I band. The qualitative analysis supports the presence of both α-helices and β-sheets in the nAChR with a high proportion of α-helices. The quantitative analysis by curve fitting suggest roughly 40% of α-helices, 35% β-sheets, 20% unordered structures and 6% β-turns. These results are consistent with the transmembrane topology model of the nAChR including 4 transmembrane α-helices per subunit. This would account for roughly 20% of transmembrane α-helices in the nAChR since each of the 20 putative segments is roughly between 25-30 amino acid residues in length.

According to the analysis of the amide I band and $^{1}H/^{2}H$ exchange kinetics, the nAChR does not experience a large secondary or tertiary structure change upon ligand

and lipid induced desensitization. The results therefore support small localized changes in structure in the desensitized state.

The $^{1}H/^{2}H$ exchange kinetics of the nAChR revealed a population of exchange resistant hydrogen peptides representing roughly 25% of the protein and likely located in the solvent inaccessible environment of the lipid bilayer. In addition, after prolonged exposure to $^{2}H_2O$, the amide I band displayed a remaining intensity at 1655 cm^{-1} indicative of a majority of transmembrane α-helices in the nAChR. These preliminary results, by providing insights into the secondary structure of the transmembrane domain of the nAChR, drove us to further investigate this controversial question.

Chapter 4- Secondary Structure of the Channel Forming Transmembrane Segments of the nAChR

1. Introduction

A detailed picture of the spatial organization of the transmembrane segments in the nAChR is crucial for the elucidation of the mechanism of channel gating, but is still missing. Initially, hydrophobicity analysis identified four hydrophobic segments in the nAChR, named M1, M2, M3 and M4, assigned to four transmembrane α-helices. Several investigations attempted to determine the secondary structure of the transmembrane segments in the nAChR, and at the present, the majority support the α-helical nature of the five M2 channel lining segments (Giraudat et al., 1987; Revah et al., 1990; Unwin, 1993; Akabas et al., 1994; Blanton and Cohen, 1994 and 1996). In contrast, the secondary structure of the M1, M3 and M4 segments is still controversial. Both M3 and M4 exhibit an α-helical exposure of photoactivatable hydrophobic probes to the lipid bilayer, while the labeling of M1 correlates with a slightly distorted α-helix, due to the presence of a proline residue (Blanton and Cohen, 1994 and 1996). Site-directed mutagenesis experiments also support an irregular structure for the M1 segment which is partially exposed to the channel lumen (Akabas and Karlin, 1995). Recently, NMR spectroscopy reported an α-helical secondary structure for a synthetic peptide corresponding to the M3 transmembrane segment in the nAChR (Lugovsky et al., 1998). West et al. (1997) probed the structure of the N-terminal extracellular domain of the nAChR by CD spectroscopy and estimated 12% α-helix, 51% β-sheets, 18% β-turns and

20% of irregular structure. These results, in conjunction with those presented in chapter 3, support a majority of transmembrane α-helices in the nAChR.

Even though the great majority of membrane proteins have α-helical transmembrane segments, the presence of transmembrane β-strands was proposed in the nAChR. In a CD study, Mielke and Wallace (1988) identified a relatively low amount (20%) of α-helices, insufficient for both transmembrane and extramembraneous helices. Also, on the electron micrographs, Unwin (1993) observed a diffuse pattern of electron density in the periphery of the ion channel assigned to five or seven transmembrane β-strands. The presence of both α-helices and β-sheets in the transmembrane domain of the nAChR was also suggested based on FTIR spectra of proteolysed nAChR (to remove the extramembraneous domains) and molecular modeling studies (Görne-Tschelnokow et al., 1994; Ortells and Lunt, 1996).

Hydrogen-deuterium experiments on the nAChR exhibit changes in the shape of the amide I band as a result of the isotopic exchange of peptide hydrogen for deuterium. In addition, the intensity of the amide II band correlates with the degree of exchange in the nAChR and showed that after prolonged exposure to ^2H_2O, roughly 25% of the hydrogen peptides are left unexchanged. These appear to be a large number of exchange resistant α-helices due to the strong intensity remaining at 1655 cm^{-1} after prolonged exposure to ^2H_2O, typical of unexchanged α-helices, and are likely located in the solvent inaccessible hydrophobic environment of the bilayer. The first goal of this chapter is to further examine the secondary structure of the exchange resistant core of the nAChR and gain insights into the secondary structure of the transmembrane domain.

Nondenaturing alkaline exchange conditions that led to the exchange of most of the "25%" exchange-resistant peptide hydrogens confirmed the presence of a large proportion of exchange resistant α-helical peptides in the nAChR. In contrast, the data suggest few, if any, exchange resistant β-strands. Since the 25% exchange-resistant hydrogen peptides is highly α-helical, this data support an essentially α-helical secondary structure for the M1-M4 transmembrane segments.

The second goal of this chapter was the isolation of the transmembrane domain of the nAChR and secondary structure characterization by FTIR spectroscopy. Two approaches have been taken to achieve this objective. First, I used various proteolytic enzymes (proteinase k, trypsin and pronase) to digest the extramembraneous domains of affinity-purified nAChR. Secondly, as a collaborative project with Dr. Michael Blanton, using FTIR spectroscopy, I investigated the secondary structure of the transmembrane segment M4 from the γ subunit (γ-M4) and a fragment containing the transmembrane segments M2 and M3 from the β-subunit, both purified at Texas Tech University. Both approaches support a high percentage of α-helices in the transmembrane segments of the nAChR.

2. Experimental procedures

2.1 nAChR purification from *Torpedo californica*

Please refer to section 2.1 of chapter 3 for a complete description of the affinity purification of the nAChR.

2.2 Proteolysis of the nAChR and 16.5% Tris-Tricine SDS-PAGE

2.2.1 Proteolysis

In the first set of experiments, the nAChR was proteolyzed with 1:1 (proteinase k/nAChR w/w ratio) proteinase K (serine endopeptidase cleaving primarily after the carboxyl group of N-substituted hydrophobic amino acids), at 37 °C in incubation buffer for 24 h. After 3 and 7 h, the same amount of enzyme was added to maximize the degradation of extramembraneous domains. An aliquot of the mixture was removed and proteolysis was inhibited by 5 mM PMSF. The incubation mixture was agitated for 1 h on ice in 1 M NaCl to remove aggregated peptides. The membrane fraction was collected by centrifugation at 100 000 g for 1 h (Görne-Tschelnokow et al., 1994). A ratio of 0.05:1 (tryspin/nAChR w/w ratio) of trypsin (serine endopeptidase hydrolyzing specifically the carboxylic side of the basic amino acids Arg and Lys) was added to a second aliquot and 0.05:1 (pronase/nAChR w/w ratio of pronase (mixture of several unspecific endo and exopeptidases generally digesting proteins down to single amino acids) was added to a third aliquot and both reactions were incubated for 1 h at 37°C. The reactions were stopped and the nAChR was collected as described above.

In a second set of experiments, the nAChR membranes were disrupted first by incubation for 24 h either in 1 M sucrose or in the presence of 0.01% saponin (plant glycoside that form holes in membranes), and then, microcentrifuged and resuspended in incubation buffer (50 mM phosphate, 150 mM KCl, pH 8.0). The nAChR was

subsequently incubated with 0.05:1 (pronase/nAChR w/w ratio) of pronase for 24 h. The reactions were stopped and the nAChR was collected as described above.

2.2.2 16.5% Tris-Tricine SDS-PAGE

Peptidic fragments of the nAChR were treated prior to loading on the gel, first 10-20 μl aliquots containing roughly 20 μg of sample were mixed with 2% SDS (trace amount) and dried under N_2 (g). The dry samples were redissolved in 20 μl trifluoroacetic acid (TFA) and TFA was evaporated under N_2 (g). Samples were put on ice and mixed with 20 μl cold sample buffer (Hennessey and Scarborough, 1989) and separated using a discontinuous Tris-Tricine 16.5% separating, 10% spacer and 4% stacking gel (with 3% of crosslinker) according to Schägger and von Jagow (1987). These gels are designed for superior resolution of peptides and small proteins for the range from 1 to 70 kDa. The ability of this method for resolving proteins in the 5 to 30 kDa range is based mainly on the introduction of tricine as the trailing ion. The gels were stained by Coomassie Blue.

2.3 Preparation of proteolytic fragments γ-M4 and β-8K of the nAChR

Two fragments of the nAChR were prepared at Texas Tech University by John Corbin and Michael Blanton and sent to us for FTIR analysis. For details of the procedure, please refer to Corbin et al. (1998). One fragment, γ-M4, contains the transmembrane segment M4, it corresponds to residue 446 to 485 of the γ-subunit and has the following primary sequence: VIDKACFWIALLLFSIGTLAIFLTGHFNQVPEF-

PFPGDPR, where the underlined residues are though to be membrane located. This fragment is roughly 5 kDa in size. The other fragment, the β-M2-M3 segment, corresponds to residue 249 to 307 of the β-subunit and has the following primary sequence: MSLSISALLAVTVPLLLLANKAPETSLVPIINYLMPIMILVAPSVILS-VVVILNLHH and is roughly 8 kDa in size.

2.4 FTIR spectroscopy

FTIR spectra were acquired either on a Bio-Rad FTS-40 or on a Bio-Rad FTS-40A spectrometer equipped with either a mercury cadmium telluride or a deuterated triglycine sulfate detector for transmission and attenuated total reflectance (ATR) measurements, respectively. Each spectrometer was purged with dry air (dew point, 100°C) from a separate Balston air-dryer. The ATR crystals were cleaned before use by soaking in chromic acid for 30 minutes and then rinsed thoroughly with distilled water. All spectra were recorded at 2 cm^{-1} resolution. Spectral deconvolution was performed according to the method of Kauppinen et al., 1981 with γ' (full width at half height) of 17.0 cm^{-1} and resolution enhancement factor of K = 2.2. Prior to deconvolution, all spectra were stringently examined for the presence of water vapor using the mild spectral deconvolution procedure described in Reid et al. (1996) and if present they were eliminated by spectral subtraction.

$^1H/^2H$ exchange. FTIR spectra were recorded during the time course of peptide $^1H/^2H$ exchange using the ATR technique. An aliquot of reconstituted nAChR was carefully spread and dried on the surface of the germanium element as described above,

however, the sample was rehydrated with ^1H_2O TR buffer after mounting the reflection element in the ATR cell. After purging the water vapours, a spectrum averaging 256 scans was recorded. Then, the ^1H_2O buffer was removed and ^2H_2O buffer, pH 7.0 was added into the ATR cell. As soon as the ATR cell was filled with ^2H_2O (roughly 1 minute), FTIR spectra were automatically recorded over a period of 12 hours with increasing number of scans (varying from 50 to 1500 scans/spectrum).

To record spectra under conditions of "extensive" peptide $^1H/^2H$ exchange, the nAChR samples were first exposed to ^2H_2O for 3 days at 4 °C, pH 7.0, to exchange roughly 75% of the hydrogen peptides. The nAChR samples were then deposited on the surface of the reflection element as described above and rehydrated with TR buffer in ^2H_2O at the appropriate pH (50 mM CAPS buffer was used above pH 9.0), and further incubated for an additional 20 h while FTIR spectra averaging 1500 scans/spectrum were recorded.

Thermal denaturation. 125 μg of nAChR samples pre-incubated in ^2H_2O for 3 days at 4 °C were centrifuged and resuspended in ^2H_2O buffer at the noted pH before deposition on the surface of a CaF_2 window. The nAChR samples were carefully dried with a gentle stream of nitrogen and rehydrated with 10 μl of ^2H_2O buffer at the noted pH. FTIR spectra were recorded upon increases in temperature using a thermostatically controlled transmission cell. Spectra averaging 256 scans were typically recorded at 2-4°C intervals between 25-75°C. The nAChR was equilibrated for roughly 15 min at each temperature before data acquisition. The melting temperatures taken from the thermal denaturation curves are reported as the mean ± standard error. They represent the average of three experiments except for the denaturation experiment at pH

11.0 for the nAChR in asolectin which is the average of two experiments and is reported as the mean ± range.

Secondary structure of the transmembrane segments. The isolated transmembrane segments of the nAChR were deposited on the surface of the reflection element as described above, but much smaller aliquots of sample (as little as 50 μg) were used due to the limited amount available. FTIR spectra averaging 256 scans were recorded in the dry state and upon rehydration with ^1H_2O and ^2H_2O TR buffer vapours by flushing N_2 (g) in the plastic tubing connected to the ATR cell where a small amount of buffer (100-200 μl) was deposited.

3. Results

3.1 Secondary structure of the exchange resistant core of the nAChR

As presented in chapter 3, FTIR spectra of affinity-purified nAChR reconstituted in EPC/DOPA/Chol membranes recorded as a function of time after exposure to ^2H_2O buffer reveal a number of spectral changes associated with the isotopic exchange of peptide hydrogens for deuterium. These changes include a decrease in intensity of the amide II band which is correlated with the level of exchange of the nAChR. After prolonged exposure (3 days, 4°C and pH 7.0), a substantial amount of peptides are left unexchanged. The subtle spectral changes in the amide I band represent the downshift in frequency of secondary structure components as they exchange for deuterium. In the first 12 hours of exposure, a decrease in intensity at 1655 cm^{-1} is observed, coupled to an

increase in intensity around 1630 cm^{-1}. Similar downshifts in frequency have been observed for numerous proteins and assigned to the downshift of both α-helices and β-sheets (Susi et al., 1967; Olinger, Hill, Jakobsen and Brody, 1986; Haris, Lee and Chapman., 1986; Baenziger and Chew, 1997).

The presence of a remaining intensity at 1655 cm^{-1} after 3 days of exposure of the nAChR to ^2H_2O supports the presence of unexchanged α-helices. Those exchange resistant α-helical hydrogen peptides are likely located in the solvent inaccessible hydrophobic environment of the lipid bilayer. In order to quantitatively determine the level of unexchanged peptides in the nAChR after 3 days of ^2H_2O exposure, I first established the exchange conditions necessary to yield a complete exchange in the nAChR. Several factors influence the rates and extent of $^1H/^2H$ exchange such as prolonged exposure, increased pH, increased temperature and membrane "fluidity". The effect of increasing the incubation time, temperature and pH and also the effect of detergents on the $^1H/^2H$ exchange level were tested. We achieved complete exchange under the following exchange conditions: first, incubation for 3 days at 4 °C and pH 7.0 to exchange a majority of hydrogen peptides and then 1 hour at 95 °C and pH 11.0. Figure 4.1 compares the intensity and area of the amide II band for the nAChR in ^1H_2O (short dashed line), after 3 days of exchange (solid line) and upon complete exchange (long dashed line). Spectra in "a" were recorded at pH 7.0 and spectra in "b" were recorded at pH 2.0 in order to upshift the absorption of carboxylic acids residues which absorb around 1580 cm^{-1}, overlapping significantly with the amide II band. Comparison of either the intensity or area of the residual amide II band in the various spectra

Figure 4.1 ATR-FTIR spectra of the nAChR in asolectin membranes showing varying levels of $^{1}H/^{2}H$ exchange. Spectra were recorded at pH 7 (A) or pH 2 (B) in either $^{1}H_2O$ (dashed line), after exposure to $^{2}H_2O$ for 3 days at 4°C, pH 7.0 (solid line), 6 h in $^{2}H_2O$ at 60°C (short/long dashed line), 1 h at pH 11.0, 95°C (long dashed line). All spectra were baseline corrected between 1800 and 1350 cm^{-1} and were normalized by either comparing the intensity of the tyrosine vibration near 1516 cm^{-1} or qualitatively assessing the intensity of the amide I band.

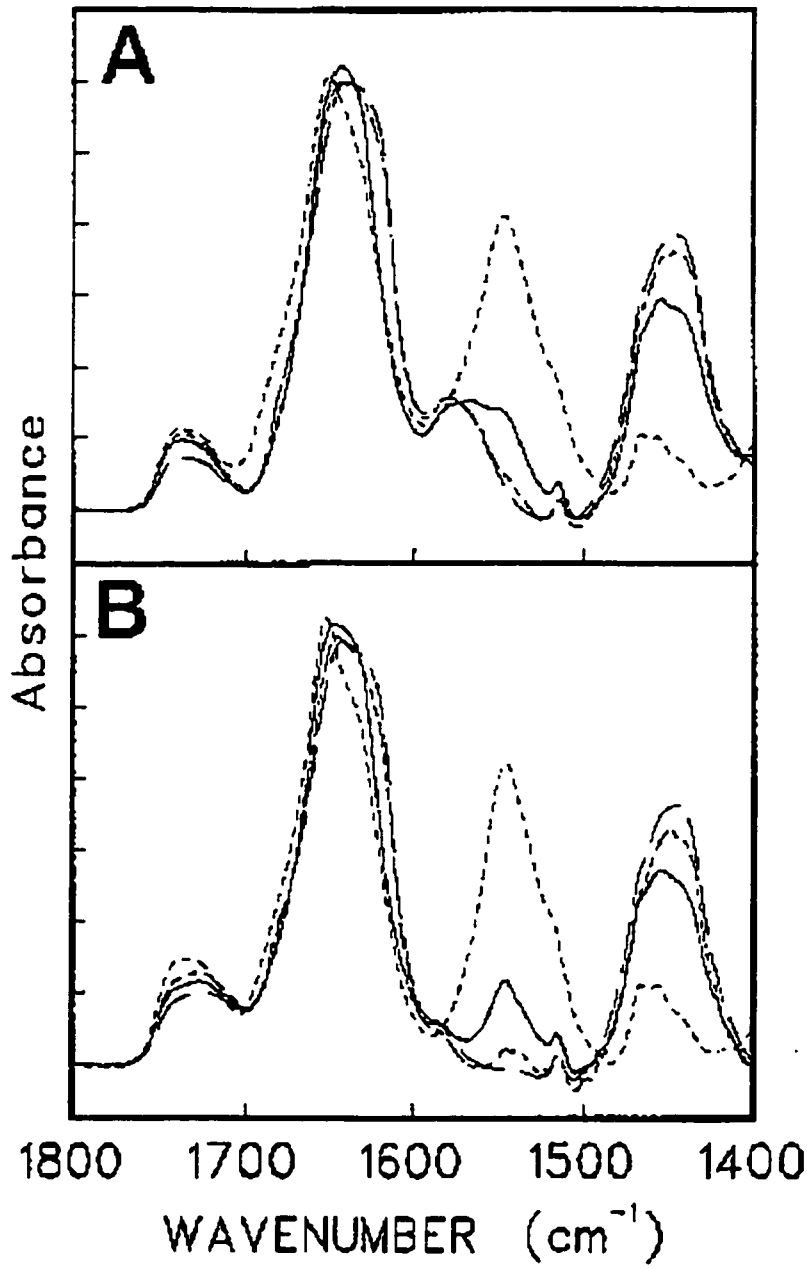
A
B
Absorbance
1800
1700
1600
1500
1400
WAVENUMBER (cm⁻¹)

presented in figure 4.1 indicates that after 3 days of exposure in ^2H_2O (solid line spectrum), roughly 25% of the protein is unexchanged. This estimation correlates well with the 25-30% of the nAChR located in the membrane by electron microscopy (Unwin, 1993) and the 20-25% of peptides predicted to form transmembrane helices by hydrophobicity plots (Noda et al., 1983 and Claudio et al., 1983). The exchange difference spectra of the nAChR, presented in chapter 3, calculated by subtracting the spectrum recorded after 3 min of exposure to ^2H_2O from those recorded at the various times emphasize the spectral changes in the amide I band in the first 12 hours of $^1H/^2H$ exchange. Careful examination of the time course of the spectral changes in both the resolution-enhanced and exchange difference spectra of the nAChR in EPC/DOPA/Chol membranes in the absence of ligands revealed distinct kinetics of $^1H/^2H$ exchange for α-helices and β-sheets. The spectral changes suggest that most of the β-sheet peptides exchange within the first 2 hours of exposure whereas most α-helical peptides exchange between 2 and 12 hours. In addition, the intensity of the exchange difference bands reflecting the $^1H/^2H$ exchange of α-helices is much smaller than those due to the exchange of β-sheets. Moreover, the remaining intensity at 1655 cm^{-1} suggests the presence of a population of unexchanged α-helices. All the above observations in conjunction with the CD spectroscopy results of West et al. (1997), which suggested a majority of β-sheets in the extracellular N-terminal domain of the nAChR, support the notion that the exchange resistant core of the nAChR is predominantly α-helical. Those exchange resistant peptides are likely located in the poorly solvent accessible, hydrophobic transmembrane domain of the nAChR.

To further investigate the secondary structure of the exchange resistant core of the nAChR, I hypothesized that if the $^{1}H/^{2}H$ exchange conditions were changed in order to increase the level of exchange in the nAChR, the spectral changes in the amide I band as a result of the higher extent of exchange would give insights into the secondary structure of the exchange resistant core of the nAChR. As presented above, increased temperature and pH increased the exchange rates of the nAChR. In addition, as seen in chapter 3, reconstitution of the nAChR into more fluid membranes such as EPC also accelerates peptide $^{1}H/^{2}H$ exchange. Before testing the effect of these physicochemical factors on the exchange kinetics of the nAChR and the resulting changes in the secondary structure sensitive amide I band, the effects of pH and membrane environment on the thermal stability of the nAChR were first examined. The objective was to establish nondenaturing exchange conditions for the enhanced $^{1}H/^{2}H$ exchange of the nAChR.

3.1.1 Thermal denaturation

Transmission-FTIR spectroscopy was used to perform thermal denaturation and identify melting temperatures of proteins (Dong, Prestrelski, Allinsom and Carpentier, 1995) including the nAChR (Fernandez-Ballester et al., 1992). The nAChR was preincubated in $^{2}H_2O$ for 3 days at 4 °C and then FTIR spectra were recorded at increasing temperature as shown in figure 4.2. The resulting spectra exhibit a number of spectral changes including a decrease in amide I intensity in the 1660-1630 cm^{-1} region coupled with the appearance of two bands: a weak band at 1680 cm^{-1} and an intense

Figure 4.2 Transmission-FTIR spectra showing thermal denaturation of the nAChR in asolectin membranes at pH 7.0 in ^2H_2O. (A) An FTIR spectrum was recorded roughly every 30 min with 3-4°C increments in temperature from 44 to 81°C (from top to bottom at 1650 cm^{-1}). (B) Same as in (A) after Fourier self-deconvolution using deconvolution parameters of γ' 17.0 and resolution enhancement factor of 2.2.

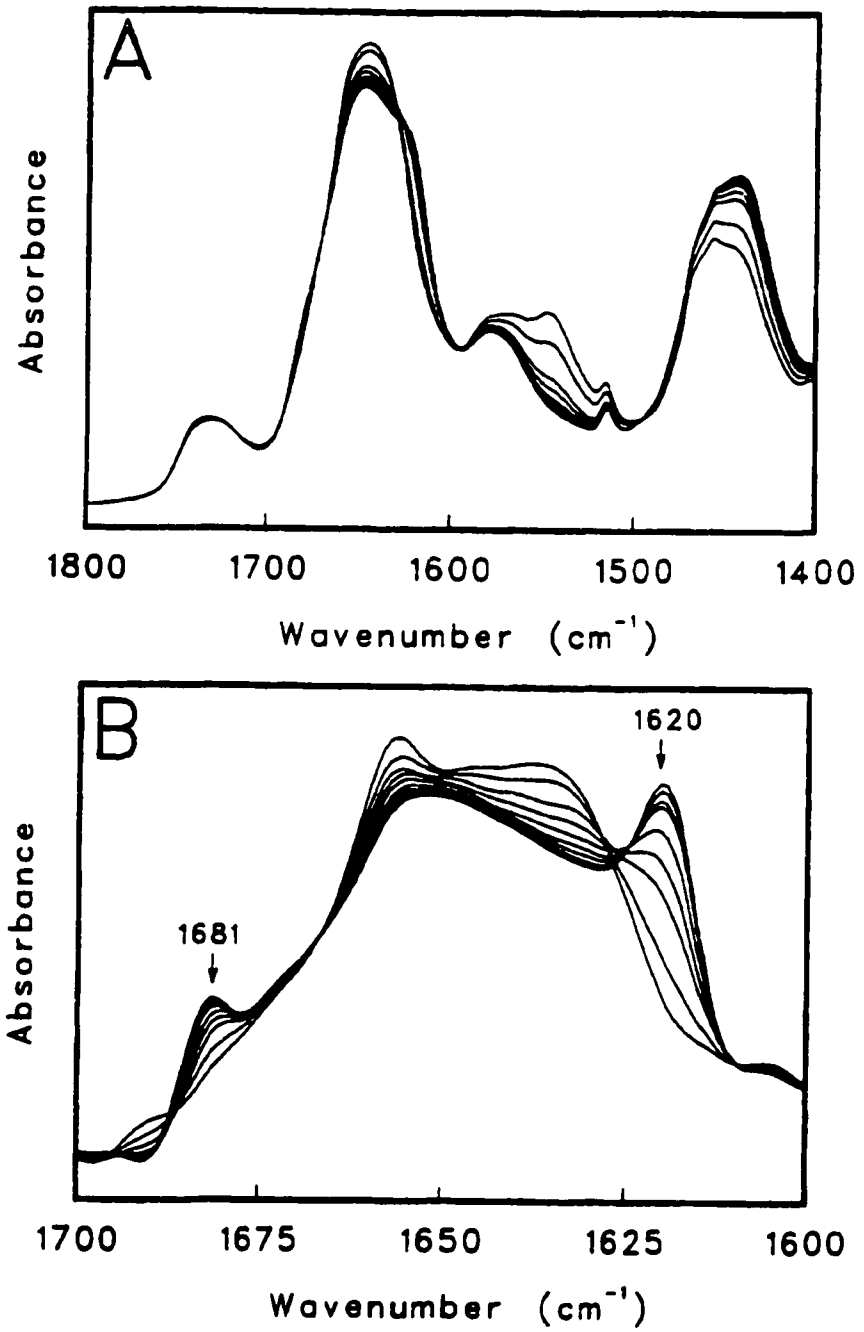
A
Absorbance
1800
1700
1600
1500
1400
Wavenumber (cm⁻¹)
B
1620
1681
Absorbance
1700
1675
1650
1625
1600
Wavenumber (cm⁻¹)

shoulder around 1620 cm^{-1} both highly characteristic of protein denaturation (Fernandez-Ballester et al., 1992; Dong et al., 1995; Knöle and Hübner, 1995). Spectral deconvolution enhances the spectral changes in the amide I band induced by temperature (figure 4.2b). In addition, elevated temperature leads to increase in the $^1H/^2H$ exchange as shown by the decrease in intensity of the amide II band.

A quantitative analysis of the increase in intensity near 1620 cm^{-1} induced by temperature reveals a sigmoidal melting curve with a melting temperature, T_m, of 57.3 ±1.1 °C for the nAChR in asolectin at pH 7.0 (figure 4.3), which is similar to the value reported for the nAChR in native membranes from studies using either differential scanning calorimetry or FTIR (Artigues, Villar, Ferraguet and Gonzalez-Ros, 1987 and Fernandez-Ballester et al., 1992). At pH 9.0, the measured T_m is 58.1 ± 1.6 °C for the nAChR in asolectin. This is similar to the value observed at pH 7.0, suggesting no perturbation in the thermal stability of the nAChR. In contrast, at pH 10.0 (data not shown) and above, T_m is significantly lower (T_m is 49.9 ± 2.0 °C for the nAChR in asolectin at pH 11.0). In the thermal denaturation experiment at pH 10.0, signs of denaturation were visible in the initial spectra suggesting the denaturation of a small percentage of the nAChR at room temperature. $^1H/^2H$ exchange experiments at pH >10.0 were only performed for comparison with studies conducted under nondenaturing conditions.

Reconstitution of the nAChR in EPC membranes lacking cholesterol and anionic phospholipids leads to a less thermally stable nAChR than upon reconstitution into asolectin. The T_m of the nAChR in both membranes are comparable at pH 7.0 (55.3 ±0.4°C in EPC), however the T_m of the nAChR in EPC at pH 9.0 is much lower (47.2

Figure 4.3 Thermal denaturation of the nAChR plotted as the percentage change in intensity at 1620 cm^{-1} versus increasing temperature. (Upper panel) nAChR in asolectin membranes at pH 7.0 (▲), pH 9.0 (■) and pH 11.0 (●). (Bottom panel) nAChR in EPC membranes at pH 7.0 (▲) and pH 9.0 (■).

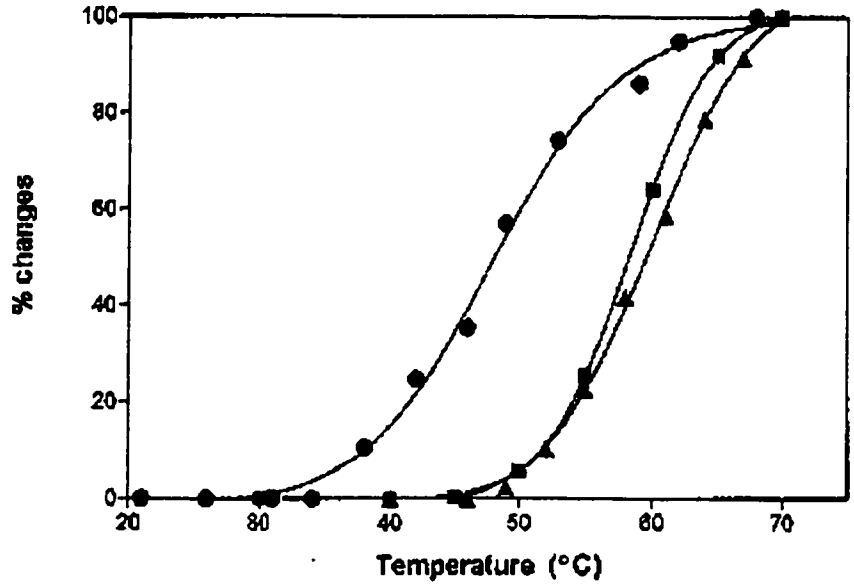
100
80
60
40
20
0
% changes
20
30
40
50
60
70
Temperature (°C)

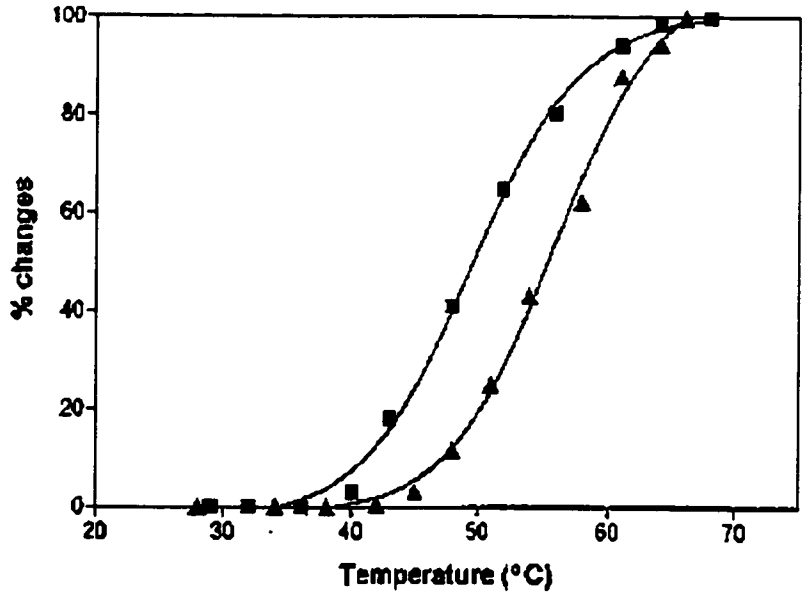
100
80
60
40
20
0
% changes
20
30
40
50
60
70
Temperature (°C)

± 2.2 °C) than that observed for the nAChR in asolectin (figure 4.3b). The initial spectra of the nAChR in EPC membranes at pH 9.0 recorded at the start of the thermal denaturation experiment do not exhibit spectral features indicative of thermal denaturation, suggesting that the nAChR retains a native secondary structure at 22.5 °C. In contrast, the initial spectrum recorded at room temperature for the nAChR in EPC at higher pH exhibits bands at 1680 and 1620 cm^{-1}, characteristic of denatured nAChR. In addition, the shape of the amide band at elevated pHs is relatively insensitive to increasing temperature, suggesting that a substantial portion of the nAChR is already in a denatured state at 22.5 °C.

3.1.2 Extent of peptide $^1H/^2H$ exchange

The effect of elevated pH and membrane environment on the $^1H/^2H$ exchange kinetics were monitored for the nAChR under conditions where the receptor retains its native conformation (pH 7.0 and 9.0 in asolectin membranes and pH 9, in EPC) as well as under conditions where a small percentage of the receptor is partially in a denatured state at room temperature (pH 11, asolectin). Protein films of the nAChR (pre-incubated in ^2H_2O buffer for three days at 4°C and pH 7.0) were deposited on the ATR crystal and exposed to ^2H_2O at the designated alkaline pH in order to achieve an increased level of $^1H/^2H$ exchange. Both the residual amide II band intensity and the spectral changes in the amide I band were monitored over the following 20 h. At the end of the experiments, the nAChR protein film was exposed to ^2H_2O buffer at pH 2.0 to shift the ionized carboxylic acid residues from 1580 cm^{-1} to their protiated form which absorb around 1700-1740cm^{-1}

Figure 4.4 Effect of pH and membrane environment of the $^{1}H/^{2}H$ exchange of the "exchange resistant" hydrogen peptides of the nAChR in asolectin. The nAChR was pre-exposed to $^{2}H_2O$ to exchange roughly 75% of the peptide N-^{1}H for N-^{2}H. The exchange kinetics of the remaining 25% N-^{1}H were then monitored over the subsequent 20h at 22.5 °C at the designated pH. (Top) Percentage of unexchanged peptides as a function of time after exposure to alkaline pH. nAChR in asolectin membranes, pH 7.0 (▼), pH 9.0 (■), pH 11.0 (▲); and nAChR in EPC membranes, pH 9.0 (O). Each curve represents the average of two experiments. (Bottom) The amide II region of spectra recorded at pH 2.0. Top spectrum at 1547 cm^{-1} is the nAChR in asolectin membranes in $^{1}H_2O$ buffer. The remaining spectra from top to bottom at 1547 cm^{-1} are nAChR in asolectin after 3 days in $^{2}H_2O$ buffer, pH 7.0 and 4 °C; the last three spectra were first pre-exposed to $^{2}H_2O$ buffer and then exposed to pH 9.0 for 20 h at 22.5 °C; nAChR in EPC membranes at pH 9.0 for 20 h at 22.5 °C; and nAChR in asolectin membranes at pH 11.0 for 1h at 95 °C to completely exchange the protein.

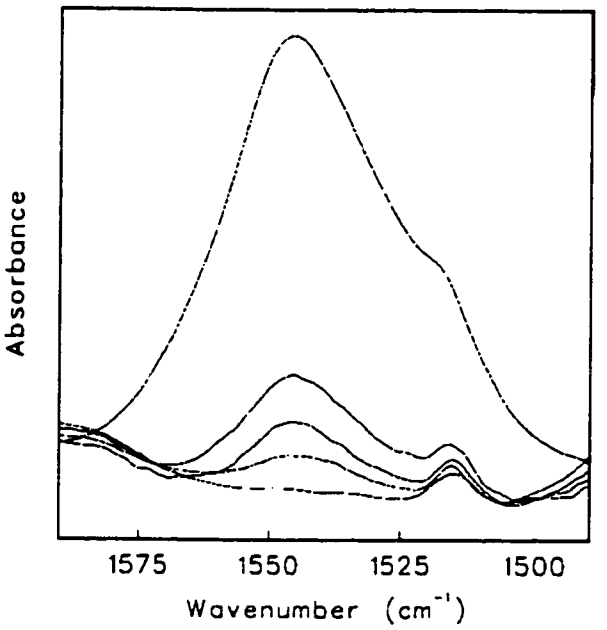
Absorbance
1575
1550
1525
1500
Wavenumber (cm⁻¹)

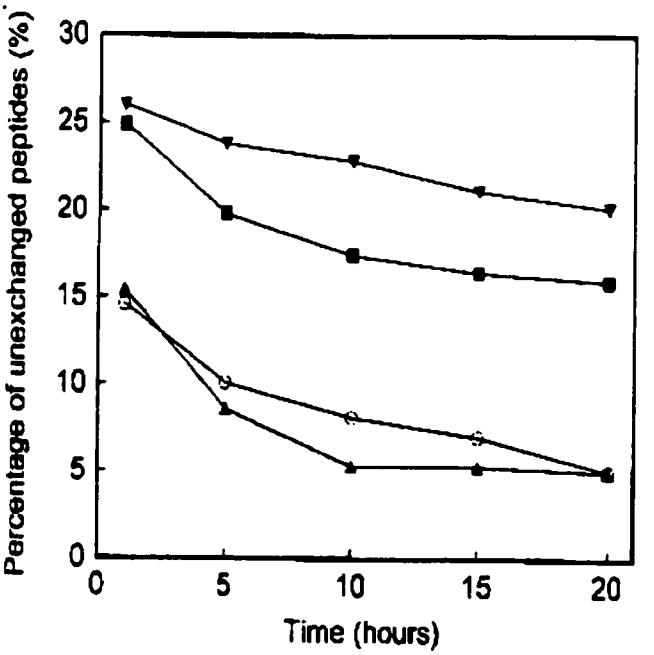
Percentage of unexchanged peptides (%)
30
25
20
15
10
5
0
0
5
10
15
20
Time (hours)

(figure 4.4b). The extent of $^{1}H/^{2}H$ exchange in the nAChR during the progression of the experiments was calculated by ratioing the intensity and area of the amide II bands and is reported as the percentage of unexchanged peptides in function of time (Figure 4.4a). Alkaline pH led to an increase in both the rate and extent of exchange in the exchange-resistant core. In all the experiments, the rate of exchange was high in the first 5 hours, except at pH 7.0 and slowed down over the course of the experiment to reach a low level toward the end. Incubation periods of up to 30 hours did not substantially increase the level of $^{1}H/^{2}H$ exchange in the nAChR. The greatest enhancement in the level of peptide $^{1}H/^{2}H$ exchange under nondenaturing conditions was found at pH 9.0 for the nAChR in EPC. Roughly 5% of the hydrogen peptides in the nAChR remain unexchanged after the 20 h incubation period. This corresponds to the exchange of roughly 80% of the normally exchange-resistant peptide hydrogens after 20 h.

3.1.3 Effect of enhanced $^{1}H/^{2}H$ exchange on the amide I band

Resolution-enhancement of the amide I band emphasizes the spectral changes induced by $^{1}H/^{2}H$ exchange and reveals the presence of secondary structure components as they downshift in frequency (fig. 4.5). Following incubation of the nAChR in asolectin at pH 7.0, 9.0 and 11.0 and nAChR/EPC samples at pH 9.0 for 20 hours, three critical observations can be made from the analysis of the amide I bands; 1) an important decrease in intensity around 1655 cm^{-1} is observed which suggests the $^{1}H/^{2}H$ exchange of α-helical peptides, 2) the lack of a downshift in frequency around 1630 cm^{-1} is

Figure 4.5 Fourier self-deconvolution of the amide I' bands in ATR-FTIR spectra of the nAChR recorded under conditions of alkaline $^{1}H/^{2}H$ exchange. The nAChR was first pre-exposed to $^{2}H_2O$ buffer for 3 days, pH 7.0 and 4°C and then exposed to $^{2}H_2O$ buffer for 20 h, at 22.5°C at the designated pH. Spectra of the nAChR in asolectin membranes (panels A-C) and in EPC membranes (D) were recorded at (A) pH 7.0, (B) pH 9.0, (C) pH 11.0, and (D) pH 9.0. Spectra in solid, long dash, and short dash lines, respectively, were recorded in (A) after 1, 10 and 20 h, in (B) after 1, 5, and 20 h, in (C) after 1,3, and 20 h, and in (D) after 1, 3, and 20 h of exposure. The spectra were autoscaled.

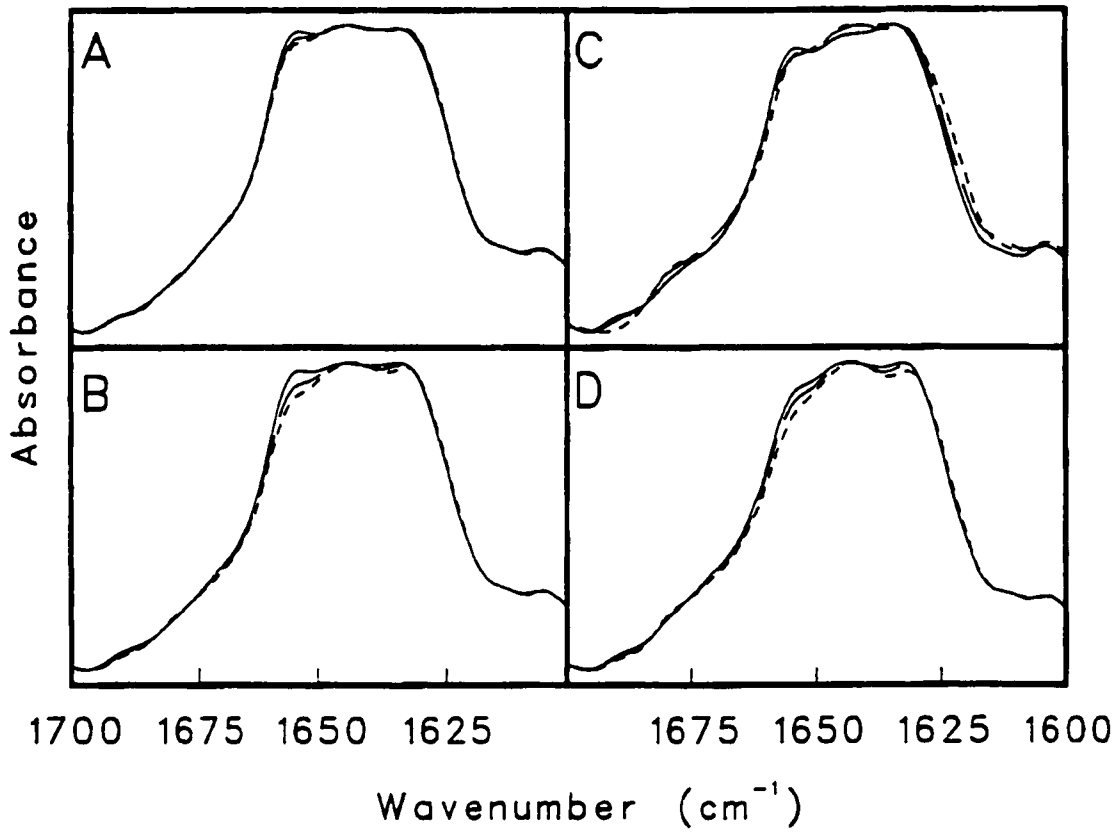
A
C
B
D
Absorbance
1700 1675 1650 1625
1675 1650 1625 1600
Wavenumber (cm^{-1})

consistent with the absence of exchange resistant β-sheets, and 3) after 20 hours of incubation, a remaining band at 1655 cm^{-1} suggests the presence of unexchanged α-helices. Both the important downshifts in frequency of the α-helical amide I component band and the residual amide I component band reflecting unexchanged α-helical peptide hydrogens suggest that the vast majority of the exchange-resistant peptides in the nAChR are in an α-helical conformation.

The nAChR in asolectin at pH 9.0 exchanges to a larger extent upon longer incubation periods (several days at room temperature) as well as at higher temperature (40°C). However, no further exchange of α-helices is observed and a shoulder around 1620 cm^{-1} and a band at 1680 cm^{-1} were visible (data not shown). Similarly, exchange experiments conducted at pH 10.0 (data not shown) and pH 11.0 at 22.5°C (Figure 4.5a) and pH 11.0 at 30°C and 40°C (data not shown) displayed comparable spectral changes with increasing magnitude upon pH and temperature increases. The slight broadening of the amide I band around 1620 cm^{-1} could be assigned to partial protein denaturation or $^{1}H/^{2}H$ exchange of β-sheets. The majority of these spectral changes was assigned to pH (and/or temperature) induced denaturation since the broadening is associated with a band at 1680 cm^{-1} highly typical of protein denaturation. Such a band is not observed upon exchange of ordered secondary structures. In addition, upon protein denaturation, the amide I band between 1630 and 1670 cm^{-1} changes from a symmetrical contour to an asymmetrical shape with an increase in intensity around 1655 cm^{-1}. As a result, at higher pHs, the amide I band does not display the decrease in intensity at 1655 cm^{-1} observed in the pH 9.0 experiment but exhibits an increase in intensity at 1655 cm^{-1}. The lack of decrease in intensity at 1655 cm^{-1} suggests a structural modification in the nAChR under

those conditions. Alkaline treated nAChR are more sensitive to heat induced denaturation, therefore, their stability could be decreased as well upon prolonged incubation. Note that the spectra reported in figure 4.5b (nAChR in EPC) also exhibit to a small extent the spectral changes characteristic of protein denaturation and were also detected to a larger magnitude in exchange experiments at pH 10.0 (data not shown). However, the level of protein denaturation observed in figure 4.5b is very subtle. While I cannot state unequivocally that there are no exchange-resistant β-strands in the nAChR, if they are present in the exchange resistant core of the nAChR, their proportion is very small.

3.2 Isolation and secondary structure of the transmembrane domain from the nAChR

3.2.1 Isolation of the transmembrane domain of the nAChR by proteolysis

In an attempt to isolate the transmembrane domain of the nAChR for secondary structure analysis by FTIR spectroscopy, affinity purified nAChR was incubated with various proteolytic enzymes (proteinase k, trypsin and pronase). In contrast to a previous study (Görne-Tschelnokow et al., 1994), incubation with proteinase k for a prolonged time led only to partial degradation of the nAChR, the resulting fragments were roughly 34 and 23 kDa in size (fig. 4.7, lane 2) compared to 40-65 for the native subunits (fig. 4.6, lane 2). The same results were obtained upon incubation of the nAChR with proteinase k first followed by either trypsin (fig. 4.7, lane 3) or tryspin and pronase (fig.

Figure 4.6 Proteolysis of the nAChR in DMPC membranes by pronase. Top panel: 16.5% Tris-tricine SDS-PAGE of the nAChR in DMPC membranes after osmotic shock followed by proteolysis with 0.05:1 pronase:nAChR (w:w ratio) for 24 hrs (lane 4). Lane 2 shows the four intact subunits of the nAChR (between the two arrows), calculated molecular weights are 66, 56, 52 and 48 kD for the δ, γ, β and α subunits, respectively. Lane 1: broad range standards and lane 3: kaleidoscope polypeptide standards. Bottom panel: ATR-FTIR spectra of the intact nAChR in asolectin membranes (solid line) and the proteolyzed nAChR (same as lane 4)(dashed line) in $^{1}H_2O$. The spectra were normalized with the intensity of the amide I band and the contribution of buffer was subtracted from the spectra.

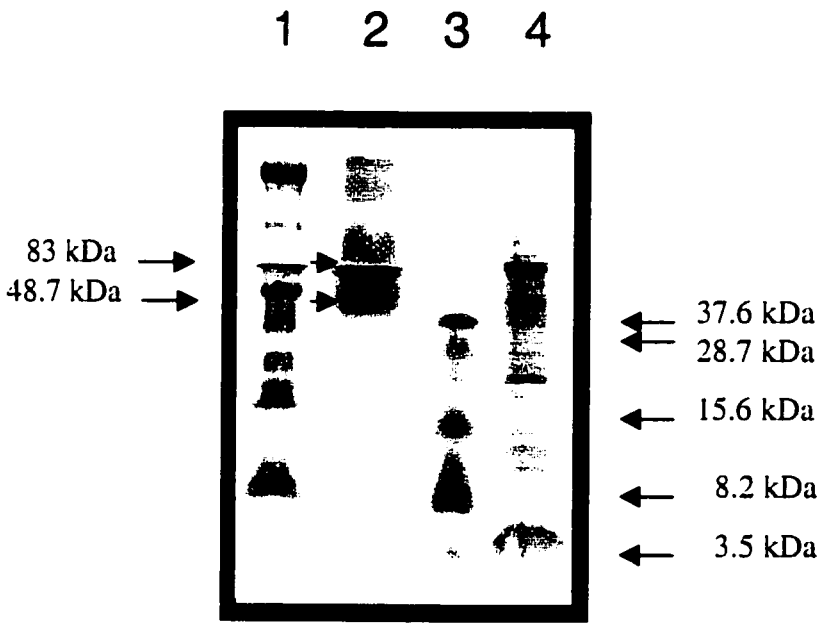
1 2 3 4
83 kDa
48.7 kDa
37.6 kDa
28.7 kDa
15.6 kDa
8.2 kDa
3.5 kDa

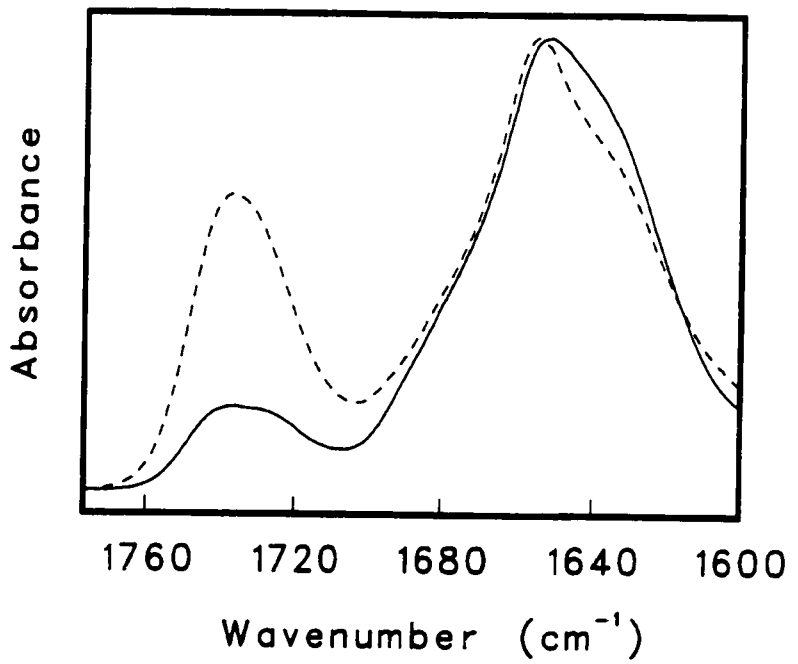
Absorbance
1760
1720
1680
1640
1600
Wavenumber (cm⁻¹)

Figure 4.7 Proteolysis of the nAChR in asolectin membranes by various proteases. Top panel: 16.5% Tris-tricine SDS-PAGE of the nAChR in asolectin membranes after proteolysis by 1:1 proteinase K:nAChR (w:w ratio) for 24 hrs (lane 2), followed by 0.05:1 trypsin:nAChR (w:w ratio) for 1 h (lane 3) or 0.05:1 pronase:nAChR (w:w ratio) for 1 h (lane 4). Lane 1: kaleidoscope polypeptide standards. Bottom panel: ATR-FTIR spectra of the intact nAChR in asolectin membranes (solid line) and the proteolyzed nAChR (same as lane 2)(dashed line) in $^{1}H_2O$. The spectra were normalized with the intensity of the amide I band and the contribution of the buffer was subtracted.

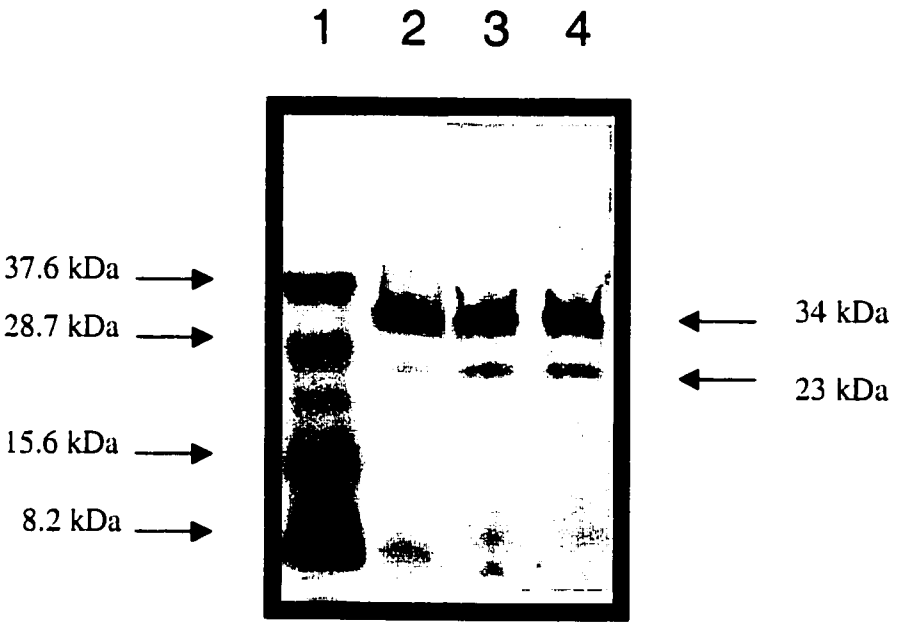
1 2 3 4
37.6 kDa
28.7 kDa
15.6 kDa
8.2 kDa
34 kDa
23 kDa

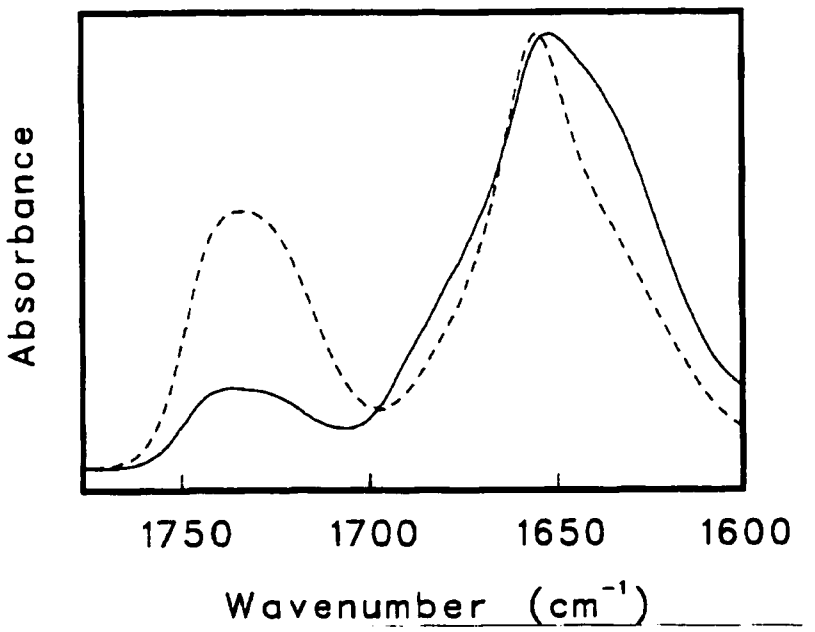
Absorbance
1750
1700
1650
1600
Wavenumber (cm^{-1})

4.7, lane 4). Wennogle and Changeux (1980) reported similar results upon treatment of membrane-rich nAChR with trypsin or pronase for 12 hours, followed by an additional 40 minutes in the presence of 1% Triton X-100. Since roughly 1/3 of the nAChR was cleaved, these results suggest that the intracellular domain of the nAChR is not accessible for the proteases as expected for sealed membrane vesicles.

To facilitate the accessibility of the protease to the intracellular domain, the nAChR was subjected to membrane disruption by either osmotic shock or saponin treatment. Subsequent incubation with pronase resulted in increased proteolysis. The most extensive digestion of the nAChR was performed upon either osmotic shock or saponin treatment of the nAChR in EPC/DOPA/Chol membranes followed by pronase incubation for 24 h. The resulting fragments were below 3.7 kDa in size which corresponds to proteolytic fragments of less that 34 amino acids in length (fig.4.8). Compared to the size of the subunits, four segments of 3.7 kDa represent between 25 to 35% of each subunit which correlates well with the predicted size of the transmembrane domain (Unwin, 1993). Membrane disruption prior to proteolysis was also reported in proteolysis studies on the nAChR (Giraudat et al., 1985) and of other membrane proteins (Scarborough and Hennessey, 1990; Vigneron, Ruysschaert and Goormaghtigh, 1995; Raussens, De Jongh, Pézolet, Ruysschaert and Goormaghtigh, 1998).

Figure 4.8 Proteolysis of the nAChR in EPC:DOPA:Chol membranes by pronase under membrane disruption conditions. Top panel: 16.5% Tris-tricine SDS-PAGE of the nAChR in EPC:DOPA:Chol membranes after either osmotic shock (lane 2) and saponin treatment (lane 3) followed by proteolysis with 0.05:1 pronase:nAChR (w:w ratio) for 24 hrs. Lane 1: kaleidoscope polypeptide standards. Bottom panel: ATR-FTIR spectra of the intact nAChR in asolectin (solid line) and the proteolyzed nAChR (same as lane 3)(dashed line). The spectra were normalized with the intensity of the amide I band.

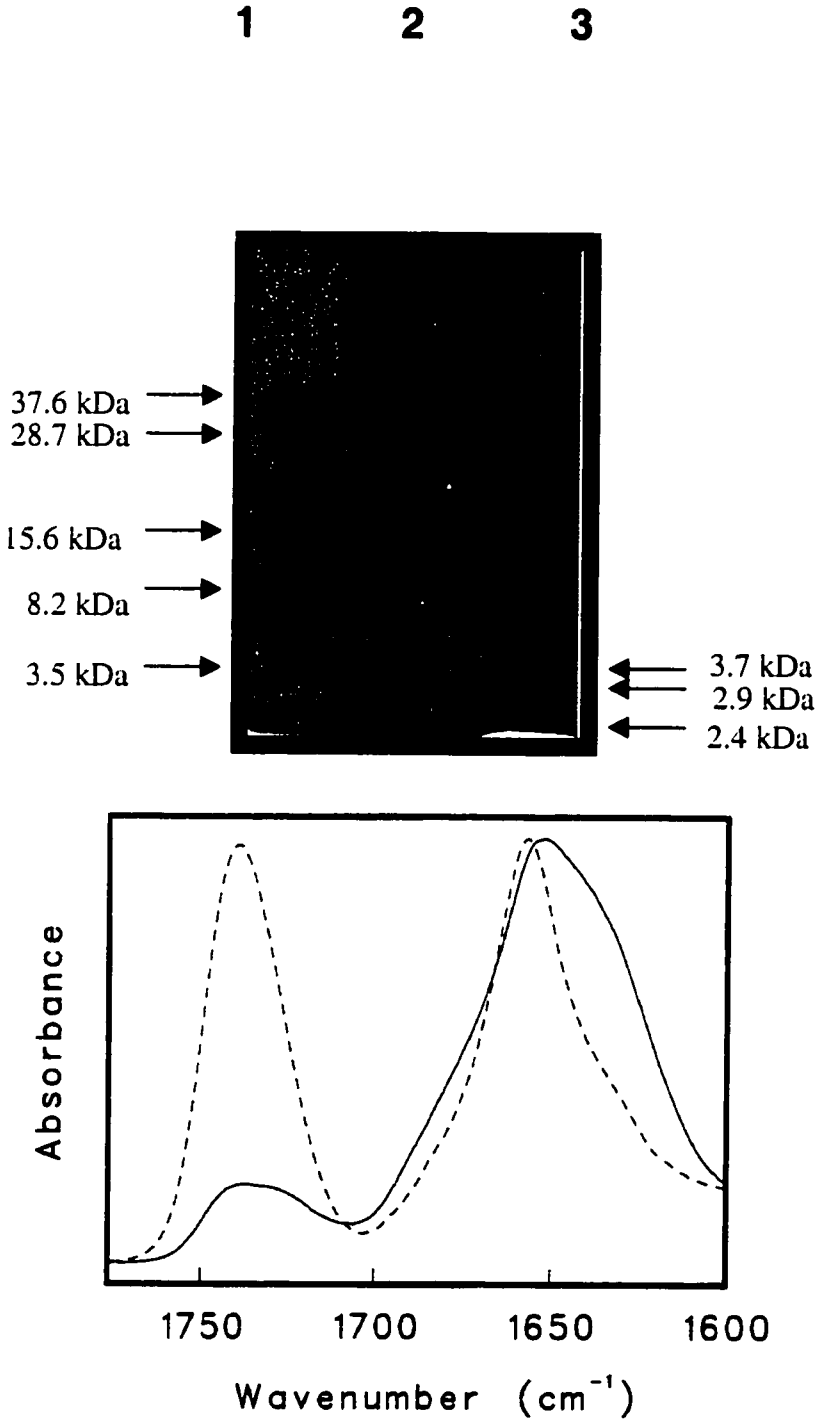
1
2
3
37.6 kDa
28.7 kDa
15.6 kDa
8.2 kDa
3.5 kDa
3.7 kDa
2.9 kDa
2.4 kDa
Absorbance
1750
1700
1650
1600
Wavenumber (cm-1)

3.2.2 Secondary structure of the transmembrane domain of the nAChR

To determine the secondary structure of proteolyzed nAChR, I recorded FTIR spectra and examined qualitatively the shape of the secondary structure-sensitive amide I band (between 1600 and 1700 cm^{-1}). Upon increased proteolysis of the nAChR, there is a gradual decrease in the shoulder around 1630 cm^{-1} and an overall narrowing of the 1655 cm^{-1} band (dash line spectra of figs. 4.6b-4.7b-4.8b) compared to the amide I shape of the intact nAChR (solid line). These spectral changes are highly typical of both a decrease in the proportion of β-sheets and an increase in α-helices, respectively. Moreover the increase in the frequency in the maximum intensity of the amide I band seems to correlate with a slight increase in the frequency of absorption of transmembrane α-helices as seen in bacteriorhodopsin (Lee et al., 1985), proteolyzed Na,K-ATPase (Heimburg, Esmann and Marsh, 1997) and glycophorin A (Challou, Goormaghtigh, Cabiaux, Conrath and Ruysschaert, 1994) as well as transmembrane peptides (Zhang, Lewis, Henry, Sykes, Hodges and McElhaney, 1995a; Zhang, Lewis, Henry, Hodges and McElhaney, 1995b; Ludlam, Arkin, Liu, Rothman, Rath, Aimoto, Smith, Engelman and Rothschild, 1996). The relative increase in intensity of lipid carbonyl vibration between 1700 and 1760 cm^{-1} suggests an increase in the lipid-to-protein ratio upon cleavage of the extramembranous domains since the proportion of "protein" is significantly reduced.

The sharp amide I band located at 1655 cm^{-1} for transmembrane domains of the nAChR strongly suggests a majority of α-helices while the weak absorption around 1627 cm^{-1} could be assigned to β-sheets, or other vibrations. For example, the absorption at 1627 cm^{-1} could be associated to intermolecular β-sheets, observed upon aggregation of

hydrophobic segments in other membrane proteins (Mercer, Abbott, Brazier, Ramesh, Haris and Srai, 1997), to short extended segments or as in myoglobin which does not contain any β-sheets, it could be due to vibrational motions of α-helical structures (Haris, Chapman and Benga, 1995).

FTIR spectra of transmembrane domains of the nAChR were recorded both in ^1H_2O and ^2H_2O to confirm their membrane location (fig. 4.9). The amide II band at 1547 cm^{-1} of solvent accessible N-H peptide vibration downshifts to 1450 cm^{-1} in ^2H_2O. After prolonged exposure, the remaining amide II absorption at 1547 cm^{-1} reveals a significant proportion (60% after 2 hours and 46% after 20 hours) of exchange resistant hydrogen peptides in the proteolyzed fragments. In ^2H_2O, the main amide I absorption downshifts from 1657 cm^{-1} to 1654 cm^{-1} is characteristic of the exchange of a small number of α-helical peptides. The lack of a large spectral change does not support the presence of unordered structures which downshift from 1655 to 1644 cm^{-1}.

3.3 Secondary structure of γ-M4 and β-M2-M3 transmembrane segments of the nAChR

The γ-M4 and β-M2-M3 segments were generated at Texas Tech University by proteolytic cleavage of nAChR-rich membranes, separation with SDS-PAGE and high performance liquid chromatography (HPLC) and reconstitution of the peptides in asolectin membranes (Corbin et al., 1998). The fragments were also sequenced in order to confirm their identity. Figure 4.10 reports the amide I band of FTIR spectra recorded both in ^1H_2O and ^2H_2O buffer of the transmembrane segment γ-M4. Although the spectra

Figure 4.9 ATR-FTIR spectra in the amide I and II regions of the proteolyzed nAChR (lane 3, figure 4.8, < 3.7 kDa) in $^{1}H_2O$ (dashed line) and after 20 hrs of exposure to $^{2}H_2O$ (solid line). The spectra are normalized and the buffer was subtracted.

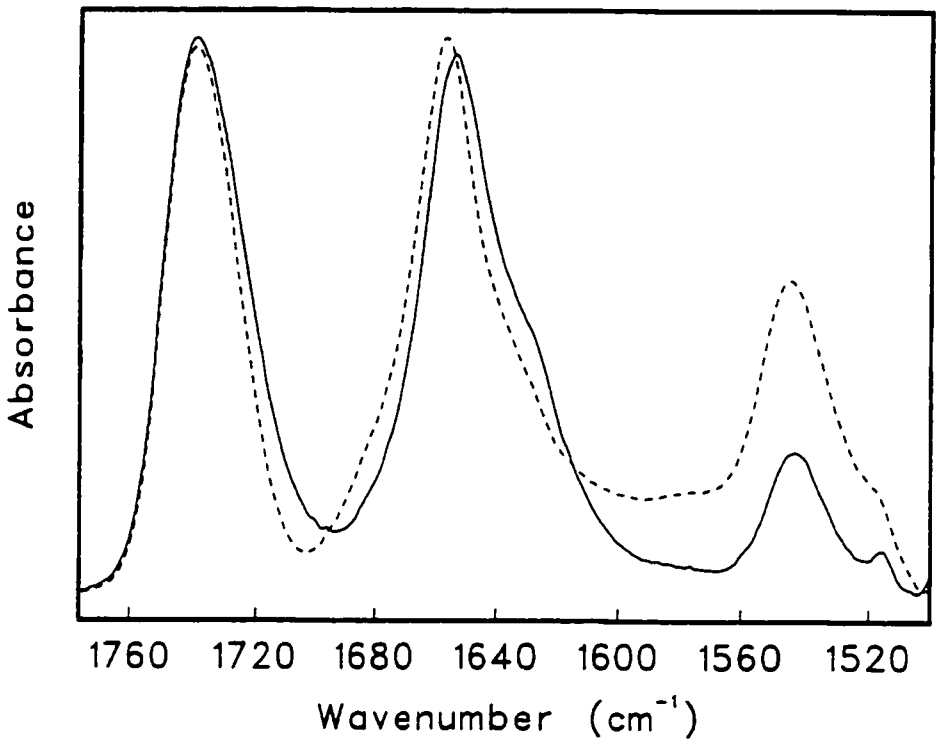
Absorbance
1760
1720
1680
1640
1600
1560
1520
Wavenumber (cm-1)

were recorded using a much smaller amount of sample (50 μg as opposed to 250 μg), the signal-to-noise ratio is very good. In ^1H_2O, the amide I band for γ-M4 is roughly symmetric with an intense peak maximum centered near 1656 cm^{-1} (fig.4.10). Also, two weak shoulders are located near 1677 and 1627 cm^{-1}. This spectral shape is highly characteristic of a high proportion of α-helices in γ-M4, however, peptides in an unordered conformation can also absorb in the 1655 cm^{-1} region in ^1H_2O. The bands at 1677 and 1627 cm^{-1} are assigned to β-sheets.

To distinguish between the contribution of α-helical and unordered structures, which both absorb at 1655 cm^{-1} in ^1H_2O, FTIR spectra of γ-M4 were recorded after exposure to ^2H_2O. In ^2H_2O, the main absorption at 1655 cm^{-1} shifts to 1653 cm^{-1} and 1640 cm^{-1}. As presented above, the former spectral change is consistent with the downshift of α-helices while the latter correlates with a downshift of unordered structures. Similar spectral changes are observed upon incubation of the peptide β-M2-M3 in ^2H_2O. Note that in ^2H_2O, the band at 1653 cm^{-1} is broader than in ^1H_2O, suggesting the overlap of both unexchanged and exchanged α-helices. The strong intensity remaining at 1653 cm^{-1} in ^2H_2O and the residual intensity at 1547 cm^{-1} (amide II band, data not shown) support an important proportion of unexchanged α-helices.

To quantify the relative amounts of secondary structures in both γ-M4 and β-M2-M3 transmembrane segments, the spectra were integrated according to the procedure described in Méthot et al. (1994). Basically, the number and frequencies of the bands revealed upon deconvolution as well as an estimate of their width and intensity are used as input parameters for the curve-fitting algorithm. The resulting curve fit is deconvolved and compared to the shape of the actual deconvolved spectrum in order to assess its

Figure 4.10 Fourier self-deconvolution of the amide I band and amide I' band from ATR-FTIR spectra of the peptide fragment γ-M4 recorded in $^{1}H_2O$ buffer (A) and $^{2}H_2O$ buffer (B). Each panel shows the absorbance (top) and deconvolved spectra (bottom).

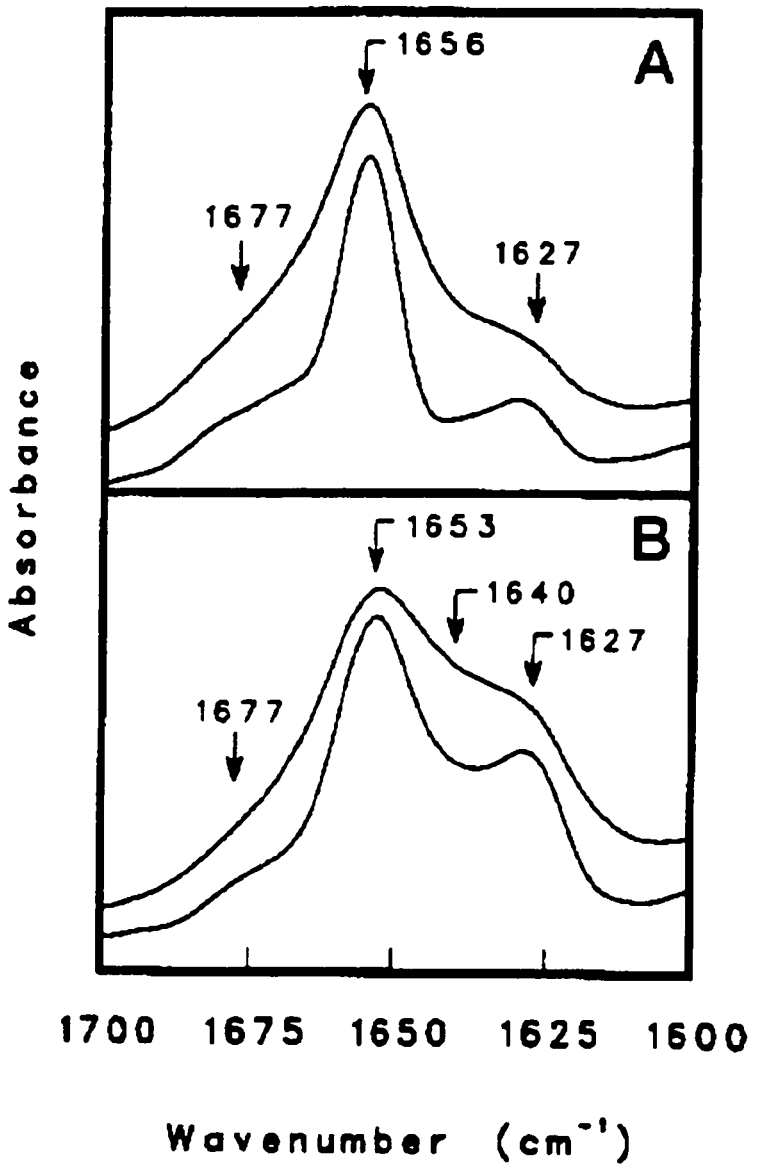
1656
A
1677
1627
1653
B
1640
1627
1677
Absorbance
1700 1675 1650 1625 1600
Wavenumber (cm⁻¹)

accuracy. The curve fit for both samples are shown in figure 4.11 and the secondary structure estimates are presented in table 4.1. The estimates suggest a high proportion of α-helical secondary structures (65% for γ-M4 and 75% for β-M2- M3) in agreement with the qualitative analysis of the FTIR spectra.

Figure 4.11 Curve-fit analysis of the amide I' band of ATR-FTIR spectra of the peptide fragments γ-M4 (A) and β-8K (B). In each panel, the solid line represents the experimental data, the dotted line spectrum superimposed onto the experimental spectrum represents the curve fit and the dotted line spectra represent the individual component bands.

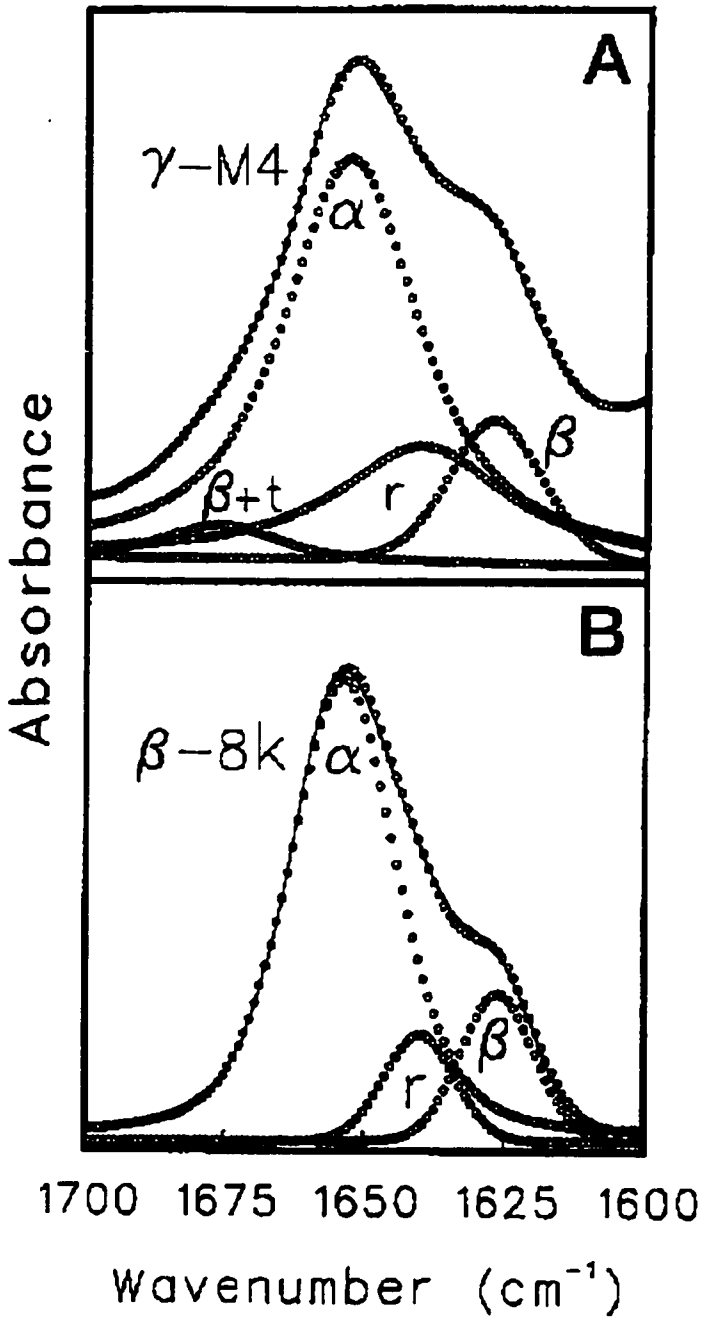
A
γ–M4
α
β
β+t
r
B
β–8k
α
β
r
Absorbance
1700 1675 1650 1625 1600
Wavenumber (cm⁻¹)

Table 4.1 Summary of secondary structure estimates from the curve fitting analysis of ATR-FTIR spectra of the peptide fragments of the nAChR.

Sample	α-helix (%)	β-sheet (%)	β-sheet + turn (%)	unordered (%)
β-8K (M2-M3)	75	15	0	10
γ-5K (M4)	65	12	3	20

4. Discussion

The objective of this work was to further examine the secondary structure of the exchange resistant core of the nAChR using a novel combination of FTIR spectroscopy and $^{1}H/^{2}H$ exchange as well as to determine the secondary structure of isolated transmembrane segments. The data show that ~25% of the nAChR peptide hydrogens are resistant to exchange after 3 days of incubation in $^{2}H_2O$ at 4°C. Most of these exchange resistant peptides can be exchanged under nondenaturing conditions at room temperature. FTIR spectra of the nAChR recorded under these enhanced exchange conditions revealed a downshift in frequency of amide I component characteristic of the $^{1}H/^{2}H$ exchange of α-helical peptides whereas a similar downshift of β-sheet component was not observed. These results support a large population of exchange resistant α-helices that are likely located in the membrane. In contrast, the lack of band shifts that can be attributed to the presence of exchange-resistant β-strands suggests an absence of transmembrane β-sheets.

The interpretation of the results is based on the assumption that the 25% exchange-resistant peptides in the nAChR are located in the transmembrane domain. The extremely low exchange rates in the transmembrane domain are explained by the hydrophobic environment of the membrane which limits water accessibility. Also, the hydrophobic transmembrane segments are involved in hydrogen bonding and are restricted to the transient unfolding/folding motions necessary for the isotopic exchange. These transient motions may be particularly restricted for the transmembrane segments which likely form a rigid structure to ensure a closed channel conformation.

The solvent inaccessibility of transmembrane peptides to hydrogen exchange is well established (for a review, see Goormaghtigh et al., 1994a). Both rhodopsin and bacteriorhodopsin exhibit a large proportion of exchange-resistant peptide hydrogens which correlates, as for the nAChR, with the proportion of the protein located in the membrane (Osborne and Nabedryk-Viala, 1977; Englander, Downer and Englander, 1982; Earnest, Herzfeld and Rothschild, 1990 and Konishi and Packer, 1977). Large numbers of exchange resistant peptides have also been observed in the multisubunit photosynthetic reaction centre and porin (Nabedryk, Andrianambininintsoa, Mäntele and Breton, 1988; Kleffel, Garavito, Baumeister and Rosenbusch, 1985).

Although the ~25% exchange-resistant peptides in the nAChR correlates well with the proportion of the nAChR which is thought to be membrane-located (Noda et al., 1983; Claudio et al., 1983; Unwin, 1993; Görne-Tschelnokow et al., 1994), the exchange-resistant peptides cannot be unequivocally attributed exclusively to the transmembrane domain.

The interpretation of the data is also based on the detection of spectral downshifts in frequency of secondary structure components. The losses of intensity centered near 1655 cm^{-1} and 1635 cm^{-1} are highly characteristic of spectral downshift of α-helices and β-sheets and have also been observed in other proteins upon exposure to ^2H_2O (Susi et al., 1967; Olinger et al., 1986; Haris et al., 1986; Heimburg and Marsh, 1993; Baenziger and Chew, 1997).

The transmembrane domain of affinity-purified nAChR was isolated by proteolytic cleavage of the solvent-exposed extramembraneous domains. The membrane-spanning segments are likely protected from proteolysis due to the inaccessibility of the

proteases to the membrane. I first tested the ability of proteinase k, trypsin and pronase which have been used previously in similar experiments to digest the nAChR. The results show that membrane disruption is required prior to proteolysis in order to achieve proteolysis of both extra and intracellular domains of the nAChR as was reported for the nAChR (Giraudat et al., 1985) and other membrane proteins (Scarborough and Hennessey, 1990; Vigneron et al., 1995; Raussens et al., 1998). Either osmotic shock or saponin treatment followed by pronase incubation resulted in complete digestion of the extramembraneous domains of the nAChR and peptidic fragments with apparent molecular weights below 3.7 kDa. This corresponds to peptides of roughly 34 amino acid residues in length and less. The suggested lengths of the transmembrane segments in the nAChR in the hydrophobic core of the membrane (30 Å), estimated from hydrophobicity plots, range from 19 to 27. However, since the overall bilayer thickness is between 40-60 Å (including the interface regions) (Yeagle, 1993) the transmembrane segments in the nAChR are likely longer, ≥ 30 amino acid in length. This correlates well with the calculated length of the fragments and suggest that the great majority of amino acid residues are embedded in the membrane. The results contradict the article by Görne-Tschelnokow et al. (1994) which report a 40% proportion of β-sheets in proteolyzed membrane rich-nAChR (60-70% pure) by proteinase k. Under the same experimental conditions reported by Görne-Tschelnokow et al. (1994) the ability of proteinase k to isolate the transmembrane domain of reconstituted nAChR was tested. Under those conditions, as well as with the use of a combination of proteases, the nAChR is only partially digested, suggesting the inaccessibility of the intracellular domain to the proteases. Görne-Tschelnokow et al. (1994) suggested the cleavage of the intracellular

domain of the nAChR due to the disappearance of the intracellular 43 kDa protein, however, Wennogle and Changeux (1980) clearly showed that detergent solubilization or sonication is required for extensive digestion of nAChR-rich membranes. Also it is well established that reconstituted membranes are impermeable to protease molecules and that membrane disruption is required for intracellular digestion (Giraudat et al., 1985; Scarborough and Hennessey, 1990; Vigneron et al., 1995; Raussens et al., 1998). In addition, proteinase k is a specific protease which is usually not competent by itself to extensively digest membrane proteins (Capasso, Hoving, Tal, Goldshleger and Karlish, 1992; Corbalán-García, Teruel, Villalaín and Gómez-Fernandez, 1994) and especially the nAChR reported to be extremely resistant to proteolytic cleavage (Wennogle and Changeux, 1980). Pronase, on the other hand, is a mixture of proteases which non-specifically digest proteins and is likely to be more effective to extensively digest proteins.

FTIR spectra of the transmembrane domains of the nAChR strongly suggests their α-helical secondary structure. The weak absorption around 1630 cm^{-1} could be assigned to a small proportion of extramembraneous β-strands since a few residues could be located outside the membrane. It is not likely that a small proportion of β-sheets resides in the transmembrane domain. The only high-resolution example of transmembrane β-sheets is in the bacterial proteins porins which contain exclusively β-strands organized in a β-barrel. In such arrangement, the β-strands are stabilized in the hydrophobic environment of the lipid bilayer by hydrogen bonding. However, a single transmembrane β-strand would have unsatisfied hydrogen bonds and would consequently be energetically unfavorable (Reinhart and Deber, 1992). The presence of both α-helices

and β-sheets in a transmembrane domain is, in addition, unlikely due to "mechanistic problems" upon insertion and oligomerization (Popot, 1993). Transmembrane α-helices in membrane proteins are thought to fold in two stages. First, independent stable α-helices are formed in the membrane and second, the helices assemble to form the tertiary fold of the protein (Popot and Engelman, 1990). Since isolated β-strands in the membrane would be energetically unfavorable due to the unsatisfied hydrogen bonds, transmembrane β-barrels fold before or during membrane insertion (Popot and Engelman, 1990). The results therefore argue against the transmembrane topology models of the nAChR that include transmembrane β-sheets (Mielke and Wallace, 1988; Unwin, 1993; Görne-Tschelnokow et al., 1994; Ortells and Lunt, 1996).

$^{1}H/^{2}H$ exchange revealed the partial inaccessibility of the transmembrane segments to solvent. Previously, the resistance to $^{1}H/^{2}H$ exchange of the transmembrane domain of the nAChR was reported (Baenziger and Méthot, 1995; Méthot and Baenziger, 1998). It is expected that isolated transmembrane segments exchange more than the transmembrane domain of an intact protein due to increased motions of free peptides. Such increase in $^{1}H/^{2}H$ exchange was also observed in the transmembrane helices of the core antenna of *R. rubrum* upon detergent induced subunit dissociation and was attributed to increased helix flexibility and breathing motions (Sturgis, Robert and Goormaghtigh, 1998).

The validity of the conclusions is based on the assumption that isolated transmembrane segments of the nAChR adopt the same secondary structure compared to the native structure. It is likely that the secondary structure observed in the isolated transmembrane segments reflect their conformation in the intact protein since

transmembrane α-helices are thought to be autonomous folding domains in absence of the rest of the protein (Popot, 1993). For example, it was shown that isolated transmembrane segments isolated from bacteriorhodopsin retain the α-helical structure of the intact protein (Ozawa, Hayashi, Masuda, Iio and Takahashi, 1997). However, there is still some uncertainty regarding the nature of the interactions between the transmembrane segments in the intact nAChR and upon cleavage of the connecting loops. The adoption of a different conformation by the proteolysed transmembrane segments could still occur after a potential change in their association, but no major modification in their secondary structure is expected.

The secondary structure of nAChR individual transmembrane segments isolated by Dr. Michael Blanton at Texas Tech University was examined by FTIR spectroscopy. A percentage of 65% and 75% of α-helices in the γ-M4 and β-M2-M3 fragments respectively, was estimated. According to hydrophobicity analysis of the primary sequence of the nAChR, 62% of the amino acid residues of γ-M4 are thought to be located within the membrane and 75% for β-M2- M3. These numbers correlate well with the estimates of the proportion of α-helical secondary structures in both fragments. The small percentage of non-α-helical secondary structures identified is likely located outside the membrane. Therefore, the α-helical secondary structure of the proteolytic fragments should reflect the secondary structure of the membrane spanning domain.

The same fragments were analyzed by CD spectroscopy by Dr. Howard H. Wang at the University of California and the α-helical content of the fragments was 10-15% higher than the observations (Corbin et al., 1998). No content of β-sheets or unordered structures was reported, however, γ-M4 was reported to contain 9% of "other" structures.

It was mentioned before that CD spectroscopy is less accurate for quantitative prediction of β-sheets (Naumann et al., 1993) and could partially explain the discrepancies with the estimations. Wang's group also studied the secondary structure of fragments including the transmembrane segments β-M1-M2- M3 and α-M4 and both were also interpreted as containing a very high proportion of α-helices.

5. Conclusion

In absence of high resolution techniques, the identification of the secondary structure of a transmembrane domain is a challenging task. I have developed several approaches, in conjunction with FTIR spectroscopy in order to shed some light on the secondary structure of the transmembrane domain of the nAChR. Those approaches have their strengths and limitations. For example, $^{1}H/^{2}H$ exchange of the intact nAChR allows the observation of a distinct topological domain without its direct isolation. On the other hand, this technique requires precaution in the interpretation and is limited to the overlap of secondary structure components in the amide bands.

Even though there is evidence that isolated transmembrane segments retain their native conformation, there is still uncertainty regarding some possible rearrangement following proteolysis. However, the secondary structure of isolated transmembrane segments is easily extracted from the FTIR spectra. Since these two different approaches converge to the same interpretation, I can confidently propose an all α-helical transmembrane domain in the nAChR and rule out all the nAChR transmembrane

topology models that include transmembrane β-sheets (Mielke and Wallace, 1988; Unwin, 1993; Görne-Tschelnokow et al., 1994; Ortells and Lunt, 1996).

In order to strengthen the observations and further characterize the organization of the transmembrane helices in the nAChR and their involvement in desensitization, I was interested in the determination of the orientation of the helices with respect to the lipid bilayer in both active and inactive conformations.

Chapter 5- Orientation of the Transmembrane Segments in the nAChR in both the Active and Inactive Conformations

1. Introduction

In the previous chapters, evidence was presented in favor of four transmembrane α-helices per subunit in the nAChR for a total of 20 transmembrane α-helices in the heteropentamer. However, the detailed quaternary structure of the transmembrane domain, for instance, the packing and orientation of the transmembrane helices is unknown. This knowledge will provide a basis for the elucidation of the mechanism of channel gating and desensitization of the nAChR.

Medium resolution electron microscopy studies suggested a funnel-shaped channel in the nAChR with the five channel lining M2 segments kinked near the middle of the membrane (Unwin, 1995, 1998 and Miyazawa et al., 1999). Tikhonov and Zhorov (1998) have built a model of the nAChR channel based on numerous experimental data. The model diplays kinked M2 helices, close to each other on the cytoplasmic side but diverging on the synaptic side. Based on NMR spectroscopy of the M2 segment, the model proposed by Opella et al. (1999) also consists of a funnel-shaped bundle in which helices are not kinked but display a right angle interhelical twist with an orientation angle of 12°.

Even though the length and primary sequence of the hydrophobic stretches of residues in the nAChR is known (table 5.1), the length of the transmembrane helices cannot be predicted. They are likely longer than the minimum 20 amino acids required to

Table 5.1 Characteristics of the transmembrane segments in the nAChR.

Transmembrane Segment	Length (amino acids)	Primary sequence (α-subunit)	Characteristics
M1	25	PLYFVVNVIIPCLLFSF LTGLVFYL	Slightly exposed to channel (Akabas and Karlin, 1995)
M2	α 19 β 18 γ 19 δ 18	M-TLSISVLLSLT VFLLVIV	Lines the channel (Hucho et al., 1986; Giraudat, 1987; Leonard, 1988; Unwin, 1993; Akabas et al., 1994)
M3	α 20 β 22 γ 22 δ 22	YMLFTMIFVISSIIITV VVI	
M4	α 19 β 19 γ 24 δ 21	ILLCVFMLICIIGTVSV FA	Surrounded by lipids (Blanton and Cohen, 1992)

span the hydrophobic core of the membrane (30 Å thick) since the overall bilayer thickness is between 40-60 Å (Yeagle et al., 1993), they are also possibly longer if they are tilted at a large angle.

In simplistic models of transmembrane topology of membrane proteins, the transmembrane α-helices are often drawn as straight and perfectly perpendicular with respect to the membrane plane. Crystal structures of membrane proteins have revealed that transmembrane α-helices are rarely straight, they are often bent, kinked and/or inclined. Little is known regarding the packing of transmembrane α-helices, however, helix-to-helix packing in soluble proteins is better characterized. Chothia, Levitt and Richardson (1981) developed a model for helix packing in soluble proteins named "ridges in grooves". Ridges along an α-helix are formed by rows of residues side chains separated in the sequence by either 3 (i,i + 3) or 4 (i,i + 4) residues. Ridges on one α-helix can pack into the grooves created by ridges on a second helix. In soluble proteins the helix-helix contact involves the i,i + 4 ridges on both helices resulting in an interaxial angle of about -50° between the two helices. The packing involving i,i + 4 ridges on one helix and i,i + 3 on the other helix gives rise to an interaxial angle of 23°, therefore a more parallel arrangement of the two helices. Similar helix packing was observed recently in crystallized membrane proteins, such as the photosynthetic reaction center (Rees, Chirino, Kim and Komiya, 1994) and cytochrome c oxidase (Tsukihara, Aoyama, Yamashita, Tomizaki, Yamaguchi, Shinzawa-Itoh, Nakashima, Yaono and Yoshikawa, 1996) and is likely to be a major protein folding motif of transmembrane α-helices.

The nature of the conformational changes in the desensitized state of the nAChR is still a matter of debate. In chapter 3, evidence suggesting that there are no global

changes in secondary structure upon desensitization was presented. However, it is unclear whether or not the transmembrane segments experience a change in orientation. In the presence of Carb, Unwin et al. (1988) and Unwin (1995) reported a rotation of the axis of the five subunits in the nAChR, of less that 10°, which would likely involve a change in the tilt of the transmembrane helices. Changes in lipid exposure of amino acid residues was observed in the M2 transmembrane segments in the presence of Carb (McCarthy and Stroud; White and Cohen, 1992). Moreover, site-directed mutagenesis and labeling experiments revealed that the M1 transmembrane segment is exposed to the channel lumen and that its exposure changes in the presence of agonist (Akabas and Karlin, 1995). In contrast, reports from Kuhlmann et al. (1991) and Baenziger and Chew (1997) did not detect conformational changes in the transmembrane domain of the nAChR in the desensitized state.

As another step toward the elucidation of the structure of the ion channel and the mechanism of desensitization in the nAChR, the goal of this chapter was to determine the average orientation of the transmembrane segments and to test whether or not there is a change in orientation in the desensitized state. Polarized ATR-FTIR spectroscopy was used to perform experiments on a model peptide and lipids. The average orientation of the transmembrane segments was then examined in both the intact and proteolyzed nAChR with respect to the lipid bilayer. Moreover, any net change in orientation of the transmembrane segments in the desensitized state stabilized with excess Carb was investigated. The results support an overall perpendicular orientation of the transmembrane segments in the proteolyzed nAChR with a calculated average tilt angle

of roughly 41°. A large change in orientation of the transmembrane segments was not detected in the desensitized state.

2. Experimental procedures

2.1 nAChR purification from *Torpedo californica*

Please refer to section 2.1 of Chapter 3 for a complete description of the affinity purification of the nAChR.

2.2 Isolation of the transmembrane domain of the nAChR by proteolysis

Please refer to section 2.2 of Chapter 4 for a complete description of the isolation of the transmembrane domain of the nAChR by proteolysis.

2.3 Preparation of pure lipid vesicles and gramicidin

Pure lipid vesicles were prepared by dissolving 3 mg of dimyristoylphosphatidylcholine (DMPC) in 500 μl of chloroform in a glass vial. After vortexing, the solvent was evaporated under nitrogen. The vial was placed under high vacuum overnight to ensure complete evaporation of the solvent. Then, the lipid film was resuspended in 300 μl of 2 mM phosphate buffer, pH 7.0, prepared in ^2H_2O. After vortexing, the lipid solution was subjected to three cycles of heating at 52°C for 30

seconds and cooling at 20°C for 30 seconds to induce multilamellar vesicles formation (Bouchard and Auger, 1993).

Gramicidin was incorporated into DMPC vesicles by dissolving 5 mg of gramicidin with 18 mg of DMPC in 500 µl of ethanol. The mixture was incubated at 52°C for 1 h and the solvent evaporated under a stream of N_2 (g) followed by high vacuum overnight. The vesicles were dissolved in 200 µl of 2 mM phosphate buffer, pH 7.0, and the solution subjected to cycles of heating and cooling as described above (Bouchard and Auger, 1993).

2.4 FTIR spectroscopy

FTIR spectra were acquired either on a Bio-Rad FTS-40 or on a Bio-Rad FTS-40A spectrometer equipped with either a mercury cadmium telluride or a deuterated triglycine sulfate detector. Each spectrometer was purged with dry air (dew point, 100°C) from a Balston air-dryer. The ATR crystals were cleaned before use by soaking in chromic acid for 30 minutes and then rinsed thoroughly with distilled water. All spectra were recorded at 2 cm^{-1} resolution.

Polarization on pure lipids and gramicidin FTIR samples for polarization were prepared according to the solvent evaporation technique (Goormaghtigh and Ruysschaert, 1990 and Fringeli and Günthard, 1981), 100 µl of lipid dispersion (with or without gramicidin, see above) was spread on the surface of the ATR element and dried by a gentle stream of nitrogen. The ATR element was placed in an ATR liquid cell as described earlier. A single diamond polarizer was installed in the sample compartment

and was controlled manually. FTIR spectra averaging 500 scans were recorded with parallel and perpendicular light either in the dry state or after rehydration with Torpedo Ringer buffer prepared either in ^1H_2O or ^2H_2O.

Polarization on intact and proteolyzed nAChR. Typically, a sample of 250 μg of intact nAChR was spread on the surface of the ATR crystal and carefully dried with a gentle stream of nitrogen. The amount of proteolyzed nAChR used was much smaller (50-100 μg) but similarly dried on the ATR element. FTIR spectra averaging 500 scans were recorded with parallel and perpendicular light either in the dry state or after rehydration using solvent vapours of TR buffer prepared either in ^1H_2O or ^2H_2O instead of bulk solvent.

3. Theory of polarization as a tool to determine α-helices tilt angles

Knowledge of the precise organization of the transmembrane segments in membrane proteins is required in order to get insights into their mechanism of action since the transmembrane segments are often involved in protein function. For instance, the crystal structure of the voltage-gated K^+ channel recently revealed a unique architecture of the transmembrane helices in the pore responsible for the selective permeability for large K^+ ions but not to small Na^+ ions (Doyle, Morais Cabral, Pfuetzner, Kuo, Gulbis, Cohen, Chait, MacKinnon, 1998). In addition, proton transfer in membrane proteins such as cytochrome c oxidase (Tsukihara et al., 1996) and bacteriorhodospin (Pebay-Peyroula, Rummel, Rosenbusch and Landau, 1997) is efficiently accomplished through hydrogen bonds, particularly in the hydrophobic

environment of the lipid bilayer. Although the structure and organization of transmembrane segments is central in membrane protein function, the structure revealing techniques available are limited. Polarized FTIR spectroscopy has been used to study the orientation of transmembrane α-helices of numerous membrane proteins such as the bacterial photosynthetic reaction center (Nabedryk and Breton, 1981; Nabedryk, Tiede, Dutton and Breton, 1982), rhodopsin (Michel-Villaz, Saibil and Chabre, 1979; Rothschild, Sanches, Hsiao and Clark, 1980), bacteriorhodopsin (Rothschild and Clark, 1979; Earnest et al., 1990), Ca^{2+}-ATPase of sarcoplasmic reticulum (Buchet, Varga, Seidler, Molnar and Martonosi, 1991), phospholamban (Arkin, Rothman, Ludlam, Aimoto, Engelman, Rothschild and Smith, 1995) and cytochrome c oxidase (Bazzi and Woody, 1985). Similarly, the orientation of the transmembrane β-sheets in porin was also investigated (Nabedryk, Garavito and Breton, 1988). The average orientation of the transmembrane helices of some of these membrane proteins: bacteriorhodospin (Pebay-Peyroula et al., 1997), cytochrome c oxidase (Tsukihara et al., 1996), photosynthetic reaction centre (Deisenhofer, Epp, Miki, Huber and Michel, 1985) and porin (Weiss, Kreusch, Schiltz, Nestel, Wlete, Weckesser and Shultz, 1991) agrees with x-ray crystallography.

The theory of polarization relevant to the work reported in this chapter is presented briefly here. For a detailed review of the theory of polarization, see Fringeli and Günthard (1981) and Goormaghtigh and Ruysschaert (1990).

The absorbance of an infrared band is proportional to:

$$|E, \delta\mu/\delta Q|^2 = |E|^2 \, |\delta\mu/\delta Q|^2 \cos^2\Gamma \qquad (1.1)$$

where E is the amplitude of the electric field of the light, $\delta\mu/\delta Q$ is the transition moment of a chemical bond, i.e. the variation of the electric dipole μ along the coordinate Q, and Γ is the angle between E and $\delta\mu/\delta Q$. In order for a vibrational transition to occur, the electric field of the light must have a component parallel to the transition dipole moment of the bond. Therefore, the polarization of the light influences the probability of absorption, making polarization spectroscopy a tool by which the orientation of chemical bonds can be obtained.

Molecular orientation is determined by the measurement of the dichroic ratio, R, which is defined as

$$R = \frac{A_{//}}{A_{\perp}} = \frac{(\overline{E}^{//} \cdot \delta\overline{\mu}/\delta Q)^2}{(E^{\perp} \cdot \delta\overline{\mu}/\delta Q)^2} \qquad (1.2)$$

where $A_{//}$ and $A_{\perp}$ are the absorbances measured with the incident radiation oriented respectively parallel and perpendicular to the plane of incidence and $E^{//}$ and $E^{\perp}$ are the components of the electric field.

The amplitude of the three components of the electric field (E_z, E_y and E_x) of the light presented in figure 5.1 have been derived by Harrick (1967) and can be calculated with the following equations in the case of thick films:

$$Ey = \frac{2\cos\theta}{(1 - n_{21}^{\,2})^{1/2}} \qquad (1.3)$$

Figure 5.1 Schematic diagram showing the attenuated total reflectance (ATR) set-up. θ is the angle on incidence; E_p and E_v are the parallel and perpendicular polarized components of the electric field of the electromagnetic radiation. E_x, E_y and E_z are the electric field components with respect to the coordinate system of the ATR plate. From Fringeli and Günthard, 1991.

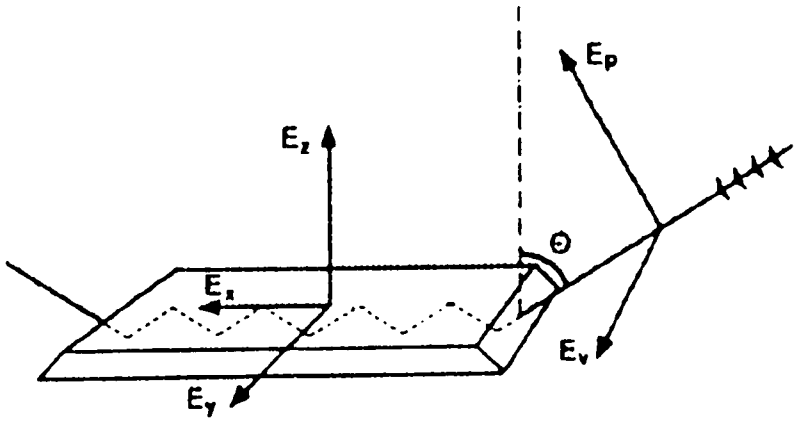
E_p
E_z
Θ
E_x
E_v
E_y

$$Ex = \frac{2\cos\theta(\sin^2\theta - n_{21}^2)^{1/2}}{(1-n_{21}^2)^{1/2}\left\{(1+n_{21}^2)\sin^2\theta - n_{21}^2\right\}^{1/2}} \tag{1.4}$$

$$Ez = \frac{2\cos\theta\sin\theta}{(1-n_{21}^2)^{1/2}\left\{(1+n_{21}^2)\sin^2\theta - n_{21}^2\right\}^{1/2}} \tag{1.5}$$

where $n_{21} = n_2/n_1$, n_1 being the refractive index of the sample, n_2 the refractive index of the ATR crystal and θ the angle of incidence. Under the experimental conditions here, with an angle of incidence, θ of 45°, the refractive index for the membranes n_1= 1.44 (Hübner and Mantsch, 1991) and for germanium crystal $n_2 = 4$, the electric field amplitudes are E_x =1.398, E_y = 1.516, and E_z = 1.625. E_y represents the electric field amplitude for perpendicular polarization and the total parallel electric field amplitude is given by:

$$E_{//} = \left(|E_x|^2 + |E_z|^2\right)^{1/2} \tag{1.6}$$

To record polarized infrared spectra of lipid vesicles, the vesicles must be oriented on the surface of the ATR element. I have used a simple technique of sample preparation on the ATR element called the solvent evaporation technique (Goormaghtigh and Ruysschaert, 1990). The membrane vesicles in solution are spread on the surface of the ATR element and dried carefully with a stream of nitrogen. While evaporating, the capillarity forces flatten the membrane which spontaneously forms multilayer arrangements (Fringeli and Günthard, 1981). Sample films are defined "thick" when the thickness of the film is much greater than the penetration depth and "thin" when the thickness is much smaller than the penetration depth. In the latter case, the light interacts

with the sample and the outside medium (water or air) as opposed to thick films where the light interacts only with the sample. I have assumed that my samples represent "thick films" and are much thicker that the penetration depth at 1600 cm^{-1}: 0.5 μm. The protein density for the gramicidin samples was ~500 $\mu g/cm^2$ whereas for the nAChR samples it was ~50 $\mu g/cm^2$. For the Ca^{2+}-ATPase from sarcoplasmic reticulum, a protein density of ~40 $\mu g/cm^2$ was defined as thick films by Buchet et al. (1991).

Molecular orientation is calculated through the evaluation of the order parameters (f), which describe the distribution of orientation. According to figure 5.2 , the angle γ is the angle between the crystal normal and the membrane normal, the angle β is between the helix axis and the membrane normal and the angle α is between the transition dipole moment and the helix axis. The angle of interest is the angle β which represents the average orientation of the α-helix with respect to the membrane normal. The observed order parameter ($f_{observed}$) is related to orientation according to:

$$f_{observed} = f_{\substack{mosaic \\ spread}} \times f_{helix} \times f_{dipole} = \left(\frac{3\cos^2\gamma - 1}{2}\right)\left(\frac{3\cos^2\beta - 1}{2}\right)\left(\frac{3\cos^2\alpha - 1}{2}\right) \qquad (1.6)$$

Figure 5.2 Orientation distribution of the membrane normal oriented at an angle γ from the plate normal, of the molecular axis oriented at an angle β from membrane normal and of the transition dipole moment oriented at an angle α from the molecular axis. From Goormaghtigh and Ruysschaert, 1990.

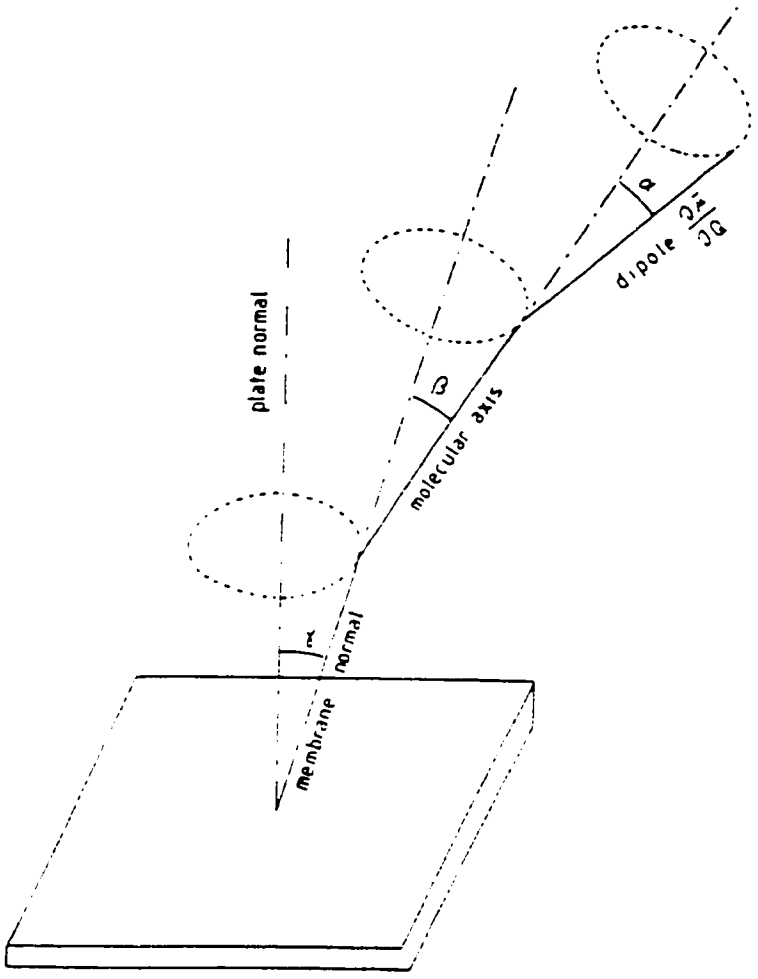
plate normal
molecular axis
dipole $\frac{\partial \chi}{\partial Q}$
membrane normal

Each of the angles decribed above has a corresponding order parameter. The individual order parameter $f_{\text{mosaic spread}}$ refers to the arrangement of the membranes on the ATR crystal, whereas f_{helix} refers to the orientation of the helices in the membrane and f_{dipole} to the orientation of the carbonyl dipole moment with respect to the helix axis. The value of ordering for the membranes can vary from 1 (perfect order) to 0 (perfect disorder). Note that a value of $f = 0$ can also represent orientation at the magic angle (54.7°). The value of ordering for the helices can vary from 1 (perpendicular orientation with respect to the membrane plane) to –0.5 (parallel orientation with the membrane plane).

Assuming an uniaxial model with fiber-type orientation for the transmembrane α-helices with an orientation normal to the ATR crystal, the order parameter f_{observed} can be obtained from the experimental R value according to (Hübner and Mantsch, 1991):

$$f(\beta) = \frac{R - 2}{R + 1.45} \bullet \frac{2}{3\cos^2 \alpha - 1} \qquad (1.7)$$

where the angle α between the transition dipole moment of the amide carbonyls and the helix axis is assumed to be 35° (Ludlam et al., 1996). This equation assumes a perfect mosaic spread.

4. Results

4.1 Polarization measurements of pure lipids and gramicidin

Gramicidin is a short peptide from the bacterium *Bacillus brevis* which forms ion channels in lipid bilayers and has been used in the past for its antibiotic properties. Gramicidin is used at the present time as a model peptide for the study of membrane protein structure and function relationship (Wooley and Wallace, 1994). Gramicidin is made of 15 alternating D- and L- amino acids which in the channel conformation is thought to adopt a right-handed $\beta^{6.3}$-helical dimer. Due to its short length, gramicidin orients predominantly perpendicularly to the membrane plane of DMPC vesicles as reported by several FTIR polarization studies (Nabedryk, Gingold and Breton, 1982; Okamura, Umemura and Takenaka, 1986; Bouchard and Auger, 1993). First, the ability of the system to detect such an orientation for both lipids and gramicidin was tested.

The ordering or disposition of the membrane vesicles on the surface of the ATR crystal is referred to as the mosaic spread and in order to detect the orientation of protein groups in transmembrane segments, it is necessary to evaluate it first. The symmetric CH_2 stretching vibration of the saturated lipid acyl chains, at 2850 cm^{-1}, is often used as a measure of the mosaic spread of the membranes since the transition dipole moment, assuming an all trans conformation, is perpendicular to the chain axis. At 2850 cm^{-1} (CH_2 symmetric stretching vibration) a dichroic ratio of $R_{CH2\ sym} = 1.22$ at 22.5 °C was calculated (Tm ~25°; Hübner and Manstch, 1991) for hydrated DMPC vesicles (figure 5.3 and table 5.2) in close agreement with the results of Hübner and Mantsch (1991) for

Figure 5.3 Polarized ATR-FTIR spectra of oriented DMPC membranes in ^2H_2O buffer at 22.5°C showing the region of the CH_2 symmetric and antisymmetric acyl chain vibrations. The spectra were recorded with the incident light either parallel (solid line) or perpendicular (dashed line) to the plane of incidence. The spectra were baseline corrected between 3000-2800 cm^{-1}.

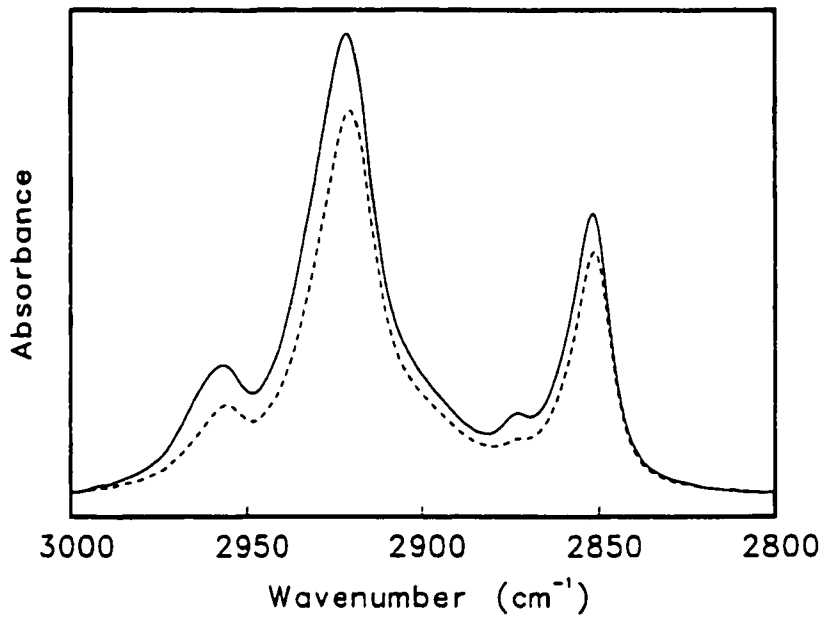
Absorbance
3000
2950
2900
2850
2800
Wavenumber (cm-1)

Table 5.2 Summary of the dichroic ratios calculated from the polarization measurements presented in Chapter 5. In some cases the average dichroic ratios are reported with the standard deviation or standard error. The values in parentheses are the calculated average tilt angles.

Sample	$R_{CH2\ sym}$	$R_{CH2\ anti}$	$R_{C=O\ lipids}$	$R_{amide\ I}$ (tilt angle)	$R_{amideII}$ (tilt angle)
Pure DMPC hydrated ^2H_2O 22.5°C n=3	1.22 ± 0	1.19 ± 0	1.38 ± 0.07		
Gramicidin/DMPC hydrated ^2H_2O 22.5°C n=4	1.26 ± 0.07	1.24 ± 0.06	1.55 ± 0.06	4.4 ± 0.3 (8.8 ± 7.8°)	1.6
nAChR/DMPC dry ^1H_2O 5°C	1.2	1.3	1.4	1.8 (64°)	1.7 (45°)
nAChR/DMPC dry ^2H_2O 5°C n=2	1.13± 0.10	1.2 ± 0.14	1.35 ± 0.07	1.6 ± 0.28	1.55 ± 0.21 (33 ± 13.7°)
nAChR/DMPC hydrated ^2H_2O 22.5°C n=2	1.31 ± 0	1.35 ± 0.07	1.5 ± 0	1.65 ± 0.21	1.6 ± 0.28 (29 ± 24°)
nAChR/DMPC ^2H_2O pH 2.0 22.5°C	1.3	1.4	1.5	1.75	1.5 (19°)
nAChR/Asolectin hydrated ^2H_2O, 22.5°C	1.6	1.6	1.6	1.95 ± 0.06 (58°) n=4	1.83 ± 0.10 (40°) n=4
Transmembrane domain (3.7 kDa)/ EPC/PA/Ch dry ^1H_2O			1.8	2.1 (41°)	1.7 (0°)

fully hydrated DMPC films. Note that the dichroic ratios reported in this chapter were calculated using band heights and were not significantly different than the values obtained using band areas. A summary of the dichroic ratios is reported in table 5.2, with calculated tilt angles. In some cases, the average of several experiments and the standard deviation is included. The order parameter calculated from the dichroic ratio of the lipid acyl chains is due to a combination of factors: the mosaic spread, the tilt and disorder of the acyl chains. The values of $R_{CH2\ sym}$ = 1.03 and 1.07 reported for dry DMPC vesicles films by Hübner and Mantsch (1991) and Bouchard and Auger (1993) were interpreted as an average tilt angle of the lipid acyl chains in the gel state of 22° and 25°, respectively. However, in the hydrated state, due to the expansion of the lipid bilayers, the acyl chains are likely not tilted. In order to evaluate the disposition of the DMPC vesicles on the ATR crystal, I have attributed the dichroic ratio of the lipid acyl chains exclusively to mosaic spread. This is an overestimation of the mosaic spread since a perfect order in the acyl chains is assumed, but in reality, this is not the case. This was clearly shown by the following results. The effect of temperature was tested on the dichroic ratio of the lipid acyl chains of DMPC vesicles containing the nAChR, below and above the melting temperature. The melting temperature of DMPC membranes containing the nAChR was first measured; T_m ~ 28.5°C, close to the value reported by Hübner and Mantsch (1991) for pure DMPC membranes: T_m ~ 25°C. The calculated dichroic ratio of the lipid acyl chains was $R_{CH2\ sym} = 1.13 \pm 0.1$ in the gel state (5°C) and a slight increase in the dichroic ratio was observed and consequently a decrease in the order parameter in the liquid crystalline state (35°C), $R_{CH2\ sym} = 1.20 \pm 0.13$, as reported by Hübner and Mantsch, 1991. The decrease in the order parameter with increasing temperature is linked to the

introduction of gauche conformers in the phospholipid acyl chain, however, likely does not represent any change in the mosaic spread. The effect of the temperature on the dichroic ratio of the lipid acyl chains in DMPC is in fact small and I neglected it to simplify the calculations. The mosaic spread of the DMPC vesicles of all experiments reported in this chapter was calculated directly from the dichoic ratio of the CH_2 symmetric stretching vibration. For example, for the pure lipid vesicles, a value of $f$ms = 0.58 was calculated.

Gramicidin gives rise to a narrow amide I band located at 1631 cm^{-1} in ^2H_2O (Fig. 5.4) (Bouchard and Auger, 1993). In the protiated form, gramicidin in membranes was shown to absorb around 1638 cm^{-1} (Nabedryk et al., 1982 and Okamura et al., 1986). Upon insertion in membranes, gramicidin orients perpendicularly to the membrane plane as confirmed by the observed high dichroic ratio ($R_{amide\ I} = 4.4 \pm 0.3$). An 8.8 ± 7.8° tilt angle was calculated using $f$mosaic spread = 0.546 and a 22.6° angle for the carbonyl transition dipole moment with respect to the helix axis. The 22.6° angle of the peptide carbonyl transition dipole moment was calculated by Nabedryk et al. (1982) by averaging the individual carbonyl transition dipole moments of the $\pi^{4.4}_{(L,D)}$ helix which has alternating D/L sequence but 4.4 residues per turn instead of 6.3 as gramicidin (Woolley and Wallace, 1994). Variations in the tilt angle of gramicidin in DMPC membranes have been reported: Nabedryk et al., 1982, $R_{amide\ I} = 3.10$ and 15° tilt; Okamura et al., 1986; $R_{amide\ I} = 4.8 \pm 0.3$ and 32 ± 2° tilt. It should be noted that none of these values take into account mosaic spread. For the sake of comparison, assuming a perfect mosaic spread in the experiments, the tilt angle of gramicidin would be 34 ± 2°. The nature of the discrepancy between these studies is likely due to differences in sample

Figure 5.4 Amide I' region of the polarized ATR-FTIR spectra of oriented DMPC vesicles containing gramicidin in $^{2}H_2O$ at 22.5 °C. The spectra were recorded with the incident light either parallel (solid line) or perpendicular (dashed line) to the plane of incidence. The spectra were baseline corrected between 1800-1500 cm^{-1}.

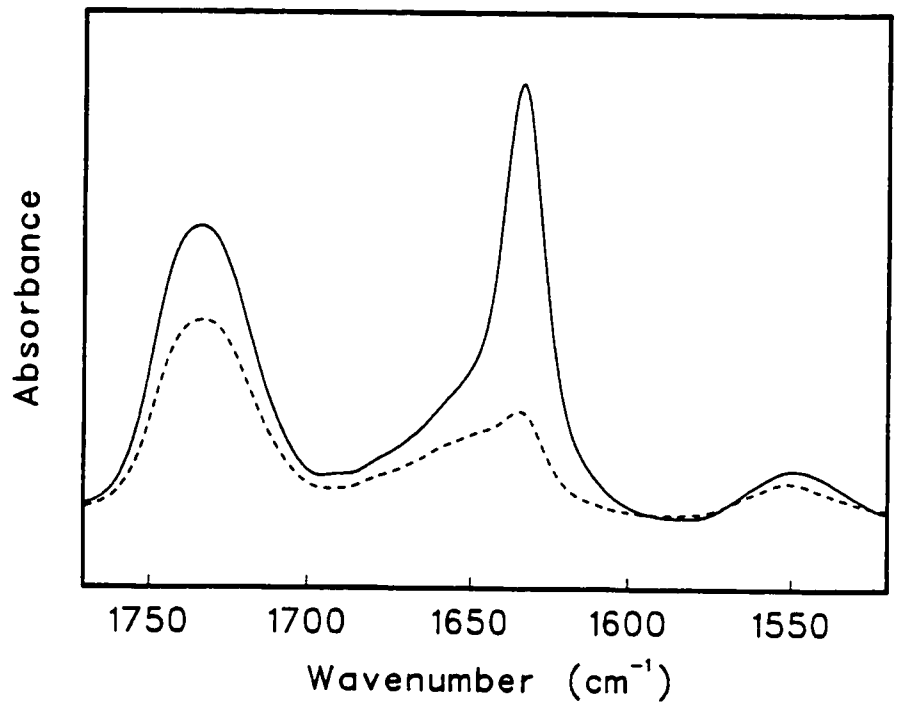
Absorbance
1750
1700
1650
1600
1550
Wavenumber (cm^{-1})

preparation and calculations. Since the polarization measurements on the pure DMPC lipids were in very close agreement with the results of Hübner and Manstch (1991) and Bouchard and Auger (1993) and since the results on gramicidin were close to the estimation of Okamura et al. (1986), we concluded that the system was reliable to measure tilt angles in the nAChR.

4.2 Orientation of the transmembrane segments in the nAChR

The major goal of this chapter was to determine the average orientation of the transmembrane α-helices in the nAChR by evaluating their tilt angle with respect to the bilayer normal. Polarization measurements were conducted on nAChR samples reconstituted in asolectin and DMPC membranes. Unsaturated acyl chains of phospholipids such as dioleoylphosphatidylcholine, the main phospholipid of asolectin, are highly disordered in the liquid crystalline phase which limits the evaluation of the mosaic spread. Indeed, the calculated dichroic ratios for both symmetric and antisymmetric CH_2 stretch was roughly 1.6 (Table 5.2). Since measurements in the gel phase for unsaturated phospholipids are difficult to achieve, the nAChR was reconstituted in saturated DMPC phospholipids in order to better evaluate the mosaic spread.

Polarized spectra of the intact nAChR were recorded in various conditions, for instance in the dry state, hydrated state, using between 125 and 500 μg of sample, etc. I measured the dichroic ratios of both amide bands of the nAChR in ^1H_2O and ^2H_2O using either the area of the band or the intensity and obtained unexpected results. Transmembrane helices oriented perpendicular to the bilayer plane usually give rise to an

opposite dichroism in the amide bands due to the opposite orientations of the transition dipole moments in the peptide bonds. The C=O transition dipole moment is mainly parallel to the helix while the N-H transition dipole moment is mainly perpendicular giving rise to a dichroic ratio in the amide I band above 2.0 and below 2.0 in the amide II band. Such an opposite dichroism was observed for example for bacteriorhodopsin ($R_{amide\ I}$ = 2.24 and $R_{amideII}$ = 0.98; Yang et al., 1987) and the EmrE multi-drug transporter in DMPC ($R_{amide\ I}$ = 2.8 and $R_{amideII}$ = 1.5). In contrast, a similar dichroism for the amide bands was observed both in ^1H_2O and ^2H_2O; $R_{amide\ I}$ = 1.8 and $R_{amideII}$ = 1.7 in ^1H_2O and $R_{amide\ I}$ = 1.4 and $R_{amideII}$ = 1.4 in ^2H_2O (fig. 5.5). Similar values for both amide bands were also reported for the myelin basic protein ($R_{amide\ I}$ = 1.64 and $R_{amideII}$ = 1.61, Nabet, Boggs and Pézolet, 1994) and Ca^{2+}-ATPase from sarcoplasmic reticulum ($R_{amide\ I}$ = 1.6 and $R_{amideII}$ = 1.57, Buchet et al., 1991). The lack of strong dichroism in the nAChR and other proteins could be due to the relatively minor contribution of the transmembrane helices to the overall absorption in the two amide bands.

Tilt angles from amide I and II dichroic ratios were calculated. The dichroic ratio of the amide I band in ^1H_2O, from the nAChR in DMPC membranes (at 5°C, see table 5.2) was $R_{amide\ I}$ = 1.8. From the dichroic ratio a calculated average tilt angle of 64° was calculated using a mosaic spread of $f$ms = 0.6 and an angle for the carbonyl dipole moment of 35° (Ludlam et al., 1996). From the dichroic ratio of the amide II band in ^1H_2O $R_{amideII}$ = 1.7, a 45° tilt was calculated with an 75° angle for the N-H dipole moment. A value of 60° is obtained for the amide I band and 42° for the amide II band if a perfect mosaic spread is assumed. In principle, the tilt angles calculated from both amide bands should converge, and as stated above, the divergence here may be explained

Figure 5.5 Polarized ATR-FTIR spectra of oriented DMPC vesicles containing the intact nAChR in $^{1}H_2O$ (A) and $^{2}H_2O$ (B) at 22.5 °C, in the amide I region. The spectra were recorded with the incident light either parallel (solid line) or perpendicular (dashed line) to the plane of incidence. The spectra were baseline corrected between 1800-1500 cm^{-1}.

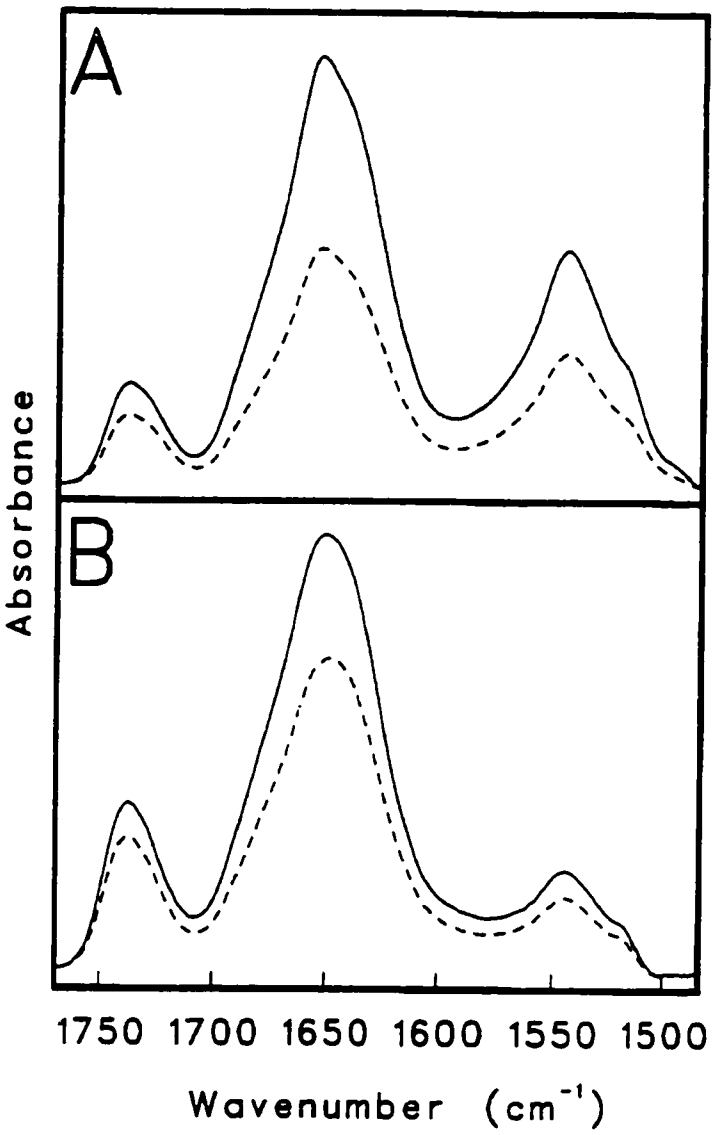
A
B
Absorbance
1750 1700 1650 1600 1550 1500
Wavenumber (cm^{-1})

by the relatively low proportion of transmembrane α-helices in the nAChR (~25%), as opposed to bacteriorhodopsin which is mainly made of transmembrane α-helices, and the overlap with other secondary structure components which on average "hides" the orientation of the transmembrane segments. Such a difference in the tilt angles calculated using both amide bands was observed before and was attributed to the spectral contribution of residue side chain vibrations (Nabet et al., 1994).

The dichroic ratio of the amide II band in ^2H_2O may be a better indication of the orientation of the transmembrane segments since the remaining N-H vibration at 1546 cm^{-1} after prolonged exposure corresponds mainly to unexchanged α-helices, many of which are likely located in the transmembrane domain. From the $R_{\text{amide II}} = 1.6 \pm 0.21$ (5°C) and $R_{\text{amide II}} = 1.6 \pm 0.28$ (22.5°C), tilt angles ranging from 29°-33° were calculated. Polarized spectra of the nAChR in DMPC were recorded in the presence of buffer prepared in ^2H_2O at pH 2.0 to upshift to absorption of carboxylic acid residues which overlaps in the amide II region and the calculated average tilt angle was roughly 19°.

Polarized FTIR spectra were recorded to evaluate the orientation of the transmembrane segments in proteolyzed nAChR. The highly characterized saturated DMPC membranes could not be used here due to the limited proteolysis observed in the nAChR reconstituted into those membranes (see fig. 4.6, upper panel, right lane). Consequently, I had to estimate the mosaic spread of the EPC:DOPA:Chol membranes in the molar ratio of 3:1:1 from the dichroic ratio at 1733 cm^{-1} of the lipid carbonyl band, $R_{C=O} = 1.8$. First, the tilt angle of the lipid carbonyls in pure DMPC vesicles was calculated from the dichroic ratio of the lipid carbonyl bands at 1733 cm^{-1}, $R_{C=O} = 1.8$.

With the calculated value of $f$dipole = -0.38, a 73° angle is obtained. This value was then used to calculate the mosaic spread of EPC:DOPA:Chol membranes, $f$ms = 0.16, 48°.

The dichroic ratio for the amide I and II bands was roughly 2.1 and 1.7, respectively, in the proteolyzed nAChR (fig. 5.6). This opposite dichroism in the amide bands is indicative of perpendicular transmembrane α-helices in the nAChR ($R_{amide\ I}$ above 2.0 and $R_{amide\ II}$ below 2.0). From the measured dichroic ratio, an average tilt angle for the transmembrane segments in the nAChR of roughly 41° was calculated from the amide I dichroism (assuming 35° angle of the carbonyl dipole moment of the peptide group) and of roughly 0° from the amide II dichroism (assuming a 75° angle of the N-H transition dipole moment) while taking into account the mosaic spread. Assuming a perfect mosaic spread, angles of 53° and 41° are obtained for the amide I and amide II bands, respectively. Again the discrepancy between the tilt angle calculated from both amide bands may be associated with the spectral contribution of other protein structures and amino acid side chains.

4.21 Effect of carbamylcholine on the orientation of the transmembrane α-helices

Quaternary rearrangements were observed in the desensitized state of the nAChR by electron microscopy at 18 Å (Unwin et al., 1988). The structural changes reported involved mainly the γ-subunit which was tilted by ~10° over a large fraction of its length.

Figure 5.6 Polarized ATR-FTIR spectra of the nAChR in EPC:DOPA:Chol vesicles containing the proteolyzed nAChR (< 3.7 kD) after 2 hours of exposure to $^{2}H_{2}O$. The spectra were recorded with the incident light either parallel (solid line) or perpendicular (dashed line) to the plane of incidence. The spectra were baseline corrected between 1800-1500 cm^{-1}.

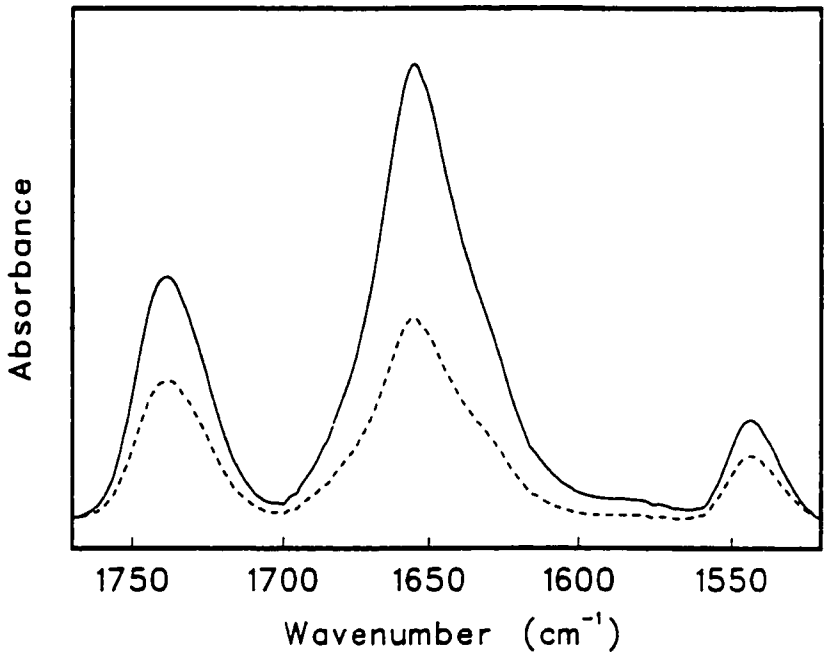
Absorbance
1750
1700
1650
1600
1550
Wavenumber (cm-1)

Localized changes were also reported in the other subunits. These structural rearrangements could possibly involve changes in the tilt of the transmembrane segments. To test this possibility, I recorded FTIR polarized spectra of the nAChR reconstituted into asolectin membranes in the absence and presence of 1 mM Carb after prolonged exposure to ^2H_2O (fig. 5.7). Note that the same protein sample was used to record the four spectra avoiding any sample artifact. In the presence of Carb, the polarized spectra did not exhibit any significant change in dichroism and it was concluded that if any change in the tilt of the transmembrane segments occurs in the desensitized state, it is too small to be detected by the current technique.

5. Discussion

Polarized FTIR spectra of pure lipids vesicles and of gramicidin containing vesicles were recorded in order to determine if the equipment (polarizer, ATR crystal, ATR stage, etc.) and sample preparation technique on the ATR element were reliable. According to Goormaghtigh and Ruysschaert (1990) a number of experimental factors can distort the polarization measurements. For instance, germanium crystals are generally used due to the hardness of their surfaces since scratched and poorly polished surfaces will not allow an excellent orientation of the membranes. Moreover, the quality of the polarizer and the alignment of the mirrors of the ATR stage influence the ability of the system to produce perfectly polarized light.

I have followed the procedure described in Bouchard and Auger (1993) for the lipid and gramicidin preparation, with a few modifications. The sample was spread on

Figure 5.7 Polarized ATR-FTIR spectra of the intact nAChR in asolectin membranes in the absence (solid line) and presence of 50 mM Carb (dashed line). The more intense spectra were recorded with the incident light parallel to the plane of incidence while the less intense spectra were recorded with perpendicular light. The spectra were baseline corrected between 1800-1500 cm^{-1}.

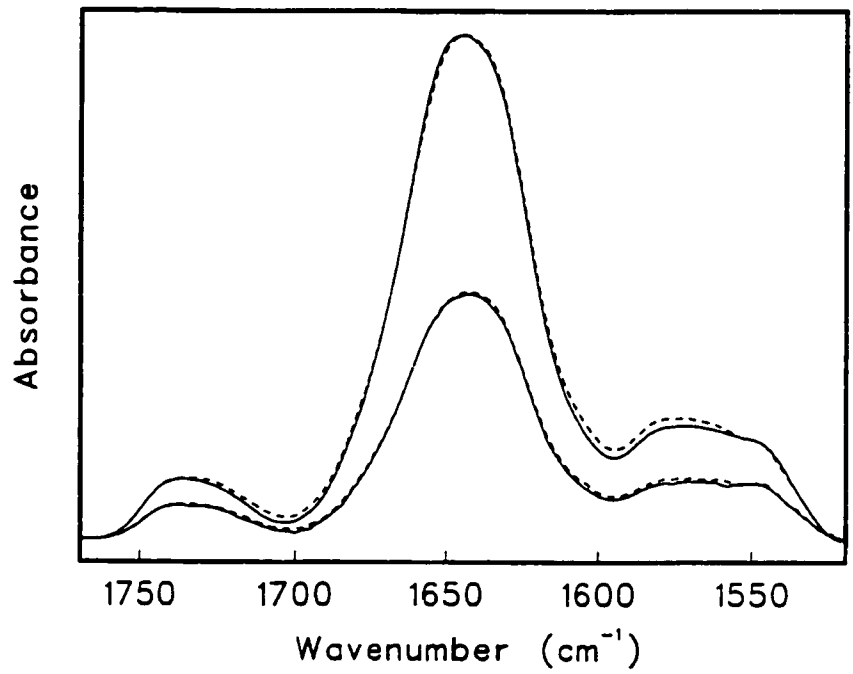
Absorbance
1750
1700
1650
1600
1550
Wavenumber (cm⁻¹)

the ATR element, but I did not use a Teflon bar to spread the sample on the surface (Fringeli and Günthard, 1981). The buffer was simply evaporated slowly using a gentle stream of N_2 (g). This technique allowed comparable mosaic spread of the DMPC vesicles to the results of Hübner and Manstch, 1991 and Bouchard and Auger, 1993 for hydrated DMPC membranes.

From the value of $R_{amide\ I} = 4.4 \pm 0.3$, a tilt angle of $8.8 \pm 7.8°$ for gramicidin in DMPC membranes was calculated, while taking into account the disordering effect of the mosaic spread. Without taking into account the mosaic spread, a tilt angle of $34 \pm 2°$ was calculated in close agreement with Okamura et al. (1986) ($R_{amide\ I} = 4.8 \pm 0.3$; tilt angle $32 \pm 2°$) but not with Nabedryk et al. (1982) ($R_{amide\ I} = 3.1$; tilt angle 15°). The variation between the tilt angles of gramicidin in DMPC membranes in those studies can be partially explained by difference in sample preparation and calculations. Since the results for the lipid dichroism were in excellent agreement with the results of Hübner and Manstch (1991) and Bouchard and Auger (1993) and since the dichroism of gramicidin in DMPC membranes was consistent with the results of Okamura et al. (1986), it was concluded that the method was reliable.

To evaluate the orientation of the transmembrane α-helices in the nAChR, two approaches were used. Their orientation was evaluated first in the intact protein reconstituted into DMPC membranes and second, in proteolyzed nAChR reconstituted into EPC:DOPA:Chol membranes in the molar ratio 3:1:1. While the dichroism in the intact nAChR was difficult to interpret, the dichroism of the proteolyzed nAChR clearly showed a perpendicular orientation with respect to the membrane surface. The calculations propose an average tilt angle in the transmembrane helices of roughly 19-33°

from the amide II dichroic ratio of the intact receptor after prolonged exposure to ^2H_2O. On the other hand, in the proteolyzed nAChR, the amide I dichroic ratio gives an average tilt angle of 41°, while the amide II gives an average tilt angle of roughly 0°. In principle, these results should converge since those vibrations are mainly due the transmembrane segments in the nAChR.

The calculation of the tilt angle of transmembrane segments in membrane proteins is associated with a large extent of uncertainty with the right estimation of the refractive index of the sample, the angle of the helix carbonyl and N-H dipole moments and the mosaic spread. A refractive index of 1.44 (Hübner and Manstch, 1991; Bouchard and Auger, 1993) was assumed for both lipid and protein samples. In contrast, values of 1.5 to 1.55 for lipids and 1.7 for proteins have been reported (Goormaghtigh and Ruysschaert, 1990).

The orientation of the transition dipole moment of the carbonyl and N-H in the peptide bonds vary from one study to the other. Values of 15° in bacteriorhodopsin, (Rothschild and Clark, 1979), 29-34° in poly-α-benzyl-L-glutamate (Miyazawa and Blout, 1961), 35° in phospholamban (Ludlam et al., 1996) and 39° in poly-α-benzyl-L-glutamate (Tsuboi, 1962) were reported for the carbonyl transition dipole moment of the peptide bonds. Similarly, variations are found in the tilt angle of the amide II vibration of the peptide groups, 75-77° in poly-α-benzyl-L-glutamate (Miyazawa and Blout, 1961 and Tsuboi, 1962) and 75° in bacteriorhodopsin (Rothschild and Clark, 1979). A transition dipole moment of 35° for the carbonyl transition dipole moment (Ludlam et al., 1996) and 75° for the N-H transition dipole moment (Tsuboi, 1962) was used since these values were representative of most of the values reported.

A major difficulty in orientation measurements with physiological lipid membranes is the precise evaluation of the mosaic spread for which little is known as opposed to model membranes as DMPC or DPPC which are better characterized. X-ray diffraction experiments have been conducted previously to determine mosaic spreads. For instance, Stamatoff, Graddick, Powers and Moncton (1979) have detected mosaic spreads of less than 15° for DPPC bilayers. Similarly, a 15° mosaic spread was reported for sarcoplasmic reticulum membranes (Buchet et al., 1991). On the other hand, Michel-Villaz et al. (1979) have estimated a mosaic spread of 31° from retinal rod outer segments sedimented in a magnetic field. From the lipid dichroism measurements, a mosaic spread around 25°, $f$ms = 0.60 was estimated for DMPC vesicles from the dichroic ratio of the CH_2 symmetric stretching vibration located at 2850 cm^{-1}. A 41°, $f$mosaic spread = 0.35 and 48°, $f$mosaic spread = 0.16 were calculated for asolectin and EPC/DOPA/Chol membranes, respectively, based on the dichroism of the carbonyl of the phospholipid head group around 1733 cm^{-1}.

Despite these uncertainties, the results suggest an overall perpendicular orientation for the transmembrane α-helices in the nAChR. The dichroism observed in the amide bands does not support the presence of transmembrane β-sheets in the nAChR oriented perpendicularly to the membrane surface since the carbonyl transition dipole moment in a β-sheet is oriented predominantly perpendicularly to the fiber axis (Goormaghtigh and Ruysschaert, 1990). Perpendicular transmembrane β-sheets would give rise to a lower dichroism in the amide I band and a higher dichroism in the amide II band.

Using polarized FTIR spectroscopy, several groups have studied the orientation of transmembranes helices in membrane proteins such as rhodopsin (40°, Rothschild et al., 1980), photosynthetic reaction center (35°, Nabedryk et al., 1982), bacteriorhodopsin (26°, Rothschild and Clark, 1979; 24-27° Earnest et al., 1990). In contrast, polarized FTIR spectroscopy detected a perpendicular orientation of the apolipophorin α-helix relative to the lipid hydrocarbon chains of DMPC vesicles (Raussens, Narayanaswami, Goormaghtigh, Ryan and Ryusschaert, 1995). The orientation of the transmembrane β-strands in porin was also revealed by polarized FTIR spectroscopy studies. Goormaghtigh et al. (1990) have calculated an average tilt angle of 35°, whereas Naberdyk et al. (1988) have reported an average tilt angle of 48°. The structure of some of the membrane proteins cited above is known at high resolution; the photosynthetic reaction center (Deisenhofer et al., 1985), bacteriorhodopsin (Pebay-Peyroula et al., 1997), and porin (Weiss et al., 1991) and the calculated tilt angles are consistent with the tilt angles revealed in the crystal structures.

In the presence of carbamylcholine, I did not detect a change in the dichroism of the amide bands which could suggest a net change in the orientation of the transmembrane segments upon desensitization. In principle, a tilt change of 10° for all 20 transmembrane segments, for example from an average 40° tilt to an average 50° tilt would give rise to a change in the dichroic ratio from 2.2 to 2.06. On the other hand, a change of only 1° in the tilt angles from 40° to 41° would change the dichroic ratio from 2.2 to 2.19. Since variations are observed in the dichroic ratios from sample to sample, the measurements in the presence of carbamylcholine were conducted on the same sample to limit the error with the use of a different sample. Since the dichroic ratio was

unchanged in the presence of Carb, it can be concluded that if any transmembrane helix experiences a change in tilt upon desensitization, it is likely small (less than 5°) and localized.

6. Conclusion

I have shown that DMPC membranes stack relatively well on the surface of the ATR crystal. Moreover, gramicidin in DMPC membranes orients quite perpendicularly to the membrane plane, with a tilt angle of roughly 9°. Polarized FTIR spectra of the isolated transmembrane domain of the nAChR are indicative of a perpendicular orientation of the transmembrane α-helices with respect to the membrane plane and the calculated average tilt angle from the dichroic ratio of the amide I band is roughly 41°. I did not detect a large change in the tilt of the transmembrane α-helices upon desensitization of the nAChR.

Chapter 6- General Discussion

Several aspects of the structure and mechanism of action of the nAChR were controversial at the beginning of this research project. Basic questions regarding the nAChR's secondary structure and mechanism of desensitization were investigated and the results presented here clarify some controversial issues of the nAChR and build on the knowledge of the nAChR. The work supports an all α-helical transmembrane domain for the nAChR with a perpendicular orientation of the transmembrane segments with respect with the lipid bilayer. In the desensitized state, the results suggest a lack of large overall changes in conformation of the protein and no important change in orientation of the transmembrane segments. These results provide a general picture of the secondary structure of the nAChR and some of the approaches used in this thesis were novel and could potentially be used to study the structure of other membrane proteins.

The results contradict the report by Unwin (1993) of electron microscopy at medium resolution (9 Å) which proposed the presence of 5 or 7 β-sheets per subunit of the nAChR. Recently, by technical and computational improvements of the electron microscopy technique, Miyazawa et al. (1999) reached 4.6 Å resolution on the structural investigation of the nAChR. Although sections of the protein were better resolved, there was no mention of the secondary structure of the transmembrane segments. Interestingly, both rhodopsin and bacteriorhodopsin displayed seven well resolved peaks of electron density at 9 Å resolution (Schertier, Villa and Henderson, 1993), which correspond to seven transmembrane α-helices. The lack of well defined electron density in the periphery of the pore in Unwin's pictures (Unwin, 1993; Miyazawa et al., 1999) could be

explained by the assumption of five-fold symmetry, or structural identity in the transmembrane domain of the nAChR. It is possible that the M2 helices are positioned similarly in the four subunits and have a comparable structure giving rise to the clear electron densities. However the position, orientation and shape of the other helices could vary from one subunit to the other resulting in a scattered electron density in the averaged pictures. This particularity of the nAChR as a pentameric protein with non-identical subunits may limit the ability of electron microscopy to better resolve its structure.

The fact that the M1, M3 and M4 transmembrane segments appear α-helical instead of β-sheets or a combination of both has implications in terms of the mechanism of coupling between the ligand binding site and channel gating in the nAChR. Even though it is established that the M2 segments are α-helical, line the ion channel and are likely involved in physically gating the ion channel in the closed state, other segments are possibly involved as well. M1 is a good candidate for the coupling binding the ligand binding site and the ion channel since residues thought to be involved in ligand binding including the highly conserved cysteine residues C192-C193 are located only roughly 20 amino acids N-terminal to the M1 segment. In addition, Akabas and Karlin (1995) have shown that the N-terminal third of αM1 contributes to the lining of the ion channel. However, the pattern of accessibility was not consistent with an α-helix or β-sheet, it was suggested that this segment of M1 adopts an irregular secondary structure. Experimental evidence from cysteine substitution experiments (Akabas and Karlin, 1995), TID labeling (Blanton and Cohen, 1994) and CD spectroscopy (Corbin et al., 1998) support an irregular secondary structure for part of M1. M1 could be largely irregular in the first third, and possibly exposed to the lumen of the channel and fold as a helix in the second

two thirds. I speculate that the transmembrane domain of the nAChR is made of M1, M2, M3 and M4 as α-helices with the N-terminal third of M1 irregular and exposed to the lumen of the channel.

The exact location of the gate in the nAChR's channel is still a matter of debate making development of channel gating models for the nAChR difficult. Basically, Unwin proposes a gate located near the middle of the membrane, where a ring of highly conserved leucine residues (L251) in the kinked M2s, by facing in the lumen of the pore would prevent ion flux (Unwin, 1995 and Miyazawa et al., 1999). According to this model, ligand binding would result in bending of the M2 segments tangentially to the central axis, displacement of the leucine side chains and opening of the gate (Unwin, 1995). This is consistent with the TID labeling results of White and Cohen (1992) in the absence and presence of agonist which initially suggested a gate formed by aliphatic leucine and valine residues. Two site-directed mutagenesis studies have shown that mutation of one or more conserved leucine residues with polar residues slowed down desensitization, increased the affinity for agonists and increased the mean open time of the channel (Labarca et al., 1995 and Filatov and White, 1995). These results support the important role of the conserved leucines in channel gating. However, Filatov and White (1995) suggested that the role of the leucine residues is to control the mean open time of the channel more than to actually form the gate of the channel.

On the other hand, Akabas and Karlin (1995) and Wilson and Karlin (1998), using the substituted-cysteine accessibility method which probed the accessibility of the mutated residues to small, cationic sulfhydryl-specific reagents, observed that a number of residues in the channel, including L251 and residues located N-terminal to L251, were

labeled by the reagent in the closed state and therefore exposed to the lumen of the channel. The labeling was consistent with the M2 segment folded in an α-helix interrupted by a stretch of three consecutive residues, L250, L251 and S252 in an extended conformation. They proposed a cytoplasmic location for the gate in the nAChR between G240 and T244, involving residues in the loop between M1 and M2. A more detailed picture of the structure of the transmembrane segments in the nAChR, especially of the M2 segments, is essential in order to better understand the mechanism of channel gating in the nAChR. Hopefully in the near future, the crystallization conditions for the nAChR will be refined and allow the elucidation of its structure at atomic resolution.

In order to provide a visual representation of the results presented in the thesis, a structural model of the channel is presented (fig. 6.1). The current knowledge regarding the location of the gate and the presence of kinks and bends is still controversial to allow a detailed model. However, the model more likely represents membrane protein structure than the other models presented so far in which the channel structure was very simplistic (Changeux, 1993). The model is a cross section of the channel, showing only the two identical α-subunits. A five-fold symmetry is assumed. Each subunit is made of a four helix-bundle motif where the helices are inclided at an angle of 18° with respect to one another (Sheridan, Levy and Salemme, 1982). Each helix-bundle is tilted substantially and form a funnel shaped channel. Such helical bundle motifs form a very compact structure and occurs in the photosynthetic reaction center (Reithmeier and Deber, 1992). The 4 transmembrane segments are α-helical except the first third of M1 which is distorded and exposed to the lumen of the channel. The M2 segments line the ion channel. The loop between M1 and M2 are located close to the channel as they may be

Figure 6.1 Schematic model of the channel of the nAChR (see text).

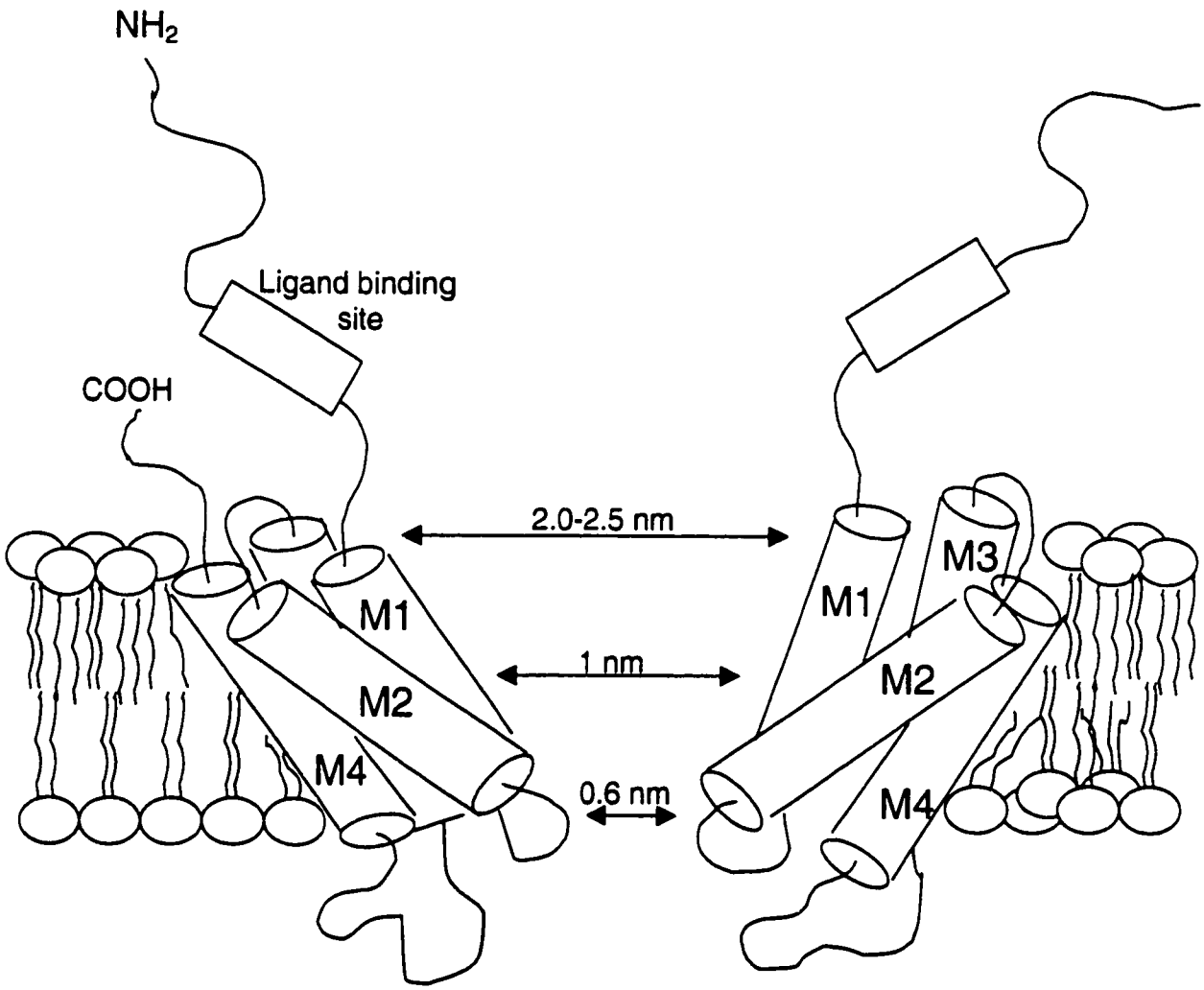
NH2
Ligand binding site
COOH
2.0-2.5 nm
M1
M2
M4
1 nm
0.6 nm
M1
M3
M2
M4

involved in channel selectivity. The M4 segments are highly exposed to the lipids. Also shown, a possible location of the ligand binding site.

The results also support a lack of change in the secondary structure and large reorganization of the nAChR in the desensitized state stabilized after prolonged exposure to agonist or upon reconstitution in membranes lacking cholesterol and anionic phospholipids. In addition, the average tilt of the transmembrane α-helices was not modified significantly in the presence of Carb. These results imply that the conformational changes involved in the desensitized state of the nAChR are small and localized. In an attempt to further investigate the changes in conformation in the desensitized state of the nAChR, I conducted preliminary experiments using polarized difference spectroscopy. This technique allows the visualization of the small conformational changes between two states of the nAChR, for instance, the resting and desensitized state and the spatial orientation of the vibrational groups. The results were preliminary, and due to the lack of time, no valid conclusion could be drawn. In the future this technique may possibly support the assignment of the difference bands to structures of the nAChR in the resting-to-desensitized spectra of the nAChR and provide detailed insights into the mechanism of desensitization.

References

Adams, P.R. (1981) Acetylcholine receptor kinetics. J. Membr. Biol. 58, 161-174.

Akabas, M.H. and Karlin, A. (1995) Identification of acetylcholine receptor channel-lining residues in the M1 segment of the α-subunit. Biochemistry 34, 12496-12500.

Akabas, M.H., Kaufmann, C., Archdeacon, P. and Karlin, A. (1994) Identification of acetylcholine receptor channel-lining residues in the entire M2 segment of the α-subunit. Neuron 13, 919-927.

Anderson, D.J., Walter, P. and Blobel, G. (1982) Signal recognition protein is required for the integration of acetylcholine receptor δ subunit, a transmembrane glycoprotein, into the endoplasmic reticulum membrane. J. Cell Biol. 93, 501-506.

Arias, H.R. (1996) Luminal and non-luminal non-competitive inhibitor binding sites on the nicotinic acetylcholine receptor. Mol. Membr. Biol. 13, 1-17.

Arkin, I.T., Rothman, M., Ludlam, C.F.C., Aimoto, S., Engelman, D.M., Rothschild, K.J. and Smith, S.O. (1995) Structural model of the phospholamban ion channel complex in phospholipid membranes. J.Mol. Biol. 248, 824-834.

Arrondo, J.L.R., Muga, A., Castresana, J. and Goñi, F.M. (1993) Quantitative studies of the structure of proteins in solution by Fourier-transform infrared spectroscopy. Prog. Biophys. Molec. Biol. 59, 23-56.

Artigues, A., Villar, M.T., Ferragut, J.A. and Gonzalez-Ros, J.M. (1987) Thermal perturbation studies of membrane-bound acetylcholine receptor from *Torpedo*: Effects of cholinergic ligands and membrane perturbants. Arch. Biochem. Biophys. 258, 33-41.

Aslanian, D., Grof, P., Galzi, J.-L. and Changeux, J.-P. (1993) A Raman spectroscopic study of acetylcholine receptor-rich membranes from Torpedo marmorata. Interaction of the receptor with carbamylcholine and (+)-tubocuranine. Biochim. Biophys. Acta 1148, 291-302.

Baenziger, J.E. and Chew, J. P. (1997) Desensitization of the nicotinic acetylcholine receptor involves a relatively large structural change in solvent accessible regions of the polypeptide backbone. Biochemistry 36, 3617-3624.

Baenziger, J.E. and Méthot, N. (1995) Fourier transform infrared and hydrogen/deuterium exchange reveal an exchange-resistant core of α-helical peptide hydrogens in the nicotinic acetylcholine receptor. J. Biol. Chem. 270, 29129-29137.

Baenziger, J.E., Miller, K.W. and Rothschild, K.J. (1993) Fourier transform infrared difference spectroscopy of the nicotinic acetylcholine receptor: Evidence for specific protein structural changes upon desensitization. Biochemistry 32, 5448-5454.

Bazzi, M.D. and Woody, R.W. (1985) Oriented secondary structure in integral membrane proteins. Biophys. J. 48, 957-966.

Bechinger, B., Kim, Y., Chirlian, L.E., Gesell, J., Neumann, J.M., Montal, M., Tomich, J., Zasloff, M. and Opella, S.J. (1991) Orientation of amphipathic helical peptides in membrane bilayers determined by solid-state NMR spectroscopy. J. Biomol. NMR 1, 167-173.

Bertrand, D., Galzi, J.-L., Devillers-Thiéry, Bertrand, S., and Changeux, J.-P. (1993) Stratification of the channel domain in neurotransmitter receptors. Curr. Opin. Cell Biol. 5, 688-693.

Bhushan, A. and McNamee, M.G. (1993) Correlation of phospholipid structure with functional effects on the nicotinic acetylcholine receptor. Biophys. J. 64, 716-723.

Blanton, M.P. and Cohen, J.B. (1992) Mapping the lipid-exposed regions in the *Torpedo californica* nicotinic acetylcholine receptor. Biochemistry 31, 3738-3750.

Blanton, M.P. and Cohen, J.B. (1994) Identifying the lipid-protein interface of the *Torpedo* nicotinic acetylcholine receptor: secondary structure implications. Biochemistry 33, 2859-2872.

Bouchard, M. and Auger, M. (1993) Solvent history dependence of gramicidin-lipid interactions: A Raman and infrared spectroscopic study. Biophys. J. 65, 2484-2892.

Brisson, A. and Unwin, P.N.T. (1985) Quaternary structure of the acetylcholine receptor. Nature 315, 474-477.

Buchet, R., Varga, S., Seidler, N.W., Molnar, E. and Martonosi, A. (1991) Polarized infrared attenuated total reflectance spectroscopy of the Ca^{2+}-ATPase of sarcoplasmic reticulum. Biochim. Biophys. Acta 1068, 201-216.

Butler, D.H. and McNamee, M.G. (1993) FTIR analysis of nicotinic acetylcholine receptor secondary structure in reconstituted membranes Biochim. Biophys. Acta 1150, 17-24.

Byler, D.M. and Susi, H. (1986) Examination of the secondary structure of proteins by deconvolved FTIR spectra. Biopolymers 25, 469-487.

Campos-Caro, A., Rovira, J.C., Vincente-Agulló, F., Ballesta, J.J., Sala, S., Criado, M. and Sala, F. (1997) Role of the putative transmembrane segment M3 in gating of neuronal nicotinic receptors. Biochemistry 36, 2709-2715.

Capasso, J.M., Hoving, S., Tal, D.M., Goldshleger, R. and Karlish, S.J.D. (1992) Extensive digestion of Na^+,K^+-ATPase by specific and nonspecific proteases with preservation of cation occlusion sites. J. Biol. Chem. 267, 1150-1158.

Castresana, J., Fernandez-Ballester, G., Fernandez, A.M., Laynez, J.L., Arrondo, J.-L., Ferragut, J.A. and Gonzalez-Ros, J.M. (1992) Protein structural effects of agonist binding to the nicotinic acetylcholine receptor. FEBS 314, 171-175.

Challou, N., Goormaghtigh, E., Cabiaux, V., Conrath, K. and Ruysschaert, J.-M. (1994) Sequence and structure of the membrane-associated peptide of glycophorin A. Biochemistry 33, 6902-6910.

Changeux, J.-P. (1993) Chemical signaling in the brain. Scientific American 269, 58-62.

Changeux, J.-P., Bertrand, D., Corringer, J.-P., Dehaene, S., Edelstein, S., Léna, C., Le Novère, N., Marubio, L., Picciotto, M. and Zoli, M. (1998) Brain nicotinic receptors: structure and regulation, role in learning and reinforcement. Brain research reviews 26, 198-216.

Chavez, R.A. and Hall, Z.W. (1991) The transmembrane topology of the amino terminus of the α subunit of the nicotinic acetylcholine receptor. J. Biol. Chem. 266, 15532-15538.

Chavez, R.A. and Hall, Z.W. (1992) Expression of fusion proteins of the nicotinic acetylcholine receptor from mammalian muscle identifies the membrane-spanning regions in the α and δ subunits. J. Cell Biol. 116, 385-393.

Chothia, C., Levitt, M. and Richardson, D. (1981) Helix to helix packing in proteins. J. Mol. Biol. 145, 215-250.

Claudio, T., Ballivet, M., Patrick, J. and Heinemann, S. (1983) Nucleotide and deduced amino acid sequences of *Torpedo californica* acetylcholine receptor γ-subunit. Proc. Natl. Acad. Sci. U.S.A. 80, 1111-1115.

Coggan, J.S., Paysan, J., Conroy, W.G., and Berg, D.K. (1997) Direct recording of nicotinic responses in presynaptic nerve terminals. J. Neurosci. 17, 5798-5806.

Colthup, N.B., Daly, L.H., and Wiberley, S.E. (1990) In: Introduction to Infrared and Raman Spectroscopy. *3rd Ed.:* Academic Press, San Diego.

Conley, E.C. (1996) In: The ion channel facts book. Extracellular ligand-gated ion channels (Academic Press, New York)

Cooley, J.W., and Tukey, J.W. (1965) Math. Comput. 19, 297.

Corbalán-Garcia, S., Teruel, J.A., Villalaín, J. and Gómez-Fernandez, J.C. (1994) Extensive proteolytic digestion of the (Ca2+ + Mg2+)-ATPase from sarcoplasmic reticulum leads to a highly hydrophobic proteinaceous residue with a mainly alpha-helical structure. Biochemistry 33, 8247-8254.

Corbin, J., Méthot, N., Wang, H.H., Baenziger, J.E. and Blanton, M.P. (1998) Secondary structure analysis of individual transmembrane segments of the nicotinic acetylcholine receptor by circular dichroism and Fourier transform infrared spectroscopy. J. Biol. Chem. 273, 771-777.

Cowan, S.W., Schrimer, T., Rummel, G., Steiert, M., Ghosh, R., Pauptit, R.A., Jansonius, J.N. and Rosenbusch, J.P. (1992) Crystal structures explain functional properties of two E. coli porins. Nature 358, 727-733.

Czajkowski, C., DiPaola, M., Bodkin, M., Salazar-Jimenez, G., Holtzman, E. and Karlin, A. (1989) The intactness and orientation of acetylcholine receptor-rich membranes from *Torpedo californica* electric tissue. Arch. Biochem. Biophys. 272, 412-420.

DiPaola, M., Czajkowski, C. and Karlin, A. (1989) The sidedness of the COOH terminus of the acetylcholine receptor δ-subunit. J. Biol. Chem. 264, 15457-15463.

Deisenhofer, J., Epp, O., Miki, K., Huber, R. and Michel, H. (1985) Structure of the protein subunits in the photosynthetic reaction centre of Rhodopseumodas viridis at 3 Å resolution. Nature 318, 618-624.

Dong, A., Prestrelski, S.J., Allison, S.D., and Carpentier, J.F. (1995) Infrared spectroscopic studies of lyophilization- and temperature-induced protein aggregation. J. Pharma. Sc. 84, 415-424.

Dousseau, F. and Pézolet, M. (1990) Determination of the secondary structure content of proteins in aqueous solutions from their amide I and amide II infrared bands. Comparison between classical and partial least-squares methods. Biochemistry 29, 8771-8779.

Doyle, D.A., Morais Cabral, J., Pfuetzner, R.A., Kuo, A., Gulbis, J.M., Cohen, S.L., Chait, B.T. and MacKinnon, R. (1998) The structure of the potassium channel: Molecular basis of K+ conduction and selectivity. Science 280, 69-77.

Earnest, T.N., Herzfeld, J. and Rothschild, K.J. (1990) Polarized fourier transform infrared spectroscopy of bacteriorhodopsin. Biophys. J. 58, 1539-1546.

Elliot, A. and Ambrose, E.J. (1950) Structure of synthetic polypeptides. Nature 165, 921-922.

Englander, S.W., Calhoun, D.B., Englander, J.J., Kallenbach, R.K., Liem, H., Malin, E.L., Mandal, C. and Rogero, J.R. (1980) Individual breathing reactions measured in hemoglobin by hydrogen exchange methods. Biophys. J. 10, 577-587.

Englander, J.J., Downer, N.W and Englander, S.W. (1982) Re-examination of rhodpsin structure by hydrogen exchange. J. Biol. Chem. 257, 7982-7986.

Englander, S.W., Downer, N.W. and Teitelbaum, H. (1972a) Hydrogen exchange. Ann. Rev. Biochem. 41, 903-924.

Englander, S.W. and Kallenbach, N.R. (1984) Hydrogen exchange and structural dynamics of proteins and nucleic acids. Quat. Rev. Biophys. 16, 521-655.

Englander, S.W. and Mauel, C. (1972b) Hydrogen exchange studies of respiratory proteins. II. Detection of discrete, ligand-induced changes in hemoglobin. J. Biol. Chem. 247, 2387-2394.

Fernandez-Ballester, G., Castresana, J., Arrondo, J.-L.R., Ferragut, J.A. and Gonzalez-Ros, J.M. (1992) Protein stability and interaction of the nicotinic acetylcholine receptor with cholinergic ligands studied by Fourier-transform infrared spectroscopy. Biochem. J. 288, 421-426.

Fernandez-Ballester, G., Castresana, J., Fernandez, M., Arrondo, J.-L.R., Ferragut, J.A. and Gonzalez-Ros, J.M. (1994) A role for cholesterol as a structural effector of the nicotinic acetylcholine receptor. Biochemistry 33, 4065-4071.

Filatov, G.N. and White, M.M. (1995) The role of conserved leucines in the M2 domain of the acetylcholine receptor in channel gating. Mol. Pharma. 48, 379-384

Fong, T.M. and McNamee, M.G. (1986) Correlation between acetylcholine receptor function and structural properties of membranes. Biochemistry 25, 830-840.

Fong, T.M. and McNamee, M.G. (1987) Stabilization of acetylcholine receptor secondary structure by cholesterol and negatively charged phospholipids in membranes. Biochemistry 26, 3871-3880.

Fringeli, U.P. and Günthard, H.H. (1981) Infrared membrane spectroscopy, In Molecular biology, biochemistry and biophysics, Vol.31, Eds.: Grell, E., (Springer-Verlag, Berlin), 270-331.

Galzi, J.-L. and Changeux, J.-P. (1992) The nicotinic acetylcholine receptor, a model of ligand-gated ion channels: Investigation of its functional organization by protein chemistry and site-directed mutagenesis, In Membrane Proteins: Structure, Interactions and Models, Eds.: A. Pullman, Netherlands, 127-146.

Galzi, J.-L., Devillers-Thiéry, A., Hussy, N., Bertrand, S., Changeux, J.-P and Bertrand, D. (1992) Mutations in the ion channel domain of a neuronal nicotinic receptor convert ion selectivity from cationic to anionic. Nature 359, 500-505.

Galzi, J.-L., Revah, F., Bouet, F., Ménez, A., Goeldner, M., Hirth, C. and Changeux. J.-P. (1991) Allosteric transitions of the acetylcholine receptor probed at the amino acid level with a photolabile cholinergic ligand. Proc. Natl. Acad. Sci U.S.A. 88, 5051-5055.

Giraudat, J., Dennis, M., Heidmann, T.H., Maumont, P.Y., Lederer, F. and Changeux, J.-P. (1987) Structure of the high-affinity binding site for noncompetitive blockers of the acetylcholine receptor: [^{3}H]Chlorpromazine labels homologous residues in the β and δ chains. Biochemistry 26, 2410-2418.

Giraudat, J., Montecucco, C., Bisson, R. and Changeux, J.-P. (1985) Transmembrane topology of acetylcholine receptor subunits probed with photoreactive phospholipids. Biochemistry 24, 3121-3127.

Glasoe, P.F. and Long, F.A. (1960) Use of glass electrodes to measure acidities in deuterium oxide. J. Phys.Chem. 64, 188-191.

Glauert, A.M., Dingle, J.T. and Lucy, J.A. (1962) Action of saponin on biological cell membranes. Nature 196, 952-955.

Goormaghtigh, E., Cabiaux, V. and Ruysschaert, J.M. (1990) Secondary structure and dosage of soluble and membrane proteins by attenuated total reflection Fourier-transform infrared spectroscopy on hydrated films. Eur. J. Biochem. 193, 409-420.

Goormaghtigh, E., Cabiaux, V. and Ruysschaert, J.M. (1994a) Determination of Soluble and Membrane Protein Structure by Fourier Transform Infrared Spectroscopy. In: Subcellular Biochemistry, vol. 23, Eds. Hilderson, H.J. and Ralston, G.B., (Plenum Press, New York), 329-450.

Goormaghtigh, E. and Ruysschaert, J.M. (1990) Polarized attenuated total reflection infrared spectroscopy as a tool to investigate the conformation and orientation of membrane components, In: Molecular Description of Biological Membranes by Computer Aided Conformational Analysis. vol. 1, Ed., Robert Brasseur, (CRC Press), 285-329.

Goormaghtigh, E., Vigneron, L., Scarborough, G.A. and Ruysschaert, J.M. (1994b) Tertiary conformational changes of the *Neurospora crassa* plasma membrane H^+-ATPase monitored by hydrogen/deuterium exchange kinetics. J. Biol. Chem. 269, 27409-27413.

Görne-Tschelnokow, U., Strecker, A., Kaduk, C., Naumann, D. and Hucho, F. (1994) The transmembrane domains of the nicotinic acetylcholine receptor contain α-helical and β structures. Embo J. 13, 338-341.

Griffiths, P.R. and Pariente, G.L. (1986) Introduction to spectral deconvolution. Trends Anal. Chem. 5, 209-215.

Haris, P.I., Chapman, D. and Benga, G. (1995) A Fourier-transform infrared spectroscopic investigation of the hydrogen-deuterium exchange and secondary structure of the 28-kDa channel-forming integral membrane protein (CHIP28) Eur. J. Biochem. 233, 659-664.

Haris, P.I., Lee, D.C. and Chapman, D. (1986) A Fourier transform infrared investigation of the structural differences between ribonuclease A and ribonuclease S. Biochim. Biophys. Acta 874, 255-265.

Harrick, N.J. (1967) In: Internal reflection spectroscopy. (John Wiley and Sons, New York).

Hartree, E.F. (1972) Determination of protein: a modification of the Lowry method that gives a linear photometric response. Anal. Biochem. 48, 422-427.

Heimburg, T., Esmann, M. and Marsh, D. (1997) Characterization of the secondary structure and assembly of the transmembrane domains of trypsinized Na,K-ATPase by Fourier transform infrared spectroscopy. J. Biol. Chem. 272, 25685-25692.

Heimburg, T. and Marsh, D. (1993) Investigation of secondary and tertiary structural changes of cytochrome c in complexes with anionic lipids using amide hydrogen exchange measurements: An FTIR study. Biophys. J. 65, 2408-2417.

Hennessey, J.P. and Scarborough, G.A. (1989) An optimized procedure for sodium dodecyl-sulphate polyacrylamide gel electrophoresis analysis of hydrophobic peptides from an integral membrane protein. Anal. Biochem. 176, 284-289.

Huang, L.-Y., Catterall, W.A. and Ehrenstein, G. (1978) Selectivity of cations and non-electrolytes for acetylcholine activated channels in cultured muscle cells. J. Gen. Physiol. 71, 394-410.

Hübner, W. and Mantsch, H.H. (1991) Orientation of specifically $^{13}C=O$ labeled phosphatidylcholine multilayers from polarized attenuated total reflection FT-IR spectroscopy. Biophys. J. 59, 1261-1272.

Hucho, F., Görne-Tschelnokow, U. and Strecker, A. (1994) β-structure in the transmembrane spanning part of the nicotinic acetylcholine receptor. TIBS 19, 383-387.

Hucho, F., Tsetlin, V.I. and Machold, J. (1996) The emerging three-dimensional structure of a receptor. Eur. J. Biochem. 239, 539-557.

Hucho, F., Oberthür, W. and Lottspeich, F. (1986) The ion channel of the nicotinic acetylcholine receptor is formed by the homologous helices MII of the receptor subunits. Febs letters 205, 137-142.

Huganir, R.L., Delcourt, A.H., Greengard, P. and Hess, G.P. (1986) Regulation of neurotransmitter receptor desensitization by protein phosphorylation. Nature 321, 774-776.

Jackson, M. and Mantsch, H.H. (1991) Protein secondary structure from FTIR spectroscopy: Correlation with dihedral angles from three-dimentional Ramachandran plots. Can. J. Chem. 69, 1639-1642.

Jackson, M. and Mantsch, H.H. (1995) The use and misuse of FTIR spectroscopy in the determination of protein structure. In: Critical reviews in biochemistry and molecular biology, 30, 95-120.

Kandel, E.R., Schwartz, J.H. and Jessell, T.M. (1995) Essentials of neural science and behavior. Eds.: Kandel, E.R., Schwartz, J.H., and Jessell, T.M.(Appleton & Lange, Norwalk, Connecticut).

Karlin, A. (1991) Explorations of the nicotinic acetylcholine receptor. Harvey Lect. 86.

Kauppinen, J.K., Moffatt, D.J., Mantsch, H.H. and Cameron, D.G. (1981) Fourier self-deconvolution: A method for resolving intrinsically overlapped bands. Appl. spec. 35, 271-276.

Kleffel, B., Garavito, R.M., Baumeister, W. and Rosenbusch, J.P. (1985) Secondary structure of a channel-forming protein: porin from *E. coli* outer membranes. EMBO J. 4, 1589-1592.

Knörle, R. and Hübner, W. (1995) Secondary structure and stability of the bacterial carbohydrate-specific recognition proteins K88ab, AFA-1, NFA-1, and CFA-1. Biochemistry 34, 10970-10975.

Konishi, T. and Packer, L. (1977) Hydrogen exchange of dark-adapted and illuminated bacteriorhodopsin. FEBS Letters 80, 455-458.

Krimm, S., and Bandekar, J. (1986) Vibrational spectroscopy and conformation of peptides, polypeptides and proteins. Adv. Protein Chem. 38, 181-364.

Kuhlmann, J., Okondo, K.O. and Maelicke, A. (1991) Desensitisation is a property of the cholinergic binding region of the nicotinic acetylcholine receptor, not of the receptor-integral ion channel. FEBS Letters 279, 216-218.

Labarca, C., Nowak, M.W., Zhang, H., Tang, L., Deshpande, P. and Lester, H.A. (1995) Channel gating governed symmetrically by conserved leucine residues in the M2 domain of nicotinic receptors. Nature 376, 514-516.

Laemmli, U.K. (1970) Cleavage of structural proteins during the assembly of the head of the bacteriophage T4. Nature 227, 680-685.

Lasalde, J.A., Tamamizu, S., Butler, D.H., Vibat, C.R.T., Hung, B. and McNamee, M.G. (1996) Tryptophan substitutions at the lipid-exposed transmembrane segment M4 of *Torpedo californica* acetylcholine receptor govern channel gating. Biochemistry 35, 14139-14148.

Lee, D.C., Hayward, J.A., Restall, C.J. and Chapman, D.C. (1985) Second-derivative infrared spectroscopic studies of the secondary structures of bacteriorhodopsin and Ca^{2+}-ATPase. Biochemistry 24, 4364-4373.

Lee, Y.-H., Li, L., Lasalde, J., Rojas, L., McNamee, M., Ortiz-Miranda, S.I. and Pappone, P. (1994) Mutations in the M4 domain of *Torpedo californica* aceylcholine receptor dramatically alter ion channel function. Biophys. J. 66, 646-65.

Léna, C. and Changeux, J.-P. (1997) Pathological mutations of nicotinic receptors and nicotine-based therapies for brain disorders. Current opinion in neurobiology 7, 674-682.

Lenormant, H. and Blout, E.R. (1953) Nature 172, 770-771

Le Novere, N., Corringer, P.-J. and Changeux, J.-P. (1999) Improved secondary structure prediction of a nicotinic receptor subunit. Incorporation of solvent accessibility and experimental data into a 2D representation. Biophys. J. 76, 2329-2345.

Leonard, R.J., Labarca, C.G., Charnet, P., Davidson, N. and Lester, H.A. (1988) Evidence that the M2 membrane-spanning region lines the ion channel pore of the nicotinic acetylcholine receptor. Science 242, 1578-1581.

Lindstrom, J., Anand, R., Gerzanich, V., Peng, X., Wang, F. and Wells, G. (1996) Structure and function of neuronal nicotinic acetylcholine receptors, In: Progress in brain research, vol. 109, Chapter 10, Eds.: J. Klein and K. Löffelholz.

Ludlam, C.F.C., Arkin, I.T., Liu, X.-M., Rothman, M.S., Rath, P., Aimoto, S., Smith, S.O., Engelman, D.M. and Rothschild, K.J. (1996) Fourier transform infrared spectroscopy and site-directed isotope labeling as a probe of local secondary structure in the transmembrane domain of phospholamban. Biophys. J. 70, 1728-1736.

Lugovskoy, A.A, Maslennikov, I.V., Utkin, Y.N., Tsetlin, V.I., Cohen, J.B. and Arseniev, A.S. (1998) Spatial structure of the M3 transmembrane segment of the nicotinic acetylcholine receptor alpha subunit. Eur. J. Biochem. 255, 455-461.

Machold, I., Weise, C., Utkin, Y., Tsetlin, V. and Hucho, F. (1995) The handedness of the subunit arrangement of the nicotinic acetylcholine receptor from *Torpedo californica*. Eur. J. Biochem. 234, 427-430.

McCarthy, M.P. and Moore, M.A. (1992) Effects of lipids and detergents on the conformation of the nicotinic acetylcholine receptor from *Torpedo californica*. J. Biol. Chem. 267, 7655-7663.

McCarthy, M.P. and Stroud, R.M. (1989a) Changes in conformation upon agonist binding, and nonequivalent labeling, of the membrane-spanning regions of the nicotinic acetylcholine receptor subunits. J. Biol. Chem. 264, 10911-10916.

McCarthy, M.P. and Stroud, R.M. (1989b) Conformational states of the nicotinic acetylcholine receptor from *Torpedo californica* induced by the binding of agonist, antagonists, and local anesthetics. Equilibrium measurements using tritium-hydrogen exchange. Biochemistry 28, 40-48.

McPhail, A.T., Semenink, G.M. and Chestnut, D.B. (1971) Crystal structures of methyltriphprylarsonium and methyltriphonylphosphonium Bis-($\alpha_1\alpha\alpha'\alpha'$-tetracyanoquinondimethanmides). J. Chem. Soc. (A), 2174-2180.

Mercer, E.A.J. , Abbott, G.W., Brazier, S.P., Ramesh, B., Haris, P.I. and Srai, S.K.S. (1997) Synthetic putative transmembrane region of minimal potassium channel protein (minK) adopts an alpha-helical conformation in phospholipid membranes. Biochem. J. 325, 475-479.

Méthot, N. and Baenziger, J.E. (1998) Secondary structure of the exchange resistant core form the nicotinic acetylcholine receptor revealed by Fourier transform infrared spectroscopy. Biochemistry 37, 14815-14822.

Méthot, N. and Baenziger, J.E. (1999) The transmembrane domain of the nAChR is made exclusively of α-helices, manuscript in preparation.

Méthot, N., Demers, C.N. and Baenziger, J.E. (1995) Structure of both the ligand- and lipid-dependent channel-inactive states of the nicotinic acetylcholine receptor probed by FTIR spectroscopy and hydrogen exchange. Biochemistry 34, 15142-15149.

Méthot, N., McCarthy, M.P. and Baenziger, J.E. (1993) Secondary structure of the nicotinic acetylcholine receptor: Implications for structural models of a ligand-gated ion channel. Biochemistry 33, 7709-7717.

Michel-Villaz, M.H., Saibil, R. and Chabre, M. (1979) Orientation of rhodopsin α-helices in retinal rod outer segment membranes studied by infrared linear dichroism. Proc.Natl.Acad. Sci USA 76, 4405-4408.

Michelson, A.A. (1891) Phil. Mag. 31, 256.

Mielke D.L. and Wallace, B.A. (1988) Secondary structural analyses of the nicotinic acetylcholine receptor as a test of molecular models. J. Biol.Chem. 263, 3177-3182.

Miyazawa, T. and Blout, E.R. (1961) The infrared spectra of polypeptides in various conformations: Amide I and II bands. J. Am. Chem. Soc. 83, 712-719.

Miyazawa, A., Fujiyoshi, Y., Stowell, M. and Unwin, N. (1999) Nicotinic acetylcholine receptor at 4.6 Å resolution: transverse tunnels in the channel wall. J. Mol. Biol. 288, 765-786.

Moore, W.K. and Krimm, S. (1975) Transition dipole coupling in amide I modes of β-polypeptides. Proc. Natl. Acad. Sci. USA 72, 4933-4935.

Nabedryk, E. and Breton, J. (1981) Orientation of intrinsic proteins in photosynthetic membranes. Biochim. Biophys. Acta 635, 515-524.

Nabedryk, E., Andrianambinintsoa, S., Mäntele, W. and Breton (1988) NATO ASI Ser., Ser A 168, 237-250.

Nabedryk, E., Garavito, R.M. and Breton, J. (1988) The orientation of β-sheets in porin. A polarized Fourier transform infrared spectroscopic investigation. Biophys.J. 53, 671-676.

Nabedryk, E., Gingold, M.P. and Breton, J. (1981) Orientation of gramicidin A transmembrane channel. Infrared dichroism study of gramicidin in vesicles. Biophys J.38,243-9.

Nabedryk, E., Tiede, D. M., Dutton, P.L. and Breton, J. (1982) Conformation and orientation of the protein in the bacterial photosynthetic reaction center. Biochim. Biophys. Acta 682, 273-280.

Nabet, A., Boggs, J.M. and Pézolet, M. (1994) Study by infrared spectroscopy of the interaction of bovine myelin basic protein with phosphatidic acid. Biochemistry 33, 14792-14799.

Naumann, D., Schultz, C., Görne-Tschelnokow, U. and Hucho, F. (1993) Secondary structure and temperature behavior of the acetylcholine receptor by Fourier transform infrared spectroscopy. Biochemistry 32, 3162-3168.

Neubig, R.R., Boyd, N.D. and Cohen, J.B. (1982) Conformations of *Torpedo* Acetylcholine receptor associated with ion transport and desensitization. Biochemistry 21, 3460-3467.

Noda, M., Takahashi, H., Tanabe, T., Toyosato, M., Furutani, S., Hirose, Y., Asai, M., Inayama, S., Miyata, T. and Numa, S. (1982) Primary structure of the α-subunit precursor of *Torpedo californica* acetylcholine receptor deduced from cDNA sequence. Nature 299, 793-797.

Noda, M., Takahashi, H., Tanabe, T., Toyosato, M., Kikyotani, S., Furutani, Y., Hirose, T., Takashima, H., Inayama, S., Miyata, T. and Numa, S. (1983) Structural homology of *Torpedo californica* acetylcholine rceptor subunits. Nature 302, 528-532.

Ochoa, E.L.M., Chattopadhyay, A. and McNamee, M.G. (1989) Desensitization of the nicotinic acetylcholine receptor: molecular mechanisms and effect of modulators. Cell. Mol. Neurobiol. 9, 141-178.

Okamura,E., Umemura, J. and Takenaka, T. (1986) Orientation of gramicidin D incorporated into phospholipid multibilayers: a Fourier transform infrared-attenuated total reflection spectroscopic study. Biochim. Biophys. Acta 856, 68-75.

Olinger, J.M., Hill, D.M., Jakobsen, R.J. and Brody, R.S. (1986) Fourier transform infrared studies of ribonuclease in H_2O and ^2H_2O solutions. Biochim. Biophys. Acta 869, 89-98.

Opella, S.J., Marassi, F.M., Gesell, J.J., Valente, A.P., Kim, Y., Oblatt-Montal, M. and Montal, M. (1999) Structures of the M2 channel-lining segments from the nicotinic acetylcholine and NMDA receptors by NMR spectroscopy. Nat. Struc. Biol. 6, 374-379.

Ortells, M.O. and Lunt, G.G. (1994) The transmembrane region of the nicotinic acetylcholine receptor: is it an all-helix bundle ? Receptors and Channels 2, 53-59.

Ortells, M.O. and Lunt, G.G. (1996) A mixed helix-beta-sheet model of the transmembrane region of the nicotinic acetylcholine receptor. Proteins Engineering, 9, 51-59.

Osborne, H.B. and E. Nabedryk-Viala (1977) The hydrophobic heart of rhodopsin revealed by infared ^1H-^2H exchange study. FEBS Letters 84, 217-220.

Ozawa, S., Hayashi, R., Masuda, A., Iio, T. and Takahashi, S. (1997) Reconstitution of bacteriorhodopsin from a mixture of a proteinase V8 fragment and two synthetic peptides. Biochm. Biophys. Acta 1323, 145-153.

Pebay-Peyroula, E., Rummel, G., Rosenbusch, J.P. and Landau, E.M. (1997) X-ray structure of bacteriorhodopsin at 2.5 Å from microcrystals grown in lipidic cubic phases. Science 277, 1676-1680.

Popot, J.-L. (1993) Integral membrane protein structure: transmembrane α-helices as autonomous folding domains. Current opinion in Structural Biology, 3, 532-540.

Popot, J.-L. and Engelman, D.M. (1990) Membrane protein folding and oligomerization: The two-stage model. Biochemistry 29, 4031-4037.

Prestrelski, S.J., Byler, D.M. and Liebman, M.N., (1991) Comparison of various molecular forms of bovine tryspin: correlation of infrared spectra with x-ray crystal structures. Biochemistry 30, 133-143.

Raines, D.E. and Krishnan, N.S. (1998) Agonist binding and affinity state transitions in reconstituted nicotinic acetylcholine receptors revealed by single and sequential mixing stopped-flow fluorescence spectroscopies Biochim.Biophys. Acta 1374, 83-93.

Rankin, S., Addona, G.H., Kloczewiak, M.A., Bugge, B. and Miller, K.W. (1997) The cholesterol dependence of activation and fast desensitization of the nicotinic acetylcholine receptor. Biophys. J. 73, 2446-2455.

Rath, P., DeGrip, W.J. and Rothschild, K.J. (1998) Photoactivatin of rhodospin causes an increased hydrogen-deuterium exchange of buried peptide groups. Biophys. J. 74, 192-198.

Raussens, V., De Jongh, H., Pézolet, M., Ruysschaert, J.-M. and Goormaghtigh, E. (1998) Fourier transform infrared spectroscopy study of the secondary structure of the gastric H+,K+-ATPase and of its membrane-associated proteolytic peptides. Eur. J. Biochem. 252, 261-267.

Raussens, V., Narayanaswami, V., Goormaghtigh, E., Ryan, R.O. and Ryusschaert, J.-M. (1995) Alignment of the apolipophorin-III α-helices in complex with dimyristoylphosphatidylcholine. J Biol. Chem. 270, 12542-12547.

Rees, D.C., Chirino, A. J., Kim, K.-H. and Komiya, H. (1994) Membrane protein structure and stability: Implications of the first crystallographic analyses. In: Membrane protein structure. Ed. Stephen H. White, 3-26.

Reid, S.E., Moffatt, D.J. and Baenziger, J.E. (1996) The selective enhancement and subsequent subtraction of atmospheric water vapour contributions form Fourier transform infrared spectra of proteins. Spectrochimica Acta. 52, 1347-1356.

Reithmeier, R.A.F. and Deber, C.M. (1992) Intrinsic membrane protein structure: Principles and prediction. From: The structure of biological membranes. Ed.: Philip Yeagle, CRC Press, Boca Raton.

Revah, F., Galzi, J.-L., Giraudat, J., Haumont, P.-Y., Lederer, F. and Changeux, J.-P. (1990) The noncompetitive blocker [^{3}H]chlorpromazine labels three amino acids of the acetylcholine receptor γ-subunit: Implications for the α-helical organization of regions MII and for the structure of the ion channel. Proc. Natl. Acad. Sci.USA 87, 4675-4679.

Rothschild, K. J. and Clark, N.A. (1979) Polarized infrared spectroscopy of oriented purple membrane. Biophys. J. 25, 473-488.

Rothschild, K. J., Sanches, R., Hsiao, T.L. and Clark, N.A. (1980) A spectroscopic study of rhodopsin alpha-helix orientation. Biophys. J. 31, 53-64.

Sabatini, D.D., Kreibich, G., Morimoto, T. and Adesnik, M. (1982) Mechanisms for the incorporation of proteins in membranes and organelles. J. Cell. Biol. 92, 1-22.

Scarborough, G.A. and Hennessey, J.P. (1990) Identification of the major cytoplasmic regions of the *neurospora crassa* plasma membrane H^+-ATPase using protein chemical techniques J. Biol. Chem. 265, 16145-16149.

Schägger, H. and von Jagow, G. (1987) Tricine-sodium dodecyl sulphate-polyacrylamide gel electrophoresis for the separation of proteins in the range from 1 to 100 kDa. Anal. Biochem. 166, 368-379.

Schiebler, W. and Hucho, F. (1978) Membranes rich in acetylcholine receptor: characterization and reconstitution to excitable membranes from exogenous lipids. Eur. J. Biochem. 85, 55-63.

Schertier, G.F.X., Villa, C. and Henderson, R. (1993) Projection structure of rhodopsin. Nature 362, 770-772.

Schmidt, J. and Raftery, M.A. (1973) A simple assay for the study of solubilized acetylcholine receptors. Anal. Biochem. 52, 349-354.

Sheridan, R.P., Levy, R.M., and Salemme, F.R. (1982) α-helix dipole model and electrostatic stabilization of 4-α-helical proteins. Proc. Natl.Acad. Sci. U.S.A. 79, 4545-4549.

Smith, I.C.P. (1984) In: Membrane fluidity. Ed.: Morris Kates (Plenum, New York) 133-168.

Smith, B.C. (1996) In: Fundamentals of Fourier transform infrared spectroscopy. CRC Press, Boca Raton, FL.

Stamatoff, J.B., Graddick, W.F., Powers, L. and Moncton, D.E. (1979) Direct observation of the hydrocarbon chain tilt angle in phospholipid bilayers. Biophys. J. 25, 253-262.

Stroud, R.M., McCarthy, M.P. and Shuster, M. (1990) Nicotinic acetylcholine receptor superfamily of ligand-gated ion channels. Biochemistry 29, 11009-11023.

Sturgis, J., Robert, B. and Goormaghtigh, E. (1998) Transmembrane helix stability: the effect of helix-helix interactions studied by Fourier transform infrared spectroscopy Biophys. J. 74, 988-994.

Surewicz, W.K. and Mantsch, H.H. (1988) New insight into protein secondary structure from resolution-enhanced infrared spectra. Biochim. Biophys. Acta 952, 115-130.

Surewicz, W.K. and Mantsch, H.H. and Chapman, D. (1993) Determination of protein secondary structure by Fourier transform infrared spectroscopy: a critical assessment. Biochemistry 32, 389-394.

Susi, H., Timasheff, S.N. and Stevens, L. (1967) Infrared spectra and protein conformations in aqueous solutions. J. Biol. Chem. 242, 5460-5466.

Swope, S.J., Moss, S.J., Blackstone, C.D. and Huganir, R.L. (1992) Phosphorylation of ligand-gated ion channels: a possible mode of synaptic plasticity. FASEB Journal 6, 2514-2523.

Tikhovov, D.B. and Zhorov, B.S. (1998) Kinked-helices model of the nicotinic acetylcholine receptor ion channel and its complexes with blockers: Simulation by the Monte Carlo minimization method. Biophys. J. 74, 242-255.

Tobimatsu , T., Fujita, Y., Fukada, K., Tanaka, K-I., Mori, Y., Konno, T., Mishina, M. and Numa, S. (1987) Effects of substitution of putative transmembrane segments on nicotinic acetylcholine receptor function. Febs Letters, 222, 56-62.

Tsuboi, M. (1962) Infrared dichroism and molecular conformation of α-form poly-γ-benzyl-L-glutamate. Journal of polymer science 59, 139-153.

Tsukihara, T., Aoyama, H., Yamashita, E., Tomizaki, T., Yamaguchi, H., Shinzawa-Itoh, K., Nakashima, R., Yaono, R. and Yoshikawa, S., (1996) The whole structure of the 13-subunit oxidized cytochrome c oxidase at 2.8 Å. Science 272, 1136-1144.

Unwin, N. (1993) Nicotinic acetylcholine receptor at 9 Å resolution. J. Mol. Biol. 229, 1101-1124.

Unwin, N. (1995) Acetylcholine receptor channel imaged in the open state. Nature 373, 37-43.

Unwin, N. (1998) The nicotinic acetylcholine receptor of the *Torpedo* electric ray. J. Struc. Biol. 121, 181-190.

Unwin, N., Toyoshima, C. and Kubalek, E. (1988) Arrangement of the acetylcholine receptor subunits in the resting and desensitized states, determined by cryoelectron microscopy of crystallized Torpedo postsynaptic membranes. J. Cell biol. 107, 1123-1138.

Vigneron, L., Ruysschaert, J.M. and Goormaghtigh, E. (1995) Fourier transform infrared spectroscopy study of the secondary structure of the reconstituted *Neurospora crassa* plasma membrane H^+-ATPase and of its membrane-associated proteolytic peptides J. Biol. Chem. 270, 17685-17696.

Wagner, K., Edson, K., Heginbotham, L., Post, M., Huganir, R.L. and Czernik, A.J. (1991) Determination of the tyrosine phosphorylation sites of the nicotinic acetylcholine receptor. J. Biol. Chem. 266, 23784-23798.

Weiss, M.S., Kreusch, A., Schiltz, E., Nestel, U., Welte, W., Weckesser, J. and Shultz, G.E. (1991) The structure of porin from Rhodobater capsulatus at 1.8 Å resolution. FEBS lett. 280, 379-382.

Wennogle, L.P. and Changeux, J.-P. (1980) Transmembrane orientation of proteins present in acetylcholine receptor-rich membranes from *Torpedo marmorata* studied by selective proteolysis. Eur. J. Biochem. 106, 381-393.

West, A. P., Bjorkman, P.J., Dougherty, D.A. and Lester, H.A. (1997) Expression and circular dichroism studies of the extracellular domain of the α-subunit of the nicotinic acetylcholine receptor. J. Biol. Chem. 272, 25468-25473.

White, S.H., (1994) Hydropathy plots and the prediction of membrane protein topology. In: Membrane protein structure, Ed.: Steven H. White (Oxford University Press) 97-126.

White, B.H. and Cohen, J.B. (1992) Agonist-induced changes in the structure of the acetylcholine receptor M2 regions revealed by photoincorporation of an uncharged nicotinic noncompetitiveantagonist. J. Biol. Chem. 267, 15770-15783.

Wilson, G.G. and Karlin, A. (1998) The location of the gate in the acetylcholine receptor channel. Neuron 20, 1269-1281.

Woolley, G.A. and Wallace, B.A. (1994) Membrane protein structure: Lessons from gramicidin. In: Membrane protein structure, Ed.: Stephen H. White (Oxford Press, New York) 314-334.

Wu, C.-S., Sun, X.H. and Yang, J.T. (1990) Conformation of acetylcholine receptor in the presence of agonists and antagonists. J. Protein Chem. 9, 119-126.

Yager, P. Chang, E.L., Williams, R.W. and Dalziel, A.W. (1984) The secondary structure of acetylcholine receptor reconstituted in a single lipid component as determined by raman spectroscopy. Biophys. J. 45, 26-28.

Yeagle, P.L. (1993) In: The membrane of cells, Eds.: Academic Press, San Diego, CA.

Yee, G.H. and Huganir, R.L. (1987) Determination of the sites of cAMP-dependent phosphorylation on the nicotinic acetylcholine receptor. J.Biol. Chem. 266, 23784-23789.

Zhang, Y.-P., Lewis, R.N.A.H., Henry, G.D., Sykes, B.D., Hodges, R.S. and McElhaney, R.N. (1995a) Peptide models of helical hydrophobic transmembrane segments of membrane proteins. 1. Studies of the conformation, intrabilayer orientation, and amide hydrogen exchangeability of Ac-K2-(LA)12-K2-amide. Biochemistry 34, 2348-2361.

Zhang, Y.-P., Lewis, R.N.A.H., Henry, G.D., Hodges, R.S. and McElhaney, R.N. (1995b) Interaction of a peptide model of a hydrophobic transmembrane alpha-helical segment of a membrane protein with phosphatidylethanolamine bilayers: differential scanning calorimetric and Fourier transform infrared spectroscopic studies. Biophys. J. 68, 847-857.

Nathalie Méthot

Home address:
69 Plein-Air Street
Hull, Québec
J8Z 2S6
phone: (819) 776-2478

Work address:
University of Ottawa
Department of Biochemistry, Microbiology and Immunology
451 Smyth Road, Ottawa, K1H 8M5
phone: (613) 562-5800 x 8168
fax: (613) 562-5440

Spoken and written languages: English and French
Canadian citizen

Education

- Ph.D. in Biochemistry. Thesis title: Secondary Structure of the Channel Forming Transmembrane Segments from the Nicotinic Acetylcholine Receptor. University of Ottawa, 1993-99.

- B.Sc. in Science, Honours in Biochemistry. Thesis title: Secondary Structure of the Nicotinic Acetylcholine Receptor by FTIR spectroscopy, University of Ottawa, 1990-93.

Scholarships/Fellowships

- Post-doctoral industrial fellowship from NSERC, 1999-2001.
- Ph.D. scholarship from N.S.E.R.C., 1996-98.
- Ph.D. scholarship from F.C.A.R., 1995-98.
- Excellence scholarship from the School of Graduate Studies and Research, University of Ottawa, 1996-99.
- Travel scholarships from the Department of Biochemistry Microbiology-Immunology and the School of Graduate Studies, University of Ottawa, 1994-96.
- Second language scholarship from the government of Québec, 1992-93.

Work experience

- Part-time teaching at La cité collégiale, Ottawa. Responsibilities: Teaching a 3 credit course: Analyses instrumentales I. September 1999-December 1999.

- Research assistant at Adherex Technologies, Ottawa. Responsibilities: Peptide synthesis and purification directed toward treatment of breast and ovarian cancer. June 1999-

- Graduate student/Research assistant in the laboratory of Dr. John E. Baenziger at the Department of Biochemistry, Microbiology and Immunology, University of Ottawa. Responsibilities: Conduction of research oriented on the elucidation of the structure-function relationship of the nicotinic acetylcholine receptor. Techniques and skills: FTIR spectroscopy, computer processing, protein purification, proteolysis, SDS-PAGE, organic chemistry, scientific writing and presentation of research results. 1993-99.

- Project coordinator for the preparation of a poster competition at the University of Ottawa, School of Graduate Studies and Research. Responsibilities: Presentation of workshops on preparing effective research posters, assist graduate students in the preparation of posters, preparation of a programme and organization of the event. May to September 1998.

- Teaching assistant in the Department of Biochemistry. Responsibilities: Correcting exams and proctoring, 1993-96.

- Teaching assistant in the teaching laboratories of the Departments of Chemistry and Biochemistry-Microbiology-Immunology. Responsibilities: Explaning experimental theory and concepts, supervising and offering direction to students during laboratory periods, correction of laboratory reports and evaluation of the students, 1992-98.

Publications

Refereed papers

- The transmembrane domain of the nicotinic acetylcholine receptor contains exclusively α-helical transmembrane segments. (1999) Manuscript in preparation.

- Secondary structure of the exchange resistant core from the nicotinic acetylcholine receptor probed directly by infrared spectroscopy and hydrogen deuterium exchange, Méthot, N., and Baenziger, J.E., (1998) *Biochemistry*, 37(42), 14815-14822.

- Secondary structure analysis of individual transmembrane segments of the nicotinic acetylcholine receptor by CD and FTIR spectroscopy; Corbin, J., Méthot, N., Wang, H.H., Baenziger, J.E., and Blanton, M.P. (1998) *J. Biol. Chem. 273*, 771-777.

- Structure of both ligand and lipid dependent channel-inactive states of the nicotinic acetylcholine receptor probed by FTIR spectroscopy and hydrogen exchange; Méthot, N., Demers, C.N., and Baenziger, J.E. (1995) *Biochemistry 34*, 15142-15149.

- Fourier transform infrared and hydrogen/deuterium exchange reveal an exchange resistant core of α-helical peptide hydrogens in the nicotinic acetylcholine receptor; Baenziger, J.E. and Méthot, N., (1995) *J. Biol. Chem. 270*, 29129-29137.

- Secondary structure of the nicotinic acetylcholine receptor: implications for structural models of a ligand-gated ion channel; Méthot, N., McCarthy, M.P., and Baenziger, J.E. (1994) *Biochemistry 33*, 7709-7717.

Conferences

Poster presentations

- Baenziger, J.E., Chew, J.P., McCarthy, M.P. and Méthot, N., (1994), *Biophys. J. 66(2)*, A212. in New Orleans, Louisiana.
- Méthot, N. and Baenziger, J.E.(1994) *Biophys. J. 66(2)*, A212. in New Orleans, Louisiana.
- Baenziger, J.E., Chew, J.P., and Méthot, N., (1995), *Biophys. J. 68(2)*, A377. San Francisco, California.
- Méthot, N. and Baenziger, J.E. (1995) *Biophys. J. 68(2)*, A377. San Francisco, California.
- Méthot, N. and Baenziger, J.E. (1996) *Biophys. J.*, Baltimore, Washington.
- Baenziger, J.E, Ryan S.E., Méthot, N. and Demers C. (1996) ACFAS meeting in Montréal, Québec.
- Méthot, N. and Baenziger, J.E. (1997) CFBS annual meeting in Québec City, Québec.
- Méthot, N. and Baenziger, J.E. (1999) *Biophys. J.*, Baltimore, Washington.

Verbal communications

- Méthot, N. and Baenziger, J.E. (1997) ACFAS meeting in Trois-Rivières, Québec.
- Méthot, N. and Baenziger, J.E. (1998) ACFAS meeting in Québec City, Québec.

Social Involvement

- Member of the American Biophysical Society since 1993.
- Member of L'Association Canadienne-Française pour l'Avancement des Sciences since 1996.
- Member of the Canadian Biophysical Society since 1997.
- Member of the Graduate Studies Committee in Biochemistry, University of Ottawa, 1995-98.
- Treasurer for the Graduate Students Association in Biochemistry, 1994-95.
- Organization of volleyball tournaments in the Faculty of Medicine, 1994-95.
- Organization of poster presentations in the Department of Biochemistry, 1996 and 1998.
- Presentation of a tutorial workshop offered by the Teaching and Learning Center, University of Ottawa, 1998.